

Azərbaycan Milli Elmlər Akademiyası
Fizika-Riyaziyyat və Texnika Elmləri Bölməsi
Fizika İnstitutu

3

Fizika

Cild

XI

2005

Bakı ✱ Elm

THE DERIVATIVE-GRAPHICAL INVESTIGATIONS OF THE POLYETHYLENE SYSTEM OF THE LOW DENSITY AND TlInSe_2

E.M.GOJAYEV, R.M.SARDARLI*, S.S.OSMANOVA, N.A.EYUBOVA*, E.A.ALLAHYAROV

Azerbaijan Technical University, 1025, Baku, G. Javid av., 25

Institute of Radiation Problems of Azerbaijan National Academy of Sciences

*1143, Baku, G. Javid av, 31a**

The results of the differential-thermal and thermogravimetric analysis of the $\text{PELD} + x \text{ weigh \% TlInSe}_2$ ($x=0; 1; 3; 5; 10; 40$) system in the interval from 20°C till 500°C are presented in the paper. It has been revealed, that at the TlInSe_2 filling PELD the thermal stability increases till 5 weigh% and mass loss for the given composition in the comparison with the initial PELD increases till 93%, proving the full saturation. The two peaks of melting are observed on the DTA curves, the process of the thermal-oxidative breakdown takes place at 330°C and 440°C temperatures.

At high concentrations of the filler till 40 weigh % the changes of the enthalpy law is observed on DTA curves in temperature region $210\text{--}218^\circ\text{C}$.

Introduction

Nowadays the direction, connected with the modified electroactive properties of the polymers by the way of the leading of the different fillers, creating of the polymeric impurities or by the influence of the different ionizing radiations, is quickly developing [1-10].

The leading of the fillers of the inorganic nature in the polymeric matrix is the universal method of the polymer modification. The three-component semiconductor compound TlInSe_2 was led in the capacity of the fillers into polyethylene of the high density (PELD) in this aspect. This is caused by the fact, that the given phase has peculiar crystalline and band structures and is the perspective material in the visual and infrared regions of the spectrum, having the record strain-sensitivity and switching properties with memory. The unique properties of the given phase are the fact, that the parameters of the photo- and strain-elements, switches are ruled in the needed direction under influence of the electromagnetic and acoustic waves in the dependence on the mechanical deformation, contact materials, the temperature of the surroundings [11-18]. The composites with the TlInSe_2 fillers can have physico-mechanical (elasticity, facility, anti-heat and e.t.c.) [19], electrophysical (electroconductivity with switching, dielectric (ϵ , $\text{tg}\delta$) and additive properties), electroactive (strain-, pyro-sensitive), electroluminescent and other properties. Besides, the study of such compositions is important for the understanding of the mechanism of charge transfer, dissipations of the energies in polymer-semiconductor, polymer-metal heterogeneous systems for the study of the interphase phenomena, and also in processes of structure modification and properties of polymers themselves at their radiation and other types of the influence. In this connection we were carrying out the derivatographical investigations of $\text{PELD} + x \text{ weigh \% TlInSe}_2$ ($x=0; 1; 3; 5; 10; 40$) system.

Experimental part

The samples of the composition $\text{PELD} + x \text{ weigh \% TlInSe}_2$ ($x=0; 1; 3; 5; 10; 40$) were investigated on the Q-derivatograph of the MOM firm (Hungary) in the temperature interval $20\text{--}500^\circ\text{C}$. [20]. The heating rate is 5

grad/min. The dry Al_2O_3 was taken in the capacity of the standard. The samples by the type of the connection 0,3 and thickness $80\text{--}100 \text{ mkm}$ had been obtained by the way of the dry shifting of the powders of the filler and polymer with the following thermopressing at pressure 150 MPa and temperature 200°C , and further, the melt was hardened with the help of the impurity ice-water with the velocity $\sim 2000^\circ\text{C/min}$ [21]. The pressing time was 15 minutes.

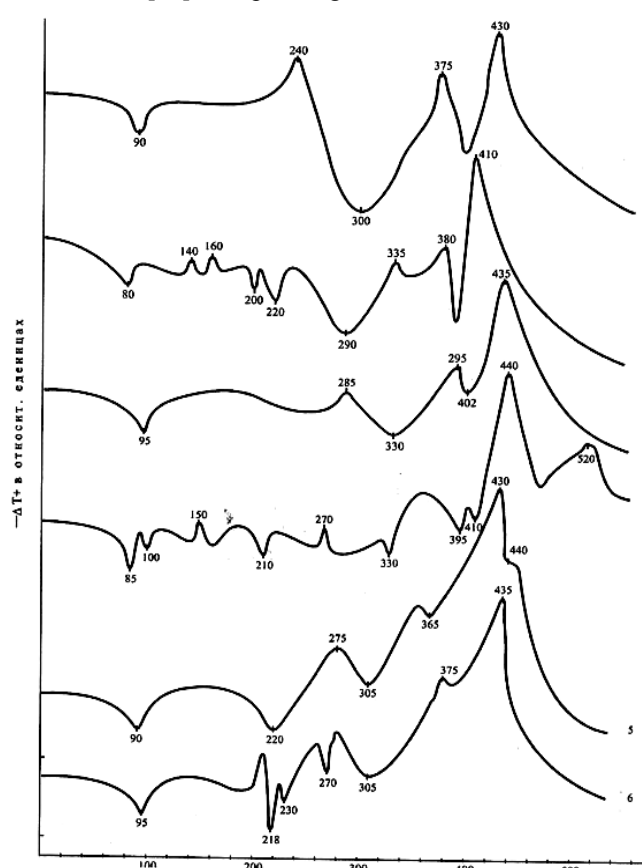


Fig.1. The differentially-thermal curves of the stoichiometric compounds of $\text{PELD} + x \text{ weigh \% TlInSe}_2$, where 1- $x=0$, 2- $x=1$, 3- $x=3$, 4- $x=5$, 5- $x=10$, 6- $x=40$ weigh %.

The results of the thermogravimetric (TG) and differential-thermal analysis (DTA) of the studied

compositions PELD + x weigh % TlInSe_2 are presented on the figures 1 and 2.

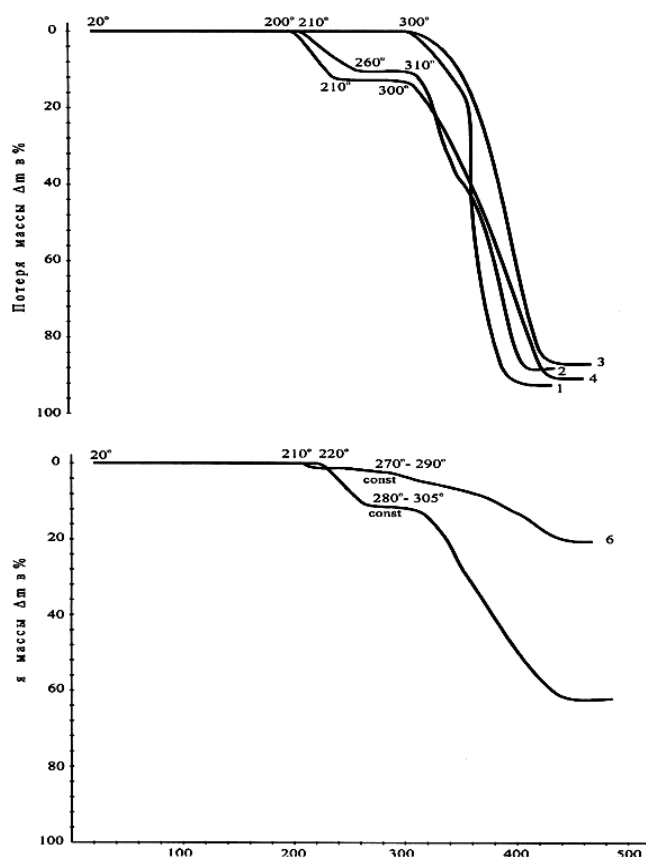


Fig.2. The thermogravimetric curves of the stoichiometric compositions of PELD + x weigh % TlInSe_2 , where 1- $x=0$, 2- $x=1$, 3- $x=3$, 4- $x=5$; 5- $x=10$; 6- $x=40$ weigh %.

The derivatogramm of the pure PELD had also fixed (Fig.1, curve 1 and curve 2) for the comparison of the changes, carrying out in PELD after the addition of формула filler. As it is seen from the fig. 1 (curve 1) the three clearly expressed endothermic effects at 90°C, 300°C, 402°C and two exothermic peaks at 240°C and 430°C are situated on DTA curve correspondingly. The second exothermic effect at 240°C is connected with the beginning of the thermal oxidation of ПЭ film. Probably, the decomposition of the transversal connection takes place on the initial thermal-oxidation. The second exothermic effect at 430°C corresponds to the second step of the thermal-oxidation and to the beginning of the process of the polymer depolymerization [21-24].

According to TG curve (curve 1) in the temperature interval 20-300°C the weight loss isn't observed, i.e. the polymer is stable till 300°C. Further, the mass loss begins from the 300°C (the disconnection of the weak connections, the endoeffect is on DTA at 300°C) and the mass loss, thermal destruction is ~ 45%. The maximum of the mass loss is observed in region 365-400°C. The bulk loss of the mass is 92%, and the residual is ashes 8%.

The four endothermic effects at 80; 200; 220 and 390°C and four exothermic effects at 140; 160; 368 and 410°C have been observed on the derivatogramm of the stoichiometric

composition 1 weigh% TlInSe_2 +99 weigh % PELD. From the comparison of these data with data on the fig.1 (curve 1) we can conclude, that the first endothermic effect at 90°C corresponds to the melting of PELD. Besides, here the two new endothermic effects at 200°C, 220°C (curve 2), accompanying by the mass loss on TG curve till 12%, appear in the samples of the compositions PELD/формула, the last probably is caused by the decomposition of the weak connections and the beginning of the oxidative processes in the filled part of PELD. The confirmation of the above mentioned are exothermic effects on curve DTA with maximums at 140 and 160°C. The exothermic effect at 140°C corresponds to the first stage of the oxidation of PELD part, filled by TlInSe_2 and the second exoeffect at 160°C corresponds to the modified part of PELD. The endothermic effect at 290°C corresponds to the depolymerization of PELD part, as filled by TlInSe_2 , so unadulterated by TlInSe_2 . The exoeffect at 368°C corresponds to thermal-oxidative destruction of the filled TlInSe_2 part of PELD and at 410°C corresponds to unaltered part of PELD.

From the comparison of DTA curves of the pure PELD and samples of the composition 1 weigh% TlInSe_2 +99weigh% PELD (fig. 1. curves 1,2 and 2. curves 1,2) is seen, that the introduction into PELD of TlInSe_2 , the new peaks are observed on DTA curve: (exoeffect) at 140°C and endothermic effects at 200 and 220°C, that proves about partial modifying of the polyethylene. That's why at the low content of TlInSe_2 the coexistence of the two different parts of the polymers – main and modified are observed in the composition content.

The partial filling of PELD, totally coinciding with the fig. 1.1, is also observed in the compound 3 weigh % TlInSe_2 +97% PELD (fig.1. curve 3). The comparison of DTAcures of these samples shows, that the decomposition of the weak connections in both parts of the investigated composition takes place at 330°C, and depolymerization process begins to carry out also at the one temperature 345°C, though the continuance of the oxidation of the depolymerization by the filled part takes place at 395°C, and by the unaltered part at 435°C. According to TG in this compound 3 weigh% TlInSe_2 +97 weigh % PELD (fig. 2. curve 3) the constancy of the compound, characterizing the thermostability of the filled part is observed in the temperature region 300-330°C, and the destruction of the weak connections of both parts of polymer is observed from 330°C, accompanying by the mass loss of the quantity 14,7%. The thermostability of the filled part of PELD with the addition 3 weigh % TlInSe_2 increases on 50-60°C and corresponds to 300-305°C.

From the derivatogramm of the compound 5 weigh % TlInSe_2 +95 weigh % PELD (fig. 1.4 and 2.4) is followed, that the two endothermic effects at 85 and 100°C, characterizing the melting of the crystals of the investigated compound, are observed on the curve DTA. The appearance of these endothermic peaks (fig.1, curve 4) can be connected with the creation of new crystal formation of the polyethylene on the surface of the particles TlInSe_2 , which melt at 100°C. It is need to note, that the increase of the crystallinity of the polyethylene is observed at the addition of other types of the fillers [21]. Thus, from these data is

followed, that at the definite ratio of the components in PELD/TlInSe₂ system the semiconductor fillers are the crystallization centers, moreover new-formed crystallites have the increased melting point (second melting peak at 100°C). The exoeffect at 150°C corresponds to I stage of the oxidation of the filled part of PELD. The endoeffect at 210°C corresponds to the disconnection of the weak connections of this filled part of PELD. According to trend of curve TG (fig. 2.4) the weight constancy, characterizing the thermostability of the filled part of polymer, is observed in the temperature region 20-210°C. In the temperature region 210-260°C the change of the trend of curve TG in the direction of the mass loss in the quantity 12,4%, caused by the disconnection of the weak connections of the filled part is observed. The exoeffect at 270°C is caused by the first stage of the oxidation of the unaltered part of the polyethylene. The endoeffect at 330°C corresponds to the disconnection of the weak connections of the unaltered part of the polyethylene in the quantity 18,6%, the endoeffect at 395°C is probably caused by the oxidative depolymerization of the filled part, and endoeffect at 410°C is caused by the unaltered part of PELD. The exoeffect at 440°C is connected with depolymerization process. Thus the filler leads to the temperature increase of PELD depolarization.

As it is seen from the calculations of the thermogravimetric curves (fig. 2 curve 4), the most effective structure of PELD is carried out at 5 weigh % concentration of TlInSe₂ in the comparison with (fig. 2).

From the comparison of DTA curves for the different compositions of PELD/TlInSe₂ is followed, that (fig.1 and 2) the observable first endothermic effect at 80-95°C is caused by the melting point of the unaltered part of PELD for all investigated compositions on DTA curve, the endothermic effect at 100°C corresponds to the melting point of the filled part, which has own specific thermal effects, connected with processes on the borders of phase division.

The thermostability for the compounds 1; 3; 5 weigh % TlInSe₂ corresponds to 290°C. The thermostability of the polymer increases on 35-45°C because of the no saturation of TlInSe₂ with the increase of the percent concentration of TlInSe₂ from 10 till 40 weigh %. The two regions of PELD are revealed on the thermogravimetric curve, beginning from 10 weigh % TlInSe₂ in PELD: the first region of the mass loss is observed in the temperature region 220-280°C, caused by the filled TlInSe₂ part of PELD, further the constancy

region is observed on TG curve in the temperature region 280-305°C, characterizing the thermostability of the filled part of the polymer. The small mass loss at 305-345°C characterizes the disconnection of the weak connections of the both parts of PELD, the depolymerization of both parts is also carried out at 345°C, but thermal-oxidative destruction divides into two parts at the temperature 430°C and 440°C.

At high contents of the fillers till 40 weigh% on DTA curve the character peaks at 215-218°C with the change of enthalpy sign are observed, which are character for the crystal transfers by the type crystal-crystal and TlInSe₂ filler.

As it is seen from (fig.1, curve 6 and fig.2, curve 6) the derivatogramm consists from two diagrams: low-temperature region characterizes filled part of PELD TlInSe₂ (from 205 till 270°C), and high-temperature – from 290 till 435°C of unaltered of PELD. It is need to note, that with the increase of the percent concentration of TlInSe₂ the maximal temperature of the decomposition of the compound PELD + x weigh % increases from 380°C for the initial PELD till 410°C for the compound 40 weigh% TlInSe₂. The gross mass loss for the initial PELD at the heating from 20°C till 500°C is 92%, at the increase of the concentration TlInSe₂ from 1 till 5 weigh % the mass loss decreases till 88-87%, that proves about connection of particles of TlInSe₂ by the polyethylene. The mass loss for the compound with 5 weigh % TlInSe₂ increases in the comparison with the initial PE till 93% that proves again, that effective filling of the polyethylene is carried out at the concentration 5 weigh % TlInSe₂. For the composition 5 weigh % TlInSe₂ the mass loss in the comparison with the initial PE increases till 93% that again is proved, that effective modifying of PE structure carries out at the 5 weigh % TlInSe₂ concentration.

Conclusion

The derivatographic investigations of PELD + x weigh % TlInSe₂ system show, that thermal stability of the composition increases at the filling till 5 weigh % of PE. It is obtained the new material, having high work temperature for the creation on it base the more perspective piezo-elements, than initial phase. Each phase at the high percents of TlInSe₂ is special, the change of the enthalpy sign is observed on DTA curve at the temperature interval 215-218°C.

-
- | | |
|---|---|
| <p>[1] M.Q. Shaxtaxinskiy, M.A. Kurbanov, B.A. Guseynov, Yu.N. Qazaryan, M.A. Ramazanov, M.M. Kuliev, A.A. Garaqashov. Visokomolek. soed., 1987, t. 29B, № 1, s. 3-5.</p> <p>[2] Q.A. Lusheykin. Polimernie pyezoelektriki. M., Ximiya, 1990, 176 s.</p> <p>[3] A.V. Qoroxov, V.I. Zakrevskiy, I.M. Sokolova, V.N. Tairov, G.P. Timosinov. Plasticheskie massi, 1988, № 6, s. 29-30.</p> <p>[4] R.M. Aliguliev. Relaksatsionnaya spektrometriya polimernih dielektrikov. Baku, Elm, 1997, 287 s.</p> <p>[5] A.P. Tyutnev, A.V. Vannikov, G.S. Mingaleev, V.S. Saenko. Elektricheskie yavleniya pri obluchenii polimerov. M., Energoatomizdat, 1985, 176 s.</p> <p>[6] J. Menson, L. Sperling. Polimernie smesi i kompoziti. M., Khimiya, 1979, 440 s.</p> | <p>[7] A. Nilsen. Mexanicheskie svoystva polimerov i polimernih konditsiy. M., Khimiya, 1978, 309 s.</p> <p>[8] V.Q. Nikolskiy, N.A. Mironov. Zavodskaya laboratoriya, 1973, t.39, № 10, s.1272-1275.</p> <p>[9] A.M. Magerramov, A.M. Lobanov, M.A. Bagirov, F.Q. Gilimyanov, V.I. Kruqlyak, A.A. Jafarov, I.I. Aliev. Plasticheskie massi, 1993, № 5, s. 19-21.</p> <p>[10] Q.V. Sagalaev, I.D. Simonov-Emelyanov, L.N. Babakova. Plasticheskie massi, 1974, № 2, s. 51-54.</p> <p>[11] K.R. Allakhverdiev. Opticheskie svoystva i kolebatelnye spektri sloistikh i tsepochevnykh kristallov grupp A^{III}B^{VI}, A^{III}B^{III}C₂^{VI} i tverdkh rastvorov na ikh osnove. Avtoref. Diss. dokt. fiz.-mat. nauk. Baku. 1981. c. 34.</p> <p>[12] G.D. Guseynov, G.B. Abdullaev. Dokladi AN SSSR. 1973. t.208. №5. c.1052-1054.</p> |
|---|---|

- [13] G.M. Godjaev, G.A. Allakhyarov, Kh.O. Sadikhova. Neorgan. materialı. 1994. t.30. №6. c. 859-860.
- [14] G.M. Godjaev, S.Kh. Khalilov, Kh.S. Khalilova, M.A. Guseynov, A.M. Suleymanova. İnjenerno-Fizicheskiy Jurnal. 2003. t. 76. №2. c. 76-79.
- [15] E.A. Vinogradov, N.M. Gasanlı, B.M. Javadov, V.İ. Tagirov. FTT. 1979. t. 21. №9. c. 2793-2796.
- [16] G.M. Godjaev, Z.M. Abdullaev, Sh.M. Guseynova. TsNİİ, «Elektronika». 1976. Deponirovana za №3975/76.
- [17] G.M. Godjaev, Kh.O. Sadıgova. Neorgan. materialı. 1993. t.29. №3. c. 337-339.
- [18] G.M. Godjaev, K.D. Gulmamedov. Neorgan. materialı. 2002. t.38. №12. s. 1426-1431.
- [19] L.Q. Berg. Vvedenie v termografiyu, Moskva, 1969, - 395 s.
- [20] A.M. Magerramov. Strukturnoe i radiatsionnoe modifitsirovanie elektretnikh, pyezoelektricheskikh svoystv polimernikh kompozitov. Baku, Elm, 2001, s.197-202.

E.M. Qocayev, R.M. Sərdarlı, S.S. Osmanova, N.A. Eyubova, E.Ə. Allahyarov

AŞAĞI SIXLIQLI POLİETİLEN VƏ TiInSe_2 KOMPOZİSİYALARININ DERİVATOQRAFİK TƏDQIQI

Təqdim olunmuş işdə ASPE + x çəki % TiInSe_2 ($x=0; 1; 3; 5; 10; 40$) sisteminin 20-500⁰ C temperatur intervalında differensial-termik və termoqravimetrik analizlərinin nəticələri verilmişdir. Müəyyən olunmuşdur ki, TiInSe_2 ASPE ilə 5 çəki %-ə qədər doldurulması zamanı termik davamlılıq artır və verilmiş tərkib üçün təmiz ASPE ilə müqayisədə kütlə itkisinin 93%-ə qədər artması tam doyma faktını təsdiq edir. DTA əyrilərində iki ərimə pikləri müşahidə edilir, termooksidləşmə destruksiya prosesi 330⁰ və 440⁰ C temperaturlarda baş verir.

Doldurucunun 40 çəki. %-ə qədər yüksək konsentrasiyası zamanı DTA əyrilərində 210-218⁰ C temperatur intervalında entalpiyanın işarəsinin dəyişməsi müşahidə olunur.

Э.М. Годжаев, Р.М. Сардарлы, С.С. Османова, Н.А. Эюбова, Э.А. Аллахьяров

ДЕРИВАТОГРАФИЧЕСКИЕ ИССЛЕДОВАНИЯ КОМПОЗИЦИЙ ПОЛИЭТИЛЕН НИЗКОЙ ПЛОТНОСТИ И TiInSe_2

В работе излагаются результаты дифференциально-термического и термогравиметрического анализов системы ПЭНП + x вес.% TiInSe_2 ($x=0; 1; 3; 5; 10; 40$) в интервале температур 20-500⁰ C. Выявлено, что при наполнении TiInSe_2 ПЭНП до 5 вес.% возрастает термическая устойчивость и для данного состава потеря массы по сравнению с исходным ПЭНП увеличивается до 93%, подтверждающие полное насыщение. На кривых ДТА наблюдается два пика плавления, процесс термоокислительной деструкции проходит при температурах 330 и 440⁰ C.

При высоких концентрации наполнителя до 40 вес.% на кривых ДТА в области температур 210-218⁰ C наблюдается изменения закона энтальпии.

Received: 22.07.05

THE MECHANISM OF ELECTRICAL CONDUCTIVITY IN THIN-FILM STRUCTURE ON THE BASIS OF THE ORGANIC SEMICONDUCTOR VANADIUM PHTHALOCYANINE

M.M. PANAHOV, S.A. SADRADDINOV, J.N. JABBAROV, B.SH. BARKHALOV

Baku State University

Acad. Z. Khalilov str., 23, Baku, Az-1145

The volt-ampere and capacitance-voltage characteristics in metal-semiconductor-metal (MSM) structures on the basis of vanadium phthalocyanine (VPc) organic semiconductor have been investigated. It is revealed that at the absence in the MSM-structure of the high-resistive interface barriers, nonlinear CVC at high electric fields is a result of the field assisted thermal emission of charge carriers from traps (Poole-Frenkel effect). It is also established that at low temperatures and high electric fields, when density of the charged traps is sufficiently high ($> 10^{24} \text{ m}^{-3}$), Coulomb potentials overlapped and a barrier lowering becomes proportional to electric field intensity and the modified Frenkel-Poole effect becomes predominant.

INTRODUCTION

High light and thermal resistance, ability to form of a continuous film by evaporation in vacuum at moderate temperatures makes the organic semiconductor vanadium phthalocyanine (VPc) a valuable material for the solution of a number of tasks of microelectronics.

Choosing the appropriate material for electrodes, using known techniques it is possible to create ohmic [1-3] as well as rectifying [3-6] electrical contacts to a surface of metal-organic semiconducting compounds of the phthalocyanine series.

For some phthalocyanine compounds the charge transport and rectifying of an alternating current phenomena were investigated in layered structures («sandwiches»), which electrical contacts were formed by using identical or different metals [3, 5-7].

For study the structures on the basis of the phthalocyanine with non-blocking contacts more often a method of space-charge-limited currents (SCLC) is used [8]. In phthalocyanine single crystals with silver electrodes ohmic (linear) current-voltage characteristics (CVC) were observed that passes further in nonlinear one. In many experimental works, at the absence of the blocking contacts in phthalocyanine thin film structures, nonlinear CVC are interpreted by the charge carrier injections in bulk from electrodes [8, 9].

EXPERIMENTAL PART

Our studies of the electrical properties of structures on the basis of the evaporated VPc layers have shown that at absence in the structure of blocking electrodes, nonlinear CVC is a result of the field assisted thermal emission of charge carriers from traps.

Double additional cleaning of the industrial VPc powder by vacuum sublimation has ensured reproducibility of our results. Investigated structures were obtained by consecutive thermal vapor deposition in a vacuum ($p \approx 10^{-3} \text{ Pa}$) the bottom Ag electrode, the VPc layer and the top Ag electrode on a non-heated ceramic substrate. On the same substrate were obtained simultaneously eight identical on topology «sandwich» samples, distinguished only by thickness of the VPc layer, that being within the limits of 0.4-2.0 μm . All measurements were carried out in a vacuum 10^{-3} Pa .

The study of the temperature-field dependences of the electrical conductivity for VPc have shown, that nonlinear

CVC of the Metal/VPc/Metal structures are stipulated by Frenkel-Poole emission, which study allows to receive the information about the charge carriers localization centers in a semiconductor [10].

For study of electrical properties of the high-resistance films it is necessary previously to establish the diagram of distribution of the applied voltage in MSM-structure, which is determined, mainly, by the basic properties of the metal/semiconductor interface. An effective way of an establishing of distribution of the voltage in MSM-structures is a study of the conduction and capacity at various temperatures and frequencies [11]. The capacity of the Ag/VPc/Ag structure in a wide temperature range practically does not depend on temperature (Fig. 1). Besides for structures with the identical electrode areas, but with various thickness of a VPc layer ($d = 0.67\text{-}1.30 \mu\text{m}$) electrical capacity $C \sim d^{-1}$ (insert in a fig. 1). These data unequivocally testify to absence of the electrical field discontinuities in the considered structure [11]. In this case equivalent circuit of a sample is represented by capacity, shunted by active volume resistance, and the applied constant voltage U totally drops in the VPc layer.

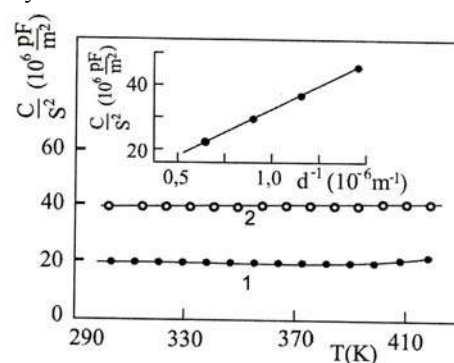


Fig.1. Dependence of capacity C on the temperature T of the Ag/VPc/Ag structure with various thicknesses d of the VPc layer, μm : (1 - 1.30; 2 - 0.67). Insert - C/d vs d^{-1} .

The dependence of the current I on the applied voltage U in Ag/VPc/Ag structure is given in fig. 2. At low voltages with the increase of the voltage U the current I grows linearly, and at large voltages - non-linearly. It has appeared that at the large voltages the dependence $I/U \propto \exp(U^{1/2})$ takes place. At passing to rather thick VPc films the character of dependence is preserved, however inclination α of a linear part of dependence $\lg(I/U)$ on $U^{1/2}$ appreciably decreases, and the value of the product $\alpha d^{1/2}$ practically remains constant.

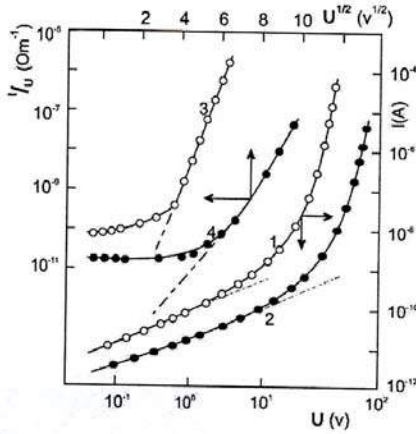


Fig. 2. Dependence of a current I on the applied voltage U in the Ag/VPc/Ag structure (1 and 2) and I/U on $U^{1/2}$ (3 and 4) at different thickness of VPc films, μm : 1- 0.67 (1 and 3) and 1.30 (2 and 4). The electrodes area $S=1.15 \text{ mm}^2$.

At the absence a high-resistance interface barriers in the MSM-structure the linear dependence $\lg I/U$ on $U^{1/2}$ may be connected with Poole-Frenkel emission [12, 13], when the process of thermal excitation of the charge carriers from traps is facilitated by the applied electrical field. It can be checked up by studying temperature dependence of a current at various voltages and establishing of characteristic parameters.

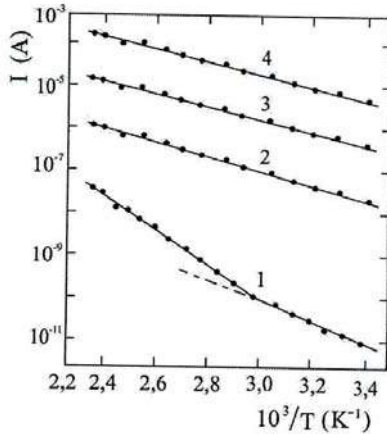


Fig. 3. The temperature dependences of the current I in the structure Ag/VPc/Ag at different applied voltages, V: 1 – 0.4; 2 – 10; 3 – 20 and 4 – 30. Thickness of VPc film $d = 0.67 \text{ }\mu\text{m}$.

In a fig. 3 are given the temperature dependence of a current at various fields in VPc film. In a weak field ($F < 6 \cdot 10^5 \text{ V/m}$) current I exponentially depends on T and also is described by two activation energies: 0.56 and 0.75 eV (in account per κT). The value $E_0 = 0.56 \text{ eV}$ is a depth of the dominant trapping levels. The second value characterizes intrinsic conductivity of the VPc (1.50 eV in account per 2 κT) and meets to the data given elsewhere [13]. In a strong field, when ($F \geq 10^7 \text{ V/m}$), an exponential increase of a current with the increasing of the temperature is described only by an activation energy $E_F < 0.56 \text{ eV}$, and with growth of F the value of E_F decreases according to the Frenkel's theory on the ionization of the traps:

$$E_F = E_0 - e\beta F^{1/2} \quad (1)$$

where e - electronic charge, β - Frenkel-Poole constant. The value of β can be determined from the curves of the dependence of the Frenkel's barrier lowering for the traps $\Delta\Phi = E_0 - E_F$ on $F^{1/2}$ (fig. 4.), which appears equal to $\beta = 4.25 \cdot 10^{-5} \text{ V}^{1/2} \text{ m}^{1/2}$.

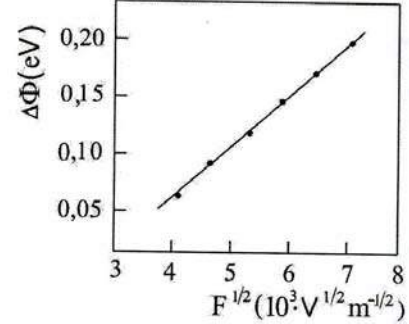


Fig. 4. The dependence of the barrier lowering $\Delta\Phi$ on $F^{1/2}$ for Ag/VPc/Ag structure.

The dependences of the conductivity σ on F in Frenkel coordinates for two temperatures are given in the Fig. 5. In a weak electric field σ does not depend on F (section ab) and $\sigma = 4 \cdot 10^{-9} \text{ }\Omega^{-1} \cdot \text{m}^{-1}$ at $T = 298 \text{ K}$. Further, with the increase of F in an interval of the several orders the conductivity grows according the law $\sigma \propto \exp F^{1/2}$ (section cd), and the inclinations of straight lines decreases with increasing of the temperature. On this section σ varies according to expression:

$$\sigma \sim \exp \left(- \frac{E_0 - e\beta F^{1/2}}{kT} \right)$$

From the inclination of straight lines on a section cd we find, that $\beta = 5.1 \cdot 10^{-5} \text{ V}^{1/2} \text{ m}^{1/2}$ (at $T = 298 \text{ K}$) and $\beta = 5.5 \cdot 10^{-5} \text{ V}^{1/2} \text{ m}^{1/2}$ (at $T = 403 \text{ K}$).

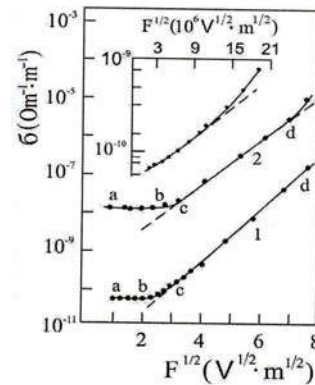


Fig. 5. Dependence of the electrical conductivity σ on $F^{1/2}$ at 298 K (1) and 403 K (2). Insert – the dependence of σ on F at 298 K.

From the theory follows, that Frenkel-Poole constant depends on the dielectric permeability ϵ and is determined from the formula [12]:

$$\beta_T = (e^3 / \pi \epsilon \epsilon_0)^{1/2} \quad (3)$$

From the dependence of capacity of structure C on d^{-1} was found, that $\varepsilon = 3.4$ for VPc (fig. 1, insert), and from the formula (3) it is obtained $\beta = 4.12 \cdot 10^{-5} \text{ V}^{1/2} \text{ m}^{1/2}$, that are in good accordance with the values found experimentally from the dependences $\Delta\Phi$ and σ on $F^{1/2}$. The ratio of the values β and β_T , experimentally determined by various ways is within the limits of 1.03-1.3.

In the σ versus $F^{1/2}$ curves a section bc (fig. 5) is observed which is narrowed with the growth of the temperature. It has appeared, that on this section σ obeys the law $\sigma \propto \exp F$. The thermally assisted field ionization, which passes to $\lg \sigma \propto F$ at rather low fields and to $\lg \sigma \propto F^{1/2}$ at high ones, is theoretically analyzed elsewhere [10]. Hence, in VPc are realized the conditions, required for the observation of such emission, and in a section bc the field dependence of conductivity is described as [10]:

$$\sigma \sim \exp \left(- \frac{E_0 - \frac{1}{2} e r F}{\kappa T} \right), \quad (4)$$

where r - distance between two next charged traps. As it is seen, at low temperatures and high fields, when density of the charged traps too large, Coulomb potentials are overlapped and a barrier lowering becomes proportional to F . From the

expression $r = \sqrt{\frac{e}{4\pi\epsilon\epsilon_0 F}}$ we find, that the traps with

$E_0 = 0.56 \text{ eV}$ are separated by 76 \AA and have concentration $2 \cdot 10^{24} \text{ m}^{-3}$. Depending on films evaporation conditions, when density of acceptors in VPc exceeds 10^{24} m^{-3} , the modified Frenkel-Poole effect becomes prevailing.

- | | |
|---|--|
| [1] C. Hamann. Phys. stat. sol., 1968, V. 26, No.1, p. 311. | [8] M. Lampert, P. Mark. Injection currents in solids. Moscow. "Mir" Publishing House, 1973 (in Russian). |
| [2] Sussman. J. Appl. Phys., 1967, V. 38, No.7, p. 2738. | [9] G. Hamann. Phys. Stat. Sol. 1968, V. 26, No.1, p. 311. |
| [3] A.P. Martynenko. Phthalocyanines - perspective materials for microelectronics. Moscow. CSRI «Electronics». 1982 (in Russian). | [10] M. Burgelman. Thin Solid Films. 1980, No.1, V.70. p. 1. |
| [4] M.I. Fedorov, V.A. Benderskiy. FTP, 1970, V.4, No. 7, p.1403 (in Russian). | [11] G.S. Nadkarny, J.G. Simmons. Appl. Phys, 1976, V.47, No.1. p.114. |
| [5] Yu. A. Vidadi., K.Sh. Kocharli, B.Sh. Barkhalov, S.A. Sadraddinov. Phys.Stat.Sol. (a), 1976, V.34, No.1, K 77. | [12] J.G. Simmons. The current flow through thin dielectric films. In: Thin Film Technology, Moscow, "Soviet radio" Publishing House, 1977, p. 375 (in Russian). |
| [6] Fu-Ren-pen, H.B. Faulkner. J. Chem. Phys., 1978, V. 68, No.7, p. 3334. | [13] F. Gutman, L. Lyons. Organic semiconductors, Moscow, 1970, p. 537 (in Russian). |
| [7] B.Sh. Barkhalov, Yu. A. Vidadi. Thin Solid Films, 1970, V. 40, No.2, p. 45. | |

M.M. Pənahov, S.A. Sədrəddinov, C.H. Cabbarov, B.Ş. Barxalov

ÜZVİ YARIMKEÇİRİCİ VANADIUM FTALOSİYANİN ƏSASINDA NAZİK TƏBƏQƏLİ STRUKTURLARDA ELEKTRİKKEÇİRİCİLİYİNİN MEXANİZMİ

Üzvi yarımkəçirici vanadium ftalosiyanın əsasında metal-yarımkəçirici-metal (MYM) strukturlarının volt-ampere və volt-tutum xarakteristikaları tədqiq olunmuşdur. Müəyyən edilmişdir ki, MYM- strukturunda yüksək müqavimətə malik potensial çəpərlərin mövcud olmadığı halda, sistemdə müşahidə olunan qeyri-xətli VAX tutma mərkəzlərində olan yükdaşıyıcıların istiliyin təsiri altında, elektrik sahəsinin dəstəyi ilə güclənən azad olunması ilə (Pul-Frenkel effekti) bağlıdır. Göstərilmişdir ki, alçaq temperaturalarda və yüksək elektrik sahələrində ($F > 10^7 \text{ V/m}$), yüklənmiş tutma mərkəzlərinin sıxlığı kifayət qədər böyük olduğu halda ($n > 10^{24} \text{ m}^{-3}$), Kulon potensialları bir-birini örtür, potensial çəpərin alçalması elektrik sahəsinin intensivliyi ilə düz mütənasib olur və modifikasiya olunmuş Frenkel-Pul effekti üstünlük təşkil etməyə başlayır.

M.M. Панахов, С.А. Садрадинов, Дж. Г. Джаббаров, Б.Ш. Бархалов

МЕХАНИЗМ ЭЛЕКТРОПРОВОДНОСТИ В ТОНКОПЛЕНОЧНОЙ СТРУКТУРЕ НА ОСНОВЕ ОРГАНИЧЕСКОГО ПОЛУПРОВОДНИКА ФТАЛОЦИАНИНА ВАНАДИЯ

Исследованы вольт-амперные и вольт-емкостные характеристики структур металл-полупроводник-металл (МПМ) на основе органического полупроводника фталоцианина ванадия. Установлено, что при отсутствии в МПМ-структуре межповерхностных потенциальных барьеров с высоким сопротивлением, наблюдаемые нелинейные ВАХ связаны с термическим высвобождением носителей заряда из центров захвата, облегченным электрическим полем (эффект Пула-Френкеля). Выявлено, что при низких температурах и высоких электрических полях ($F > 10^7 \text{ В/м}$), когда плотность заряженных ловушек достаточно высока ($N_t > 10^{24} \text{ м}^{-3}$), кулоновские потенциалы перекрываются, понижение барьера становится пропорциональным полю и начинает преобладать модифицированный эффект Френкеля-Пула.

Received: 20.07.05

MnIn₂S₄ və MnGaInS₄ MONOKRİSTALLARINDA TERMOSTİMULLAŞMIŞ DEPOLYARİZASIYA CƏRƏYANLARI

N.N.NİFTİYEV

Azərbaycan Dövlət Pedaqoji Universiteti, Az1000, Bakı, Ü.Hacıbəyov, 34

O.B.TAĞIYEV

AMEA Fizika institutu, Az.1143, Bakı, H.Cavid, 33

MnIn₂S₄ və MnGaInS₄ monokristallarında müxtəlif polarizasiya gərginliklərində termostimullaşmış depolyarizasiya cərəyanları tədqiq edilmişdir. Sürətli yapışma səviyyələrinin mövcudluğu aşkara çıxarılmışdır. Bu monokristallarda tələlərin yerləşmə dərinliyi, konsentrasiyası və tutulma en kəsikləri təyin edilmişdir.

Yarımkeçirici və dielektriklərdə yapışma səviyyələrinin parametrlərini tədqiq etmək üçün istifadə olunan üsullardan biri termostimullaşmış depolyarizasiya metodudur.

Bu işdə MnIn₂S₄ və MnGaInS₄ monokristallarında müxtəlif polarizasiya gərginliklərində termostimullaşmış depolyarizasiya cərəyanlarının (TD C) tədqiqi nəticələri verilmişdir.

MnIn₂S₄ monokristal kimiyyəvi köçürmə metodu ilə alınmışdır. Rentgenquruluş analiz göstərdi ki, MnIn₂S₄ kubik quruluşa malik olub (*f.q.Fd 3m*), qəfəs sabiti $a=10,71\text{Å}$ –*a* bərabərdir[1]. MnGaInS₄ monokristal Bricmen metodu ilə alınmışdır. Rentgenoqrafik tədqiqatlar göstərir ki, MnGaInS₄ monokristal qəfəs sabitləri $a=3,81$; $C=12,17\text{Å}$; $z=1$, *f.q. p3m1* olan ZnIn₂S₄ birpaketli yarımtp quruluşunda kristallaşır [2].

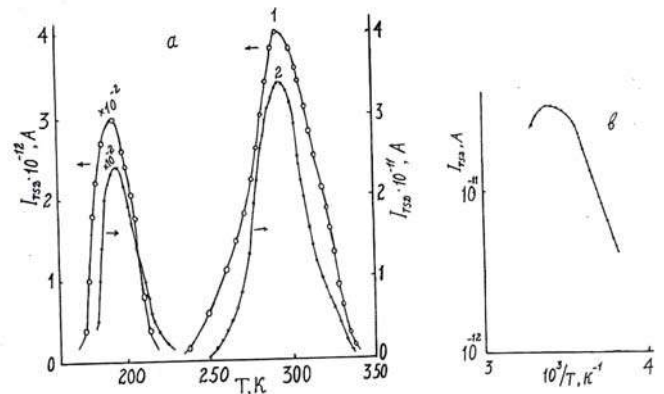
MnIn₂S₄ monokristal kimiyyəvi köçürmə metodu ilə alınmışdır. Rentgenquruluş analiz göstərdi ki, MnIn₂S₄ kubik quruluşa malik olub (*f.q.Fd 3m*) və qəfəs sabiti $a=10,71\text{Å}$ –*a* bərabərdir [1]. MnGaInS₄ monokristal Bricmen metodu ilə alınmışdır. Rentgenoqrafik tədqiqatlar göstərir ki, MnGaInS₄ monokristal qəfəs sabitləri $a=3,81$; $C=12,17\text{Å}$; $z=1$, *f.q. p3m1* olan ZnIn₂S₄ birpaketli yarımtp strukturuna kristallaşır [2].

MnIn₂S₄ və MnGaInS₄ monokristallarında TSD-nin ölçülməsi zamanı nümunədə qabaqcadan həyəcanlandırma müəyyən temperaturda (140÷400K) VAX-ın *q/* xətti oblastında gərginliyin tətbiqi ilə 10 dəqiqə ərzində həyata keçirilir. Sonra gərginliyi ayırmadan nümunə 140K temperatara kimi soyudulur. Bu temperatara çatdıqdan sonra gərginliyi ayırırlar və nümunə qısa qapanır. 1-5 dəqiqə keçdikdən sonra nümunə sabit sürətlə 400K temperatara qədər qızdırılır və eyni vaxtda xarici dövredə cərəyan ölçülür. Nümunənin qızdırılma sürəti $b=0.07\div0.6$ dər/san intervalında dəyişdirilir.

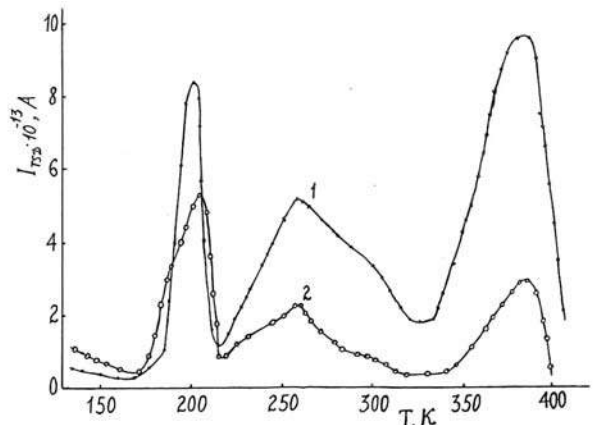
Şəkil 1a–da MnIn₂S₄ monokristal üçün müxtəlif polarizasiya gərginliklərində TSD əyriləri göstərilmişdir. Nümunəyə gərginlik VAX-ın *q/* xətti oblastında 340K temperatarda tətbiq edilmiş və bu gərginlik altında nümunə 160K temperatara kimi soyudulmuşdur. MnIn₂S₄ monokristalında TDC spektrində müxtəlif temperaturu iki maksimum aşkara çıxarılmışdır. Polarizasiya gərginliyi artdıqca TDC maksimumunu yüksək temperatur oblastına doğru sürüşür və TDC-nin qiyməti artır.

Şəkil 2-də MnGaInS₄ monokristal üçün 2 müxtəlif polarizasiya gərginliklərində TDC əyriləri verilmişdir.

Nümunəyə gərginlik VAX-ın *q/*xətti oblastına uyğun 400K temperatarda tətbiq edilmiş və bu gərginlik altında nümunə 140K temperatara kimi soyudulmuşdur. MnGaInS₄ monokristalında 400V polarizasiya gərginliyinə uyğun TDC spektrində temperatur maksimumları 202, 260 və 383 K olan üç pik müşahidə edilmişdir. Polarizasiya gərginliyi artdıqca cərəyan maksimumuna uyğun temperatur yüksək temperatur oblastına doğru sürüşür.



Şəkil 1. a) 340K polarizasiya temperaturunda və polyarizasiya gərginliyinin müxtəlif qiymətlərində TSD əyriləri (U, V); 1-300; 2-500
b) 500 V polarizasiya gərginliyində 294 K temperatara uyğun TSD cərəyan pikinin başlanğıc hissəsinin temperaturdan asılılığı.



Şəkil 2. 400K polarizasiya temperaturunda və polarizasiya gərginliyinin müxtəlif qiymətlərində TSD əyriləri (U, V); 1-400; 2-500

TDC əyrilərinin analizi üçün yapışma səviyyələrinin növünü bilmək lazımdır. Bildiyimiz kimi yapışma səviyyələrinin növünü bilmək üçün « δ » kəmiyyətindən istifadə olunur və « δ » aşağıdakı ifadədə tapılır.

$$\delta = \frac{T_2 - T_M}{T_2 - T_1}$$

Burada T_M -TSD-nin maksimumuna uyğun temperatur, T_1 və T_2 – TCD-nin maksimum intensivliyinin yarısına uyğun aşağı və yuxarı temperaturlardır. TCD maksimumlarının formalarının analizi göstərir ki, MnIn₂S₄ və MnGaInS₄ monokristalları üçün müşahidə edilən bütün maksimumlarda

$$\delta \geq e^{-1} \left(1 + \frac{2kT_M}{E_t} \right)$$

şərti ödənilir [3]. Bu şərtin ödənilməsi sürətli yapışma səviyyələrinin mövcudluğunu göstərir.

Şəkil 1b-də MnIn₂S₄ monokristalı üçün 500V polarizasiya gərginliyində 294K temperatura uyğun TDC cərəyan pikinin başlanğıc hissəsinin temperaturdan asılılıq əyrisi $\sim 10^3/T$ miqyasında göstərilmişdir. Bu əyridən tələlərin enerji səviyyəsi hesablanmışdır və $E_t=0,60\text{eV}$ [4].

MnIn₂S₄ və MnGaInS₄ monokristalları üçün tələlərin yerləşmə dərinliyi TDC-dən cərəyanın başlanğıc artımı hissəsinin temperaturdan asılılığından (Qarlik-Qibson metodu) [5], Byub metodundan [6] və TSD cərəyanı piklərinin formasından asılı olan düsturlardan [7,8], təyin edilmişdir. Aşqar tələlərin konsentrasiyası və tutulma en kəskinliyi aşağıdakı düsturlardan təyin edilir:

$$N_t = \frac{j_M N_s K T_M^2}{\alpha \tau E_t b} \quad S_t = \frac{b j_M E_t}{2 \alpha N_s g_i K^2 T_M^3} \exp \left(\frac{2 E_t}{K T_M} \right)$$

Burada: j_M – TDC maksimumuna uyğun cərəyan, b-qızdırılma sürəti, N_s – keçirici zonada hal sıxlığı, g_i – sərbəst elektronların istilik sürəti, K – Bolsman sabiti-dir. $\ln j \sim 1/T$ koordinatında j əyrinin düz xətt hissəsinin yüksək temperatur oblastında ekstrapolyasiyası nəticəsində ordinat oxundan α parçasını ayırır.

Yuxarıda göstərdiyimiz metodların köməyi ilə hesablamalar nəticəsində MnIn₂S₄ monokristalında lokal səviyyələrin parametrləri üçün aşağıdakı qiymətlər alınmışdır.

$$\begin{array}{ll} E_{t1}=0,38 \pm 0,02 \text{ eV} & E_{t2}=0,59 \pm 0,02 \text{ eV;} \\ N_{t1}=2,6 \times 10^{13} \text{ sm}^{-3} & N_{t2}=5,2 \times 10^{15} \text{ sm}^{-3} \\ S_{t1}=1,7 \times 10^{-17} \text{ sm}^2 & S_{t2}=2,3 \times 10^{-17} \text{ sm}^2 \end{array}$$

MnGaInS₄ monokristalı üçün isə lokal səviyyələrin parametrlərinin orta qiymətləri aşağıdakı kimidir.

$$\begin{array}{ll} E_{t1}=0,39 \pm 0,02 \text{ eV} & E_{t2}=0,50 \pm 0,02 \text{ eV;} \\ E_{t3}=0,70 \pm 0,02 \text{ eV} & N_{t1}=2,5 \times 10^{14} \text{ sm}^{-3} \\ N_{t2}=4 \times 10^{18} \text{ sm}^{-3} & N_{t3}=0,9 \times 10^{14} \text{ sm}^{-3} \\ S_{t1}=2,9 \times 10^{-17} \text{ sm}^2 & S_{t2}=8,5 \times 10^{-14} \text{ sm}^2 \end{array}$$

$$S_{t3}=2,4 \times 10^{-18} \text{ sm}^2$$

Beləliklə, MnIn₂S₄ və MnGaInS₄ monokristallarında müxtəlif polarizasiya gərginliklərində termostimullaşmış depolyarizasiya cərəyanları tədqiq edilmişdir. Sürətli yapışma səviyyələrinin mövcudluğu aşkara çıxarılmışdır. Bu monokristallarda tələlərin yerləşmə dərinliyi, konsentrasiyası və tutulma en kəskinliyi təyin edilmişdir.

- | | |
|--|--|
| [1] T. Kanamoto, H. Ido H., T. Kaneko. J.Phys. Japan, 1973, v.34, №2, p.554. | [6] R. Byub. Fotoprovodimost tverdx tel. M: Mir, 1960, 558 s. |
| [2] C. Batistony, L. Gastaldi, Q. Mattogno et.al. Solid State Commun., 1987, v.61, №1, p.43-46 | [7] Ə.A.Pyasta. K teorii krivix termostimulirovannoqo vozbujdeniya. Mikroelektronika, 1974, T.3, №1, s.178-180 |
| [3] P.Q. Litevçenko, V.İ. Ustinov. Aktualniye voprosi fiziki poluprovodnikovix priborov. Vilnyus, Mokslas, 1960, s.153 | [8] Q.A. Bordovskiy. Termostimulirovanniye toki kak metod opredeleniya parametrov lovuxek. Fotoprovodyaşşiyeye okislı svintsı. 1976, s.87-110. |
| [4] Yu.A.Qoroxovatskiy. Osnovi termodepolarizatsionnoqo analiza, M.: Nauka, 1981, 176 s. | |
| [5] F. Garlic, A.F. Gibson. Proc. Phys. Soc., 1948, A60, P.6, №342, p.574-590. | |

N.N. Niftiyev, O.B. Tagiyev

CURRENTS OF THERMOSTIMULATED DEPOLARIZATION IN MnIn₂S₄ AND MnGaInS₄ SINGLE CRYSTALS

The currents of thermostimulated depolarization in single crystals MnIn₂S₄ and MnGaInS₄ at the different polarizing voltage. The presence of quick capture levels are revealed. The depth levels, concentration and capture cross-sections are obtained.

Н.Н. Нифтиев, О.Б. Тагиев

ТОКИ ТЕРМОСТИМУЛИРОВАННОЙ ДЕПОЛЯРИЗАЦИИ В МОНОКРИСТАЛЛАХ

MnIn₂S₄ и MnGaInS₄

Исследованы токи терmostимулированной деполяризации в микрокристаллах MnIn₂S₄ и MnGaInS₄ при различных поляризующих напряжениях. Выявлено наличие быстрых уровней прилипания. Определены глубины залегания уровней, концентрация и сечения захвата ловушек.

Received: 15.09.05

SIXILMIŞ QAZLARIN VƏ MAYELƏRİN İSTİLİKKEÇİRMƏSİNİN TERMİKİ TƏZYİQDƏN ASILILIĞININ NƏZƏRİ TƏDQIQI

C.Y. NAZİYEV

*Azərbaycan Dövlət Neft Akademiyası
Bakı Az. 1007, Azadlıq pr.20.*

Məqalədə maye və qazlar üçün molekulyar – kinetik nəzəriyyə əsasında istilikkeçirmənin termiki təzyiqdən asılılığı baxılır və bundan ötrü hesabət tənliyi çıxarılır.

Təcrübə yolu ilə istilik-fiziki xassələrin öyrənilməsi əlbəttə ən etibarlı üsuldur. Lakin bu həmişə mümkün olmur. Bunun üçün zəngin texniki baza və kifayət qədər maliyyə vəsaiti olmalıdır. Bu səbəbdən maye və qazların xassələrinin oxşarlıq metodu ilə hesablanması, onların proqnozlaşdırılması, nəzəri və yarımnezəri yolla təyin edilməsinin xüsusi əhəmiyyəti var.

Xüsusiən sıxılmış qazlar və mayelərin istilikkeçirməsinin təzyiqdən asılılığını verən tənliyin alınması maraqlıdır [1].

Mayelərin nəzəriyyəsi qaz və bərk kristal maddələrin nəzəriyyəsinə nisbətən az inkişaf etmişdir. Bu səbəbdən onların köçürmə xassələrini öyrəndikdə müəyyən yaxınlaşma metodlarından istifadə edilir: bərk maddə və maye quruluşlarının oxşarlığından; statistik mexanikanın dürüst metodlarından və s. [2-4]. Bizi maraqlandıran maye nəzəriyyəsinə baxaq.

Kinetik nəzəriyyəyə aid olan Enskoq metodunda diametri d olan bərk sferik molekulaların yalnız cüt toqquşmaları baxılır və onların ölçülərinin son qiyməti qəbul edilir. Bu baxımdan Enskoq [5-6] sıxılmış qazın istilikkeçirməsini hesablamaq üçün belə ifadə alır:

$$\lambda = \lambda^0 b \rho \left(\frac{1}{b \rho \xi} + \frac{6}{5} + 0,7574 b \rho \xi \right). \quad (1)$$

Bir molekulun o biri molekul yanında olmasının ehtimalını səciyyələndirən əmsal ξ belə tapılır

$$\rho = k \frac{NT}{v} (1 + b \rho \xi), \quad (2)$$

$$b \rho = \frac{2}{3} \pi \frac{N}{v} d^3, \quad (3)$$

$$kN = R, \quad (4)$$

burada N – 1q. qazda molekulaların sayı; k – Bolsman sabiti; v – xüsusi həcm, b – 1q. qazda molekulaların dörd qat həcmi; R – qaz sabiti; ρ – sıxlıqdır.

Seyrəkləşdirilmiş qaz üçün

$$\lambda^0 = \frac{1981,1 (T/M)^{0,5}}{d^2 \cdot \Omega^{(2,2)} \cdot T^*}, \quad (5)$$

haradakı $T^* = kT/\varepsilon$ – gətirilmiş temperatur; $\Omega^{(2,2)}$ – toqquşma integralı; M – molekulyar kütlə; ε – potensial enerjinin minimum qiymətidir.

(1) tənliyinin dəqiqliyini artırmaq üçün sonralar təzyiq p əvəzinə (2) ifadəsində termiki təzyiq $P_t = T(\partial P / \partial T)_\rho$ işlədilmişdir [3,6]. Deməli

$$P_t = P + \alpha \rho^2 = \frac{R_\mu T \rho}{M} (1 + b \rho \xi), \quad (6)$$

burada R_μ – universal qaz sabitidir.

Yüksək temperaturlu qazlardan ötrü Enskoq tənliyində $b = b(T)$ korrelyasiya götürülməsi əhəmiyyətlidir. Bununla belə (1) tənliyi alçaq temperaturlu mayelər üçün xəta verir.

Qeyd etmək lazımdır ki, Enskoq tənliyi sıxılmış qazlar və mayelər üçün istilikkeçirmənin təzyiq və temperaturdan asılılığını keyfiyyətə düzgün göstərir. Bu bizə əsas verir ki, Enskoq tənliyi bazasında daha dəqiq olan və praktiki əhəmiyyət daşıyan yeni tənlik alaçaq.

(1) tənliyində $b \rho \xi$ kompleks kəmiyyəti (6) ifadəsindən təyin etmək məqsəduyğundur:

$$1 + b \rho \xi = \frac{M}{R_\mu \rho} \left(\frac{\partial P}{\partial T} \right)_\rho \quad (6a)$$

Bu qiyməti (1) tənliyində yerinə yazsaq alarıq

$$\lambda = \lambda^0 \frac{1 + 0,4426 b \rho \xi}{\xi} + 0,7574 \frac{M b}{R_\mu} \left(\frac{\partial P}{\partial T} \right)_\rho \lambda^0. \quad (7)$$

Molekulyar – kinetik nəzəriyyəyə görə seyrəkləşmiş qazlar üçün

$$\lambda^0 = \varepsilon \gamma \rho \bar{c} l C, \quad (8)$$

harada ki, γ – özlülük üçün sabit, \bar{c} – molekulun orta sürəti, l – molekulun orta qaçış uzunluğu, C_v – izoxor istilik tutumu, ε – əmsaldır (Eyken əmsalı). Burada sabit $\varepsilon \gamma = E$ temperaturdan asılı olacaq.

Bildiyimiz kimi

$$l = \frac{3v}{4\pi Nd_t^2}; \quad b = \frac{4}{3}\pi \frac{N}{2} d_{p,t}^3.$$

Onda

$$\lambda^0 b = \frac{E}{2} \bar{c} C_v D_p d_{p,t} \quad (9)$$

burada d_t – temperaturdan asılılığı nəzərə alan molekulun diametri; $d_{p,t}$ – həm temperatur, həm də təzyiqin təsirini nəzərə alan molekulun diametridir:

$$d_{p,t}^2 = D_p d_t^2.$$

(9) ifadəsini və $\bar{c} = \sqrt{3R_\mu T / M}$ - i nəzərə alsaq (7)

tənliyindən yaza bilərik

$$\lambda = 0,7574 \sqrt{\frac{3MT}{4R_\mu}} EC_v D_p d_{p,t} \left(\frac{\partial P}{\partial T} \right)_\rho + \lambda^0 \frac{1+0,4426b\rho\xi}{\xi} \quad (10)$$

Qəbul etsək ki,

$$A_\lambda = 0,7574 \sqrt{\frac{3MT}{4R_\mu}} EC_v D_p d_{p,t},$$

olar. Burada $A_\lambda = f(P, T)$ və ya $A_\lambda = f(\rho)$.

Hesablama göstərir ki, A_λ -nin sıxlıqdan asılılığı çox zəifdir və məhdud sıxlıq intervalında onu sabit qəbul etmək olar. (11) ifadəsində əmsal ξ çox böyük olmayan sıxlıqlarda belə şəkil ola bilər:

onda

$$\xi = 1 + 0,645b\rho + 0,287b^2\rho^2 + \dots \quad (12)$$

$$\lambda = A_\lambda \left(\frac{\partial P}{\partial T} \right)_\rho + \lambda^0 \frac{1+0,4426b\rho\xi}{\xi} \quad (11)$$

Bu qiyməti (11)-də yerinə yazsaq alarıq:

$$\lambda = \lambda^0 \frac{1+0,4426b\rho+0,2855b^2\rho^2+\dots}{1+0,645b\rho+0,287b^2\rho^2+\dots} + A_\lambda \left(\frac{\partial P}{\partial T} \right)_\rho. \quad (13)$$

Aşağı sıxlıqlarda (13) ifadəsi belə forma alır:

$$\lambda = \lambda^0 + A_\lambda \left(\frac{\partial P}{\partial T} \right)_\rho \quad (14)$$

çünki $\lim_{\rho \rightarrow 0} \beta_\lambda = 1$, burada

$$\beta_\lambda = \frac{1+0,4426b\rho+\dots}{1+0,645b\rho+\dots} \quad (15)$$

Onda ümumi şəkildə yaza bilərik

$$\lambda = \beta_\lambda \lambda^0 + A_\lambda \left(\frac{\partial P}{\partial T} \right)_\rho, \quad (16)$$

yüksək təzyiqlərdə $\beta_\lambda = f(\rho)$ olmalıdır. Belə çıxır ki, böyük təzyiqlərdə β_λ - nin sıxlıqdan asılılığını götürməliyik və

deməli $\left(\frac{\partial P}{\partial T} \right)_\rho = f(\rho)$ olduğundan

$$\beta_\lambda = f \left[\left(\frac{\partial P}{\partial T} \right)_\rho \right] \quad (17)$$

(17) – yə uyğun olaraq (15) ifadəsini belə yazmaq əlverişlidir

$$\beta_\lambda = 1 + \varphi \left[\left(\frac{\partial P}{\partial T} \right)_\rho \right]. \quad (18)$$

Onda (16) tənliyinə aşağıdakı şəkili vermək olar

$$\lambda = \lambda^0 = a_\lambda \left(\frac{\partial P}{\partial T} \right)_\rho^n, \quad (19)$$

haradakı $a_\lambda = f(\rho)$ və $n = f(\rho)$ funksiyaları ρ -dan zəif asılıdırlar. Geniş olmayan sıxlıqlar intervalllarında onları sabit qəbul etmək mümkündür.

Termodinamik funksiyaları termiki təzyiqlə ifadə etsək

$$P_t = T \left(\frac{\partial P}{\partial T} \right)_\rho \text{ alarıq}$$

$$\lambda - \lambda^0 = a_\lambda \left(\frac{P_t}{T} \right)^n \quad (20)$$

Termiki təzyiq molekulun istilik hərəkətilə yaranır. Termiki təzyiqi təyin etmək üçün aşağıdakı düsturdan istifadə etmək əlverişlidir

alınar.

$$P_t = -T \left[\left(\frac{\partial V}{\partial T} \right)_p \right] / \left(\frac{\partial V}{\partial P} \right)_T \quad (21) \quad \lambda - \lambda^0 = 1,23 \cdot 10^{-5} \left(\frac{\partial \pi}{\partial \tau} \right)_\omega^{7/8}, \quad \frac{kal}{sm \cdot san \cdot dər}, \quad (23)$$

Bu təzyiqi real qazların hal tənliklərindən hesabla-
maq olar. Məsələn Van-der-Vaalsın hal tənliyindən alı-
nır:

$$P_t = P + a\rho^2. \quad (22)$$

(19) asılılığından izafi istilikkeçirməni $(\lambda - \lambda^0)$
hesablamaq olar. Mizik və Todos [7] (19) tənliyini
metanın istilikkeçirməsinə tətbiq etmiş və yaxşı nəticə
almışdır.

Onlar metan üçün gətirilmiş parametrlərdə belə
asılılıq almışlar

tənlik $\left(\frac{\partial \pi}{\partial \tau} \right)_\omega \geq 1,00$ hallar üçün alınıb.

Burada π , τ , ω - uyğun olaraq gətirilmiş təzyiq,
temperatur və sıxlıqdır: $\pi = p/p_k$, $\tau = T/T_k$, $\omega = \rho/\rho_k$.

Qeyd etmək lazımdır ki, Mizik və Todos (19) tənliyini
empirik formada istifadə etmişlər.

(23) tənliyi loqarifmik koordinat sistemində düz xətt
verir və ona görə α_λ və n sabitlərinin tapılması asanlaşır.

[6] işdə propilenin istilikkeçirməsinin tənliyi verilib.
Burada bir-birindən az fərqlənən iki ayrı-ayrı tənlik alınır:

$$\lambda - \lambda^0 = 3,35 \cdot 10^{-2} \left(\frac{P_t}{T} \right)^{0,995}, \quad \frac{V_t}{m \cdot k}, \quad \frac{P_t}{T} < 0,302 - \text{də} \quad (24)$$

və

$$\lambda - \lambda^0 = 2,88 \cdot 10^{-2} \left(\frac{P_t}{T} \right)^{0,857}, \quad \frac{P_t}{T} > 0,302 - \text{də} \quad (25)$$

Beləliklə istilikkeçirmənin termiki təzyiqdən asılılığını verən (19) tənliyi praktiki işlənmək üçün çox əlverişlidir.

- | | |
|---|--|
| <p>[1] L.P. Filippov. O sostoëni i zadaçax issledovaniy teploprovodnosti qazov i jidkostey V kn. «Teplofizixeskiye svoystva veshestv i materialov» M.: İzd. Standartov. 1978, vip.13, s.77-86.</p> <p>[2] D. Qirşfelğder, İ. Kertiss, R. Berd. Molekulərnə te-
oriə qazov i cidkostey. M.: İL. 1961, 934s.</p> <p>[3] K. Krokston. Fizike cidkoqo sostoëniə. Statistiçes-
koye vvedenie. M.: Mir. 1978, 400s.</p> <p>[4] Fizika prostix jidkostey: Statistiçeskaya teoriya.
Pod red. Q.Temperli, Dc.Roulinsona, Dc. Raşbru-
ka. M.: 1971, 308s.</p> | <p>[5] S. Çepmen, T. Koulinq. Matematixeskə teoriə
neodnorodnix qazov. M.: İL. 1960, 510s.</p> <p>[6] Ə.M. Naziev. İssledovanie teploprovodnosti uqle-
vodorodov pri visokix davleniəx i nekotorie oso-
bennosti metodov ee izmereniə. Avtoref.diss.
...dokt.texn.nauk. M.: GNIIN. 1970, 52s.</p> <p>[7] D. Misic, G. Thodos. Physica. 1966. vol.32, №5.</p> |
|---|--|

J.Y. Naziyev

THEORETICAL RESEARCH OF THE DEPENDENCE OF THERMAL CONDUCTIVITY OF COMPRESSED GASES AND LIQUIDS ON THERMAL PRESSURE

On the base of molecular – kinetic theory of compressed gases the dependence of excessive thermal conductivity on thermal pressure is considered in this paper. Theoretical equation for calculation of thermal conductivity at high pressures is obtained.

Дж.Я. Назиев

ТЕОРЕТИЧЕСКОЕ ИССЛЕДОВАНИЕ ЗАВИСИМОСТИ ТЕПЛОПРОВОДНОСТИ СЖАТЫХ ГАЗОВ И ЖИДКОСТЕЙ ОТ ТЕРМИЧЕСКОГО ДАВЛЕНИЯ

На основе молекулярно – кинетической теории сжатых газов в статье рассматривается зависимость избыточной теплопроводности от термического давления. Получено теоретическое уравнение для вычисления теплопроводности при высоких давлениях.

Received: 16.06.05

LAX PAIR PRESENTATION OF WZNW MODEL

M.A. MUKHTAROV

*Institute of Mathematics and Mechanics
370602, Baku, F.Agaev str. 9, Azerbaijan*

One dimensional WZNW model obtained as a reduction of self-dual Yang-Mills equations has been presented in the normal Lax pair form.

1. The problem of constructing of the solutions of self-dual Yang-Mills (SDYM) model and its dimensional reductions, the one dimensional WZNW model in our case, in the explicit form for arbitrary semisimple Lie algebra, rank of which is greater than two, remains important for the present time. The interest arises from the fact that almost all integrable models in one, two and (1+2)-dimensions are symmetry reductions of SDYM or they can be obtained from it by imposing the constraints on Yang-Mills potentials [1-12].

This work is a direct continuation of [11], where the exact solutions have been derived with the use of Riemann Hilbert

Problem formalism. The aim is to apply to this problem the discrete symmetry transformation method [12] that allows generating new solutions from the old ones in much more easier way than applying methods from [11]. The Lax pair presentation of the model under consideration is the first step in this program that we hope will give us a key to construct solutions for an arbitrary semisimple algebra.

2. The one dimensional reduction of self duality equations obtained in [11] are the equations for the element f , taking values in the semisimple algebra,

$$\frac{\partial^2 f}{\partial r^2} + 2 \frac{\partial f}{\partial r} - [H, [H, f]] - 2[X^-, [X^+, f]] - 2[X^+, [X^-, f]] + 2\left[\frac{\partial}{\partial r} - H, f\right], [X^+, f] = 0 \quad (1)$$

Here H, X^\pm are generators of $A_1(SL(2, C))$ algebra

$$[X^+, X^-] = H, [H, X^\pm] = \pm 2X^\pm$$

embedded to gauge algebra in the half-integer way.

Let's rewrite (1) in the equivalent form:

$$\left[\frac{1}{2}\left(\frac{\partial}{\partial r} + H\right) - [X^+, f], -\frac{1}{2}\left[\frac{\partial}{\partial r} - H, f\right] + X^-\right] - \frac{1}{2}\left[\frac{\partial}{\partial r} - H, f\right] + X^- = 0$$

This equation after changing the variable $t = \ln r$ has the following form

$$\left[\frac{\partial}{\partial t} + \frac{1}{2}H - [X^+, f], -\frac{\partial f}{\partial t} + \frac{1}{2}[H, f] + X^-\right] - \frac{\partial f}{\partial t} + \frac{1}{2}[H, f] + X^- = 0 \quad (2)$$

Introducing the notation

$$\tilde{F} = e^{\frac{1}{2}Ht} \left(-\frac{\partial f}{\partial t} + \frac{1}{2}[H, f] + X^-\right) e^{-\frac{1}{2}Ht}, \quad (3)$$

multiplying (2) from the left side by $e^{\frac{1}{2}Ht}$ and from the right side by $e^{-\frac{1}{2}Ht}$, we obtain

$$\frac{\partial \tilde{F}}{\partial t} - [[e^{\frac{1}{2}Ht} X^+ e^{-\frac{1}{2}Ht}, e^{\frac{1}{2}Ht} f e^{-\frac{1}{2}Ht}], \tilde{F}] + \tilde{F} = 0$$

Due to the evident equality

$$e^{\frac{1}{2}Ht} X^+ e^{-\frac{1}{2}Ht} = e^t X^+$$

the last equation can be rewritten in a form

$$\frac{\partial \tilde{F}}{\partial t} - e^t [[X^+, \tilde{f}], \tilde{F}] + \tilde{F} = 0, \quad (4)$$

where $\tilde{f} = e^{\frac{1}{2}Ht} f e^{-\frac{1}{2}Ht}$.

In terms of these notations we have from (3) the following expression

$$\tilde{F} = -\frac{\partial \tilde{f}}{\partial t} + [H, \tilde{f}] + X^- e^{-t} = 0$$

Let's introduce the notation

$$F = e^t \tilde{F} = -e^t \frac{\partial \tilde{f}}{\partial t} + e^t [H, \tilde{f}] + X^- = 0$$

Then (4) has a form

$$\frac{\partial F}{\partial t} + [A, F] = 0, \quad (5)$$

where $A = -e^t [X^+, \tilde{f}]$.

The equation (5) is one-dimensional evolution equation defined by Lax pair operators and it is one of the principal criteria of equations integrability.

3. From the presentation (5) it is followed that

$$\frac{\partial}{\partial t} spF^n = 0, \text{ for } \forall n$$

and solution of the equations can be found in a form

$$F = \varphi F_0 \varphi^{-1}, \quad (6)$$

where $\varphi(t)$ takes values in the corresponding Lie group and $F_0 = F|_{t=0}$.

From equation (5) and presentation (6) it is directly followed the expression for the operator A :

$$A = \varphi' \varphi^{-1} \quad (\varphi' = \frac{\partial \varphi}{\partial t}) \quad (7)$$

Let's consider the commutator of F with X^+ :

$$\begin{aligned} [X^+, F] &= [X^+, X^-] - e' \frac{\partial}{\partial t} [X^+, \tilde{f}] + e' [X^+, [H, \tilde{f}]] = \\ &= H - e' \frac{\partial}{\partial t} [X^+, \tilde{f}] - 2e' [X^+, \tilde{f}] + e' [X^+, [H, \tilde{f}]] = \\ &= H - \frac{\partial}{\partial t} (e' [X^+, \tilde{f}]) - e' [X^+, \tilde{f}] + [H, e' [X^+, \tilde{f}]]. \end{aligned}$$

Taking into account (6) and (7) the last expression can be rewritten in a form

$$[X^+, \varphi F_0 \varphi^{-1}] = H - (\varphi' \varphi^{-1})' - \varphi' \varphi^{-1} + [H, \varphi' \varphi^{-1}].$$

Making the substitution $\varphi = e^{H\tau} q$ and introducing a new variable $\tau = e^{-t}$, we have another form of equation (1)

$$\frac{\partial}{\partial \tau} \left(\frac{\partial q}{\partial \tau} q^{-1} \right) = [q F_0 q^{-1}, X^+] \quad (8)$$

Equation (8) is one-dimensional WZNW (Wess-Zumino-Novikov-Witten) equation [16-18] and its partial exact solutions are the subject of further publications.

- | | |
|---|--|
| <p>[1] R.S. Ward, <i>Phil. Trans. R. Soc. Lond.</i> A315, 451 (1985); <i>Lect. Notes Phys.</i>, 1987, 280, 106; <i>Lond. Math. Soc. Lect. Notes Ser.</i>, 1990, 156, 246.</p> <p>[2] L.J. Mason and G.A. J.Sparling, <i>Phys. Lett.</i>, 1989, A137, 29; <i>J. Geom. and Phys.</i>, 1992, 8, 243.</p> <p>[3] S. Chakravarty, M.J. Ablowitz and P.A. Clarkson, <i>Phys. Rev. Lett.</i>, 1990, 1085.</p> <p>[4] I. Bakas and D.A. Depireux, <i>Mod. Phys. Lett.</i>, 1991, A6, 399.</p> <p>[5] M.J. Ablowitz, S. Chakravarty and L.A. Takhtajan, <i>Comm. Math. Phys.</i>, 1993, 158, 1289.</p> <p>[6] T.A. Ivanova and A.D. Popov, <i>Phys. Lett.</i>, 1992, A170, 293.</p> <p>[7] L.J. Mason and N.M.J. Woodhouse, <i>Nonlinearity</i> 1, 1988, 73; 1993, 6, 569.</p> <p>[8] M. Kovalyov, M. Legare and L. Gagnon, <i>J. Math. Phys.</i>, 1993, 34, 3425.</p> | <p>[9] M. Legare and A.D. Popov, <i>Pis'ma Zh. Eksp. Teor. Fiz.</i>, 1994, 59, 845.</p> <p>[10] A.A. Belavin and V.E. Zakharov, <i>Phys. Lett.</i>, 1978, B73, 53.</p> <p>[11] A.N. Leznov and M.A. Mukhtarov, <i>J. Math. Phys.</i>, 1987, 28 (11), 2574; <i>Prepr. IHEP</i>, 1987, 87-90. <i>Prepr. ICTP</i> 163, Trieste, Italy, 1990; <i>J. Sov. Lazer Research</i>, 13 (4), 284, 1992.</p> <p>[12] A.N. Leznov, <i>IHEP preprint-92/87</i>, 1990.</p> <p>[13] A.N. Leznov, M.A. Mukhtarov and W.J. Zakrzewski, <i>Tr. J. of Physics</i> 1995, 19, 416.</p> <p>[14] M.A. Mukhtarov, <i>Fizika</i>, 2002, v. 5, N 2, 38</p> <p>[15] M.A. Mukhtarov, <i>Fizika</i>, 2002, v. 5, N 3, 3</p> <p>[16] V.G. Knizhnik and A.B. Zamolodchikov, <i>Nucl. Phys.</i> B247 (1984) 83.</p> <p>[17] F. Bastianelli, <i>Nucl. Phys.</i> B361 (1991) 555.</p> <p>[18] A.A. Tseytlin, <i>Nucl. Phys.</i> B411 (1994) 509.</p> |
|---|--|

M.A. Muxtarov

WZNW MODELİNİN LAKSA CÜTÜ HALINDA TƏQDİM OLUNMASI

Avtodual Yanq-Mills tənliklərinin reduksiyasından alınan birölçülü WZNW modeli Laksa cütünün normal təqdim olunmasına gətirilib.

M.A. Мухтаров

ПРЕДСТАВЛЕНИЕ МОДЕЛИ WZNW В ВИДЕ ПАРЫ ЛАКСА

Одномерная модель WZNW, полученная редукцией автодуальных уравнений Янга-Миллса, сведена к нормальному представлению пары Лакса.

Received: 20.09.05

DYNAMICAL PROPERTIES OF THE ALLATOSTATIN IV NEUROPEPTIDE SIDE CHAINS IN WATER SOLUTION

M.A. MUSAYEV, L.I. VELIEVA, I.N. ALIEVA, N.M. GOJAYEV

*Baku State University, Department of Physics, Laboratory of Molecular Biophysics,
Z. Khalilov str.23, Az-1148, Baku, Azerbaijan*

The conformational flexibility of the allatostatin IV neuropeptide side chains in water solution has been investigated by the method of molecular mechanics using atom-atomic potential functions. The series of conformational maps of the potential surfaces were constructed over the angles of the side chains for lowest energy-minimized conformation of the molecule. Permissible deviations of these angles from the optimal values were determined.

1. Introduction

Allatostatins are a family of neuropeptides that inhibit juvenile hormone (JH) synthesis by the corpora allata (CA) in cockroach and related insects [1]. These peptides are produced by cells of the brain and ganglia as well as by midgut endocrine cells [2,3]. Allatostatins have also been identified and purified from muscle tissue, suggesting that these molecules may have other roles apart from regulation of JH production [4]. Here we describe in detail conformational dynamics of the allatostatin IV neuropeptide initially isolated from brains of the virgin female the cockroach *Diploptera punctata* [2,3]. The primary structure of this neuropeptide was assigned as Asp1-Arg2-Leu3-Tyr4-Ser5-Phe6-Gly7-Leu8-NH₂. To clarify the mechanism and specificity of action of the allatostatin IV neuropeptide the permissible deviations of the side chains dihedral angles each amino acid residue from the optimal values for the preferable conformation in water solution was determined. Such study may provide important information regarding the structural and conformational features important for structure-function relationship of the allatostatin IV neuropeptide.

2. Computational method

Calculations have been carried using molecular mechanics method. Molecular mechanics is a computational method designed to give accurate structures and energies of molecules. It treats molecules as collections of masses that are interacting with each other via Van der Waals, electrostatic and torsion forces between non-bonded atoms. Mathematical functions of the atomic coordinates (called potential energy functions) are used to describe these interactions. Various parameters derived from experimental observations are included in the potential energy function. The energy of Van der Waals interaction has been described by Lennard-Jones potential with parameters proposed by Momany et al.[5]. A contribution of electrostatic interactions has been taken into account in a monopole approximation according to Coulomb's law with single atomic charges proposed by Momany et al [5]. The influence of solvent is included in the dielectric constant (ϵ). Since conformations of neuropeptide have to be analyzed in an aqueous environment, the dielectric constant is assumed to equal 10 as described in [6] and hydrogen bonds calculated from the Morse potential are supposed to be weakened with maximum energy of

1.5kcal/mol at NH...CO distance $r_0=1.8\text{\AA}$ [6]. Torsion potentials and barriers to rotation about bonds C ^{α} -N(ϕ) and about side chains bonds (χ) were as proposed by Momany et al [5]. The nomenclature and conventions adopted are those recommended by IUPAC-IUB [7]. Low-energy conformational state of the allatostatin IV neuropeptide (fig.1) was found by locating the global minima on a potential energy surface using energy minimization procedure in our previous study [8]. The motions of the amino acid residues side groups are governed by the conformation of the neuropeptide main chain, and it is expected that the studies of the motions of the side groups may provide information on the allatostatin IV neuropeptide molecular structure in detail. By conformational analysis, we estimated the probability distributions of side chain angles ($\chi_1, \chi_2, \chi_3...$) each amino acid residue of the molecule. The conformational search was confined near the calculated distributions of backbone dihedral angles of each amino acid and includes the following steps:

1. Conformational maps, i.e. energy contour maps as a function of backbone angle ϕ and side chain angles χ_1, χ_2, χ_3 were constructed for calculated lowest energy conformation (Table 1) of the allatostatin IV neuropeptide keeping all bond lengths, bond angles and peptide bond dihedral angles ψ and ω fixed. The angles $\phi-\chi_1, \phi-\chi_2, \phi-\chi_3$, and $\chi_1-\chi_2$ or $\chi_2-\chi_3$ varied at intervals of 30°.

- 2 After defining low-energy regions similar conformational maps were produced for the particular $\phi-\chi_1, \phi-\chi_2, \phi-\chi_3$, and $\chi_1-\chi_2$ or $\chi_2-\chi_3$ values at a 5° step, yielding in this way the detailed potential surfaces for the side chains of the molecule.

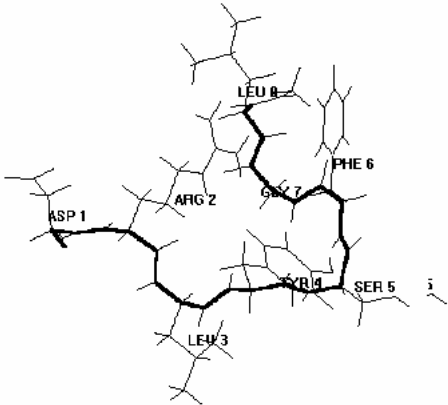
3. Structures resulting from step 2 are locally minimized.

3. Results and discussion

The results of conformational maps analysis which reflect the dynamics of functionally important side chains of the allatostatin IV neuropeptide are shown in figs.2-8. The values of dihedral angles corresponding to the optimal energy are marked by crosses; and the energy on equipotential lines is given in kcal/mol. Values for χ_1, χ_2 and χ_3 described low-energy states of the allatostatin IV side chains angles were taken from molecular mechanics calculation described above (Table 1).

Table 1.

The values of the dihedral angles (in degree) of the lowest energy conformation of the allatostatin IV neuropeptide

Residue	Dihedral angles	 <p>Fig. 1. Lowest energy conformational state of the allatostatin IV neuropeptide [8].</p>
Asp1	$\varphi=-89$, $\psi=-44$, $\omega=178$, $\chi_1=54$, $\chi_2=105$	
Arg2	$\varphi=-134$, $\psi=97$, $\omega=179$, $\chi_1=-67$, $\chi_2=174$, $\chi_3=161$	
Leu3	$\varphi=-99$, $\psi=94$, $\omega=183$, $\chi_1=54$, $\chi_2=177$, $\chi_3=182$	
Tyr4	$\varphi=-150$, $\psi=165$, $\omega=177$, $\chi_1=-67$, $\chi_2=95$, $\chi_3=180$	
Ser5	$\varphi=-71$, $\psi=-52$, $\omega=171$, $\chi_1=56$, $\chi_2=177$	
Phe6	$\varphi=-60$, $\psi=-29$, $\omega=178$, $\chi_1=62$, $\chi_2=81$	
Gly7	$\varphi=80$, $\psi=-77$, $\omega=182$	
Leu8	$\varphi=-104$, $\psi=-60$, $\omega=179$, $\chi_1=-53$, $\chi_2=176$, $\chi_3=186$	
E_{conf}	-36, 9 kcal/mol	

Three conformational maps of the potential surfaces were constructed over φ - χ_1 , φ - χ_2 , and χ_1 - χ_2 angles of the Asp1 residue in the lowest energy conformational state of the allatostatin IV neuropeptide (fig.2). These maps take into account the low-energy state of the asparagine residue, thereby displaying the minima of the potential functions at all possible values of the χ_1 and χ_2 angles. As can be seen in fig.2, the optimal positions of the Asp1 side chain are close to

minima of their torsional potential, i.e. χ_1 may populate $\pm 60^\circ$, 180° and deviations by $\pm 20^\circ$ from minimal values are possible for backbone φ angle. Calculated results indicate that χ_2 for Asp1 can take two values -60 and 100° , and the low-energy changes of this angle in the range of $\pm 15^\circ$ are allowed (fig.2). The plot of the χ_1 and χ_2 angles distributions is given in fig.3.

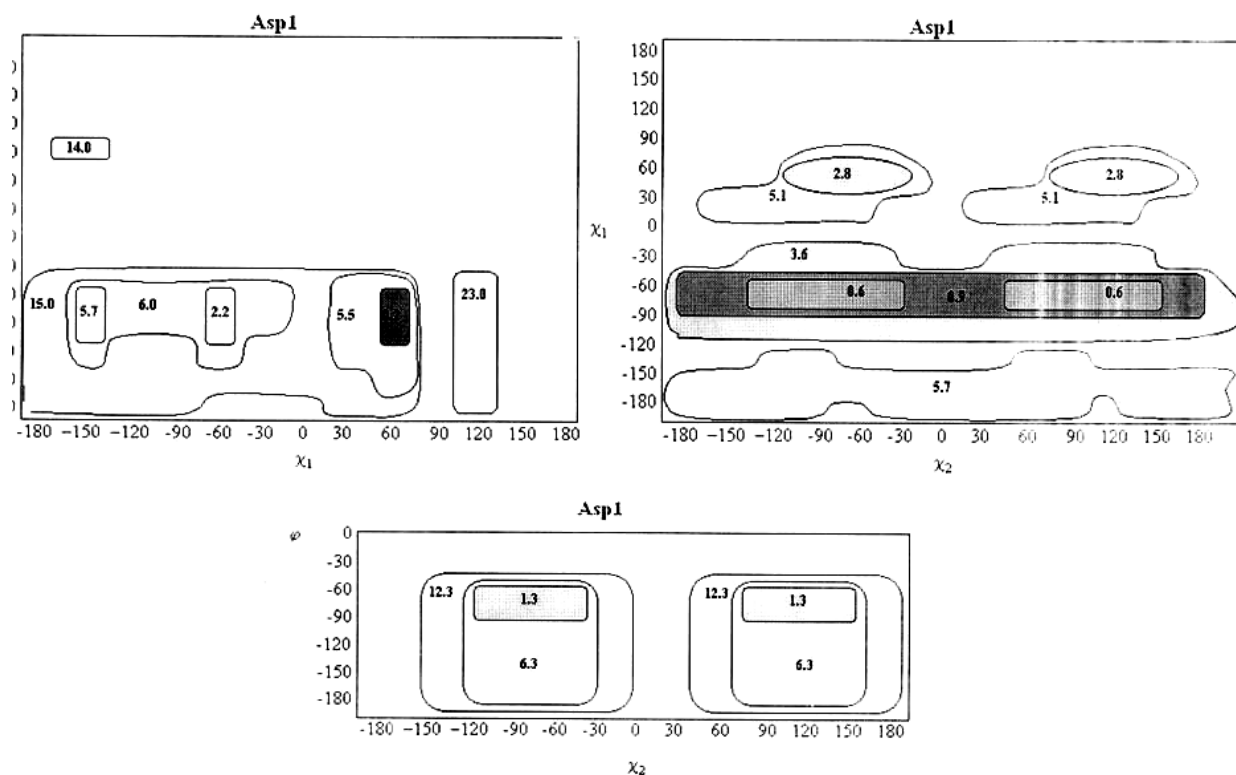


Fig. 2. Energy contours (in kcal/mol) as a function φ - χ_1 ; φ - χ_2 ; and χ_1 - χ_2 of the Asp1 for lowest energy conformation of allatostatin IV neuropeptide.

A further calculation scheme included a study of low-energy regions for the Arg2 positively charged side chain. The calculation was made by constructing three

conformational maps over the φ - χ_1 , φ - χ_2 , φ - χ_3 angles, based on low-energy structure of allatostatin IV neuropeptide (fig.4).

As can be seen from fig.4, the energies of the conformations that correspond to the positive value of the φ dihedral angle are approximately 24,1 kcal/mol higher than those with negative values. The low-energy changes from -60° to -120° of the φ angle and from -120° to -60° of the χ_1 angle are allowed. Calculated results indicate that χ_2 for Arg2 can take values -60 and 180° , and low-energy changes of this angle in the range of $\pm 15^\circ$ are allowed. There is very restricted low-energy region for one value of χ_3 for Arg2, i.e. at 180° . The permissible deviation by $\pm 5^\circ$ from optimal value of this angle is revealed. This result suggest that not only the positive charge of the amino acid residue at position 2, but also the length of the side chain seem to be important for the three-dimensional structure of the neuropeptide. Fig.5 describes distributions of the arginine χ_1 and χ_2 dihedral angles in the lowest energy conformation of the molecule.

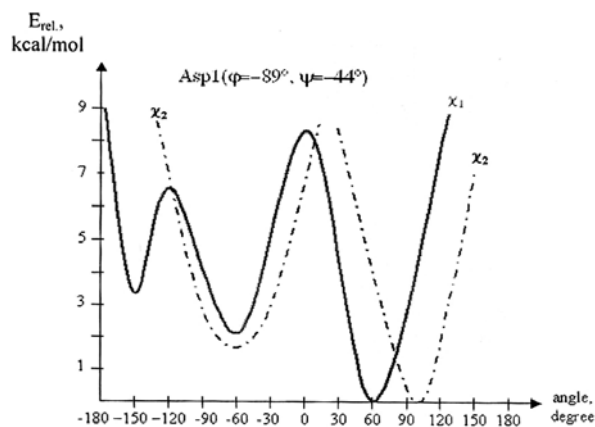


Fig. 3. A plot of the distribution of the Asp1 χ_1 and χ_2 dihedral angles. The x-axis is the value of the dihedral angle, from -180 to $+180^\circ$, with the distribution in 30° bins. The y-axis is the relative conformational energy of the molecule in kcal/mol.

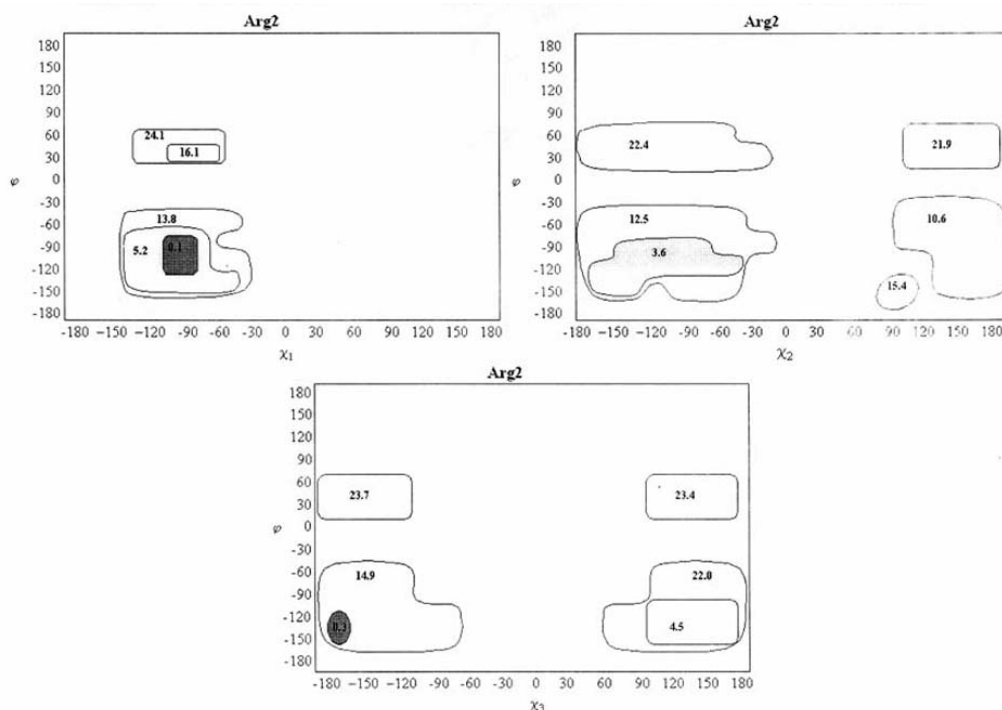


Fig. 4. Energy contours (in kcal/mol) as a function φ - χ_1 ; φ - χ_2 ; and φ - χ_3 of the Arg2 for lowest energy conformation of allatostatin IV neuropeptide.

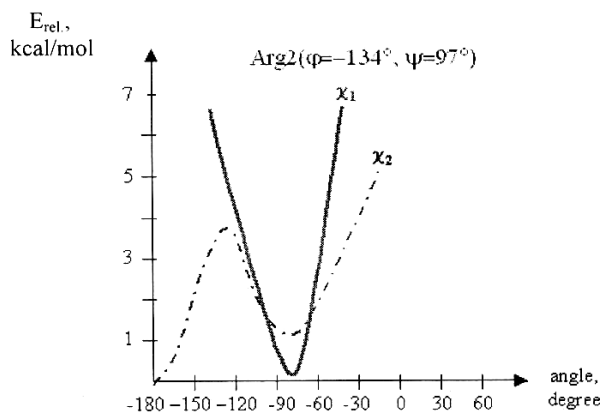


Fig. 5. A plot of the distribution of the Arg2 χ_1 and χ_2 dihedral angles.

For the leucine part of the allatostatin IV neuropeptide, the permissible deviations of the backbone φ and χ_1, χ_2 side chain angles are calculated by constructing φ - χ_1 and φ - χ_2 conformational maps. It must be noted that the dihedral angle χ_3 and χ_4 which determines the spatial state of the end group of the leucine residue, does not contribute significantly to the stabilization of the spatial structure. Conformational maps that indicate the restricted conformational mobility of the Leu3 backbone are given in fig.6. As can be seen in fig.6, the positive values of φ angle form forbidden region in conformational map. There are low-energy regions for χ_2 for Leu3, i.e. at $\pm 60^\circ$ and only one for χ_1 , which corresponds to 180° (fig.7). Through computer simulation, it was found that the effects caused by variation of χ_3 and χ_4 angles are small compared with those caused by χ_2 .

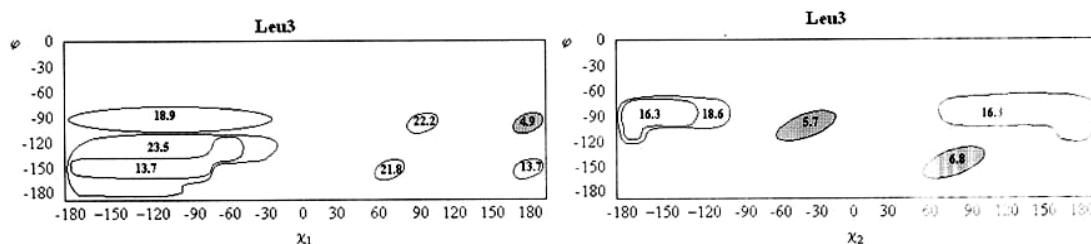


Fig. 6. Energy contours (in kcal/mol) as a function φ - χ_1 and φ - χ_2 of the Leu3 for lowest energy conformation of allatostatin IV neuropeptide.

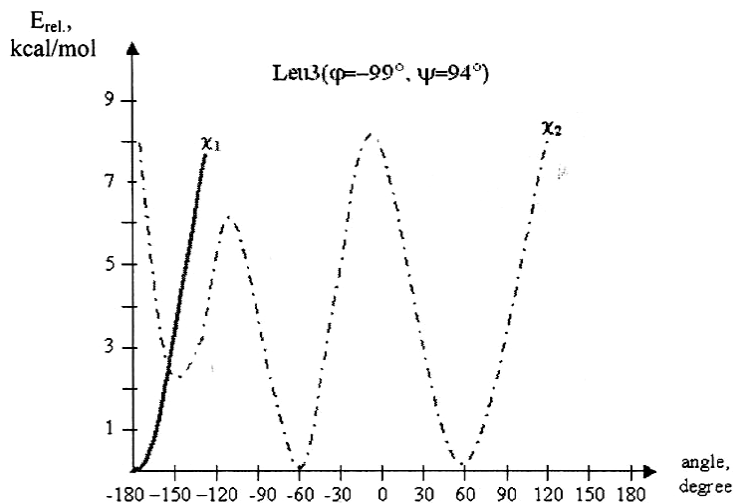


Fig. 7. A plot of the distribution of the Leu3 χ_1 and χ_2 dihedral angles.

Fig.8,a and b show the energy contours of φ , χ_1 and χ_2 angles for Tyr4. The φ angle for Tyr4 has a weak conformational mobility, i.e. its low-energy change by $\pm 5^\circ$ is possible here. Two minima for χ_2 ($\pm 90^\circ$) and only one for χ_1

(-60°) side chain angles are found (fig.9). The angle χ_3 for Tyr4, which defines the orientation of hydroxyl group OH, has a noticeable conformational flexibility.

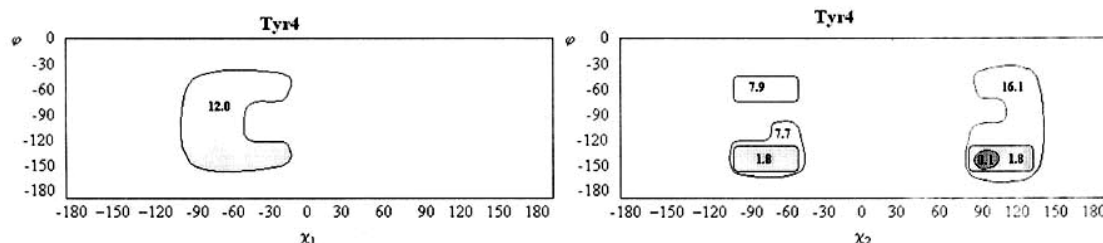


Fig. 8. Energy contours (in kcal/mol) as a function φ - χ_1 and φ - χ_2 of the Tyr4 for lowest energy conformation of allatostatin IV neuropeptide.

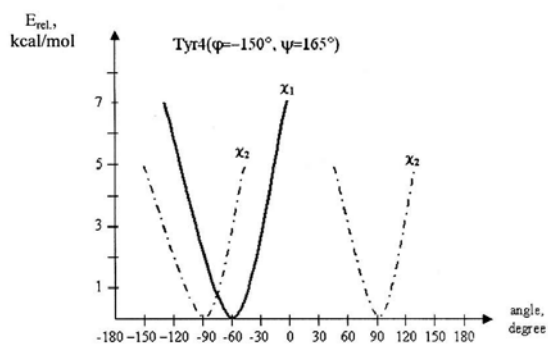


Fig. 9. A plot of the distribution of the Tyr4 χ_1 and χ_2 dihedral angles.

The side chain of the next Ser5 amino acid residue is characterized by significant conformational mobility (fig.10). In spite very fixed backbone, there are two low-energy regions in the φ - χ_2 conformational map. The low-energy changes from -180° to 180° for χ_1 and it is possible from 90° to 180° and from -60° to 180° for χ_2 (fig.11).

A further calculation scheme included a study of low-energy regions for the Phe6 side chain. Calculation was made by constructing two conformational maps over the φ - χ_1 and φ - χ_2 angles, based on low-energy structures of allatostatin IV neuropeptide. The energies of the conformations that correspond to the positive values of the φ dihedral angle are equal approximately 60 kcal/mol that higher than those with negative values. Calculated results indicate that χ_2 angle for Phe6 can take to opposite values $\pm 90^\circ$, and low-energy

changes of this angle in the range of $\pm 20^\circ$ are allowed (fig.12 and fig.13).

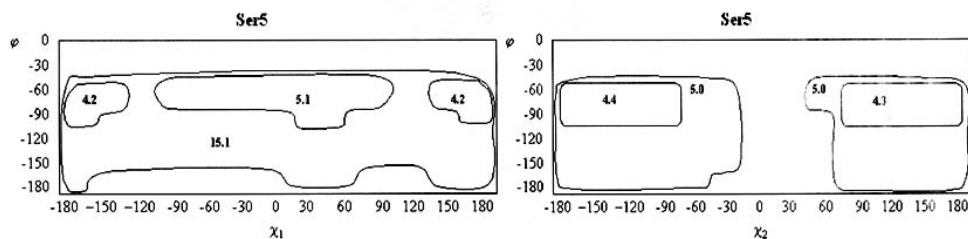


Fig. 10. Energy contours (in kcal/mol) as a function φ - χ_1 and φ - χ_2 of the Ser5 for lowest energy conformation of allatostatin IV neuropeptide.

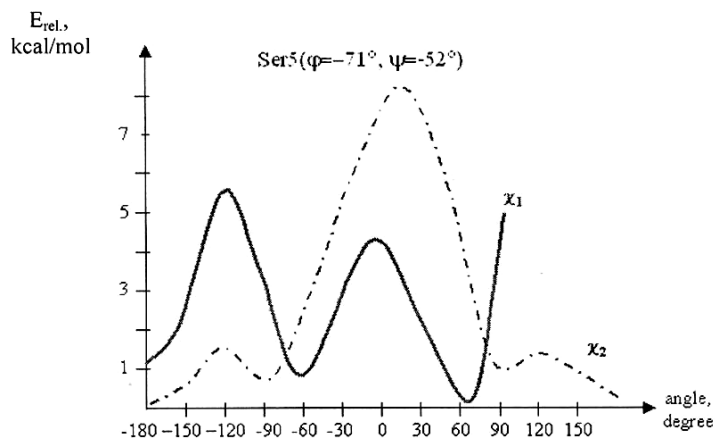


Fig. 11. A plot of the distribution of the Ser5 χ_1 and χ_2 dihedral angles.

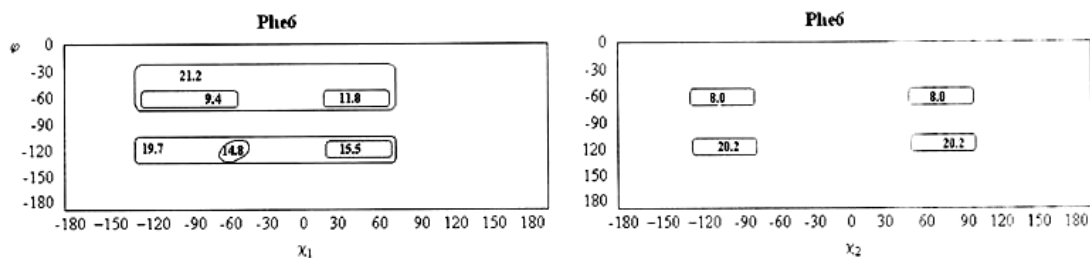


Fig. 12. Energy contours (in kcal/mol) as a function φ - χ_1 and φ - χ_2 of the Phe6 for lowest energy conformation of allatostatin IV neuropeptide.

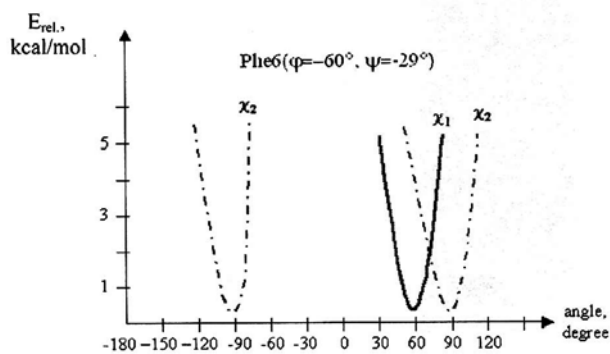


Fig. 13. A plot of the distribution of the Phe6 χ_1 and χ_2 dihedral angles.

Three conformational maps of the potential surfaces were constructed over the φ - χ_1 , φ - χ_2 , and φ - χ_3 of the Leu8 for lowest energy conformation of allatostatin IV neuropeptide. The conformational maps, which indicate the forbidden zone that correspond to the positive values of φ backbone angle

are given in fig.14,a and b. χ_1 dihedral angle may populate two states $\pm 60^\circ$, but there is only one possible state for χ_2 dihedral angle (fig.15).

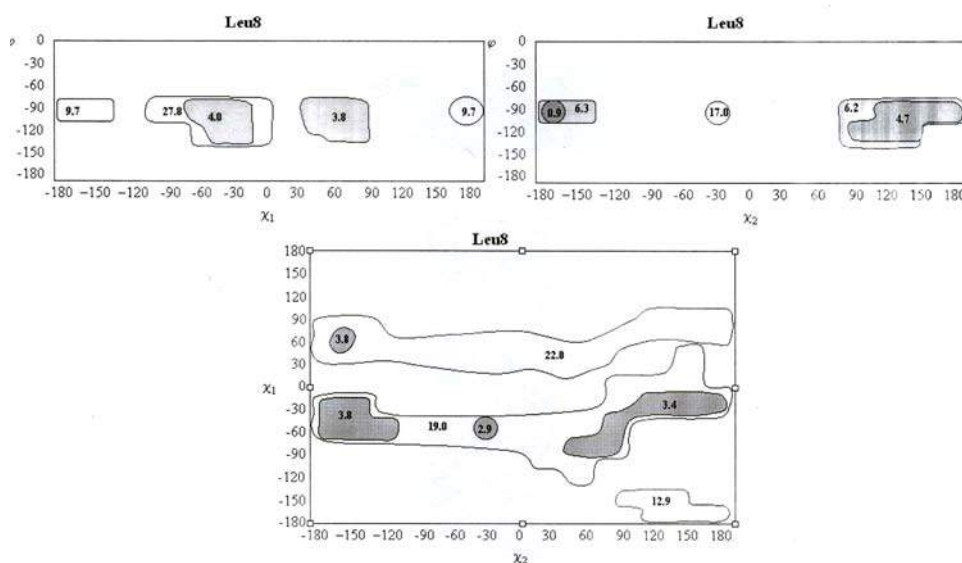


Fig. 14. Energy contours (in kcal/mol) as a function φ - χ_1 ; φ - χ_2 ; and φ - χ_3 (c) of the Leu8 for lowest energy conformation of allatostatin IV neuropeptide.

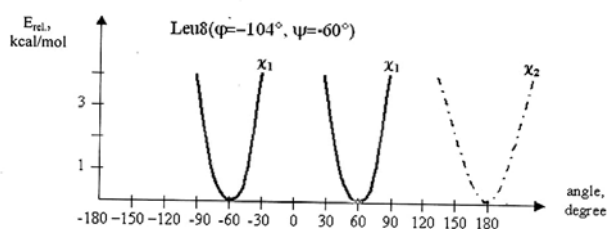


Fig. 15. A plot of the distribution of the Leu8 χ_1 and χ_2 dihedral angles.

The obtained data allow one to conclude that, in spite of considerable conformational mobility of the molecule, only Ser5 side chain has a noticeable conformational mobility. The reported results may serve as the basis for investigations of the structure-function relationship of the allatostatin IV neuropeptide.

- [1] S.S. Tobe and B. Stay, Adv.Insect Physiol., 1985, 18, 305.
- [2] A.P. Woodhead, B. Stay, S.L. Siedel, M.A. Khan, and S.S. Tobe. Proc. Natl. Acad. Sci. USA, 1989, 86, 5997.
- [3] G.E. Pratt, D.E. Fransworth, et.al Proc. Natl. Acad. Sci. USA, 1991, 88, 2412.
- [4] A.P. Woodhead, C.A. Stoltzman, and B. Stay. Arch. Insect Biochem. Physiol., 1992, 20, 253.
- [5] F.A.Momany, R.McGuire, A.W.Burgess, H.A.Scheraga. J.Phys.Chem., 1975, 79, 2361.
- [6] E.M. Popov, Int.J.Quant.Chem., 1979, 16, 707.
- [7] IUPAC-IUB Quantity, Units and Symbols in Physical Chemistry, Blackwell Scientific Publications, Oxford 39, 1988.
- [8] M.A. Musayev, L.I.Velievaya, I.N. Aliyeva. V.Kn. Tezisi dokladov I stendovikh coobshsheniy. II Rossiyskiy simpoziumpo khimii I biologii peptidov. Moskva, 2005, s. 92 (in Russian).

M.A. Musayev, L.I. Vəliyeva, İ.N. Əliyeva, N.M. Qocayev

ALLATOSTATİN IV NEYROPEPTİDİNİN SU MÜHİTİNDƏ YAN ZƏNCİRLƏRİNİN DİNAMİK XÜSUSİYYƏTLƏRİ

Atom-atom potensial funksiyalardan istifadə edilməklə molekulyar mexanika üsulu ilə allatostatin IV neyropeptidin su mühitində amin turşuları qalıqlarının yan zəncirlərinin konformasiya müəhərrikliliyi tədqiq edilmişdir. Neyropeptidin yan zəncirlərlərinin ikiüzlü bucaqlarının fırladılması yolu ilə molekulun qlobal konformasiyası üçün potensial çəpərin hündürlüyünü təsvir edən konformasiya xəritələri qurulmuşdur. İkiüzlü bucaqların öz optimal qiymətlərindən icazə verilən kənara çıxmaları müəyyən olunmuşdur.

М.А. Мусаев, Л.И. Велиева, И.Н. Алиева, Н.М. Годжаев

ДИНАМИЧЕСКИЕ СВОЙСТВА БОКОВЫХ ЦЕПЕЙ НЕЙРОПЕПТИДА АЛЛАТОСТАТИНА IV В ВОДНОЙ СРЕДЕ

Методом молекулярной механики с помощью атом-атомных потенциальных функций исследована конформационная подвижность боковых цепей аминокислотных остатков нейропептида аллатостатина IV в водной среде. Построены конформационные карты, описывающие сечения потенциальной поверхности для глобального конформационного состояния молекулы путем варьирования двугранных углов в боковых цепях нейропептида. Установлены допустимые отклонения двугранных углов от их оптимальных значений.

Received: 14.07.05

THE BLUR OF THE ORDER PARAMETER IN ARGENTUM CHALCOGENIDE IN THE REGION OF THE PHASE TRANSITION

S.A. ALIYEV

Institute of Physics of NASA, Baku-1143, G. Javid av., 33

The temperature dependence of the order parameter η in argentums chalcogenides is defined using the temperature differential coefficient of the inclusion function in the zero approximation. It is revealed, that η in the region of the phase transition (PT) is strongly blurred. It is established, that Ag_2Te , Ag_2Se and Ag_2S achieve only 69%, 52% and 49% in the phase disorder region PT correspondingly.

The order parameter η , characterizing the physical state of the phases in PT region takes the important place among the parameters, describing the PT. That's why the investigation of the temperature dependence $\eta(T)$ in PT region can add the current information about PT nature in argentums chalcogenides and give the comprehensive data about phase disorder in PT process.

According to the classic theory of PT, the η parameter is considered for the ordered system $\eta \neq 0$, and for the unordered system $\eta = 0$. In such interpretation PT can be considered as the system transfers from the ordered state into unordered one. The η parameter depends on T at the constant pressure, and achieves the zero meaning in $\text{PT}-T_0$ point, when the ordering disappears.

However, in the common case the change of η near PT can be as in spurts, so constantly. These questions had been considered in the refs [1-3], in which Landau developed his theory for PT of II type, considering them more interesting as physical ones. But the main conditions are applied for another PT also. Taking under the consideration the small meaning of η near $\text{PT}-T_0$, analyzing the thermodynamic potential $P(\eta)$, depending on η , we obtain:

$$\Phi = \Phi_0 + \alpha\eta^2 + \beta/2\eta^4, \quad (1)$$

Where Φ_0 is thermodynamic potential of the disordered phase, α and β are decomposition coefficients. Using the equilibrium conditions for the thermodynamic potential of the ordered phase at the given pressure, we obtain:

$$\alpha(T) = \alpha_0(T - T_0), \quad (2)$$

where $\alpha_0 > 0$. As β changes weakly near $\text{PT}-T_0$ point, so changed it on $\beta_0 > 0$ and limited by the quadratic member, we obtain

$$\eta^2 = \alpha_0(T_0 - T)/\beta_0, \quad (3)$$

being the main result of Landau theory for PT II.

But it is need to note, that the fluctuation of the compound and other physical values, order parameter η , also as PT parameters and the thermodynamic parameters, can be blurred because of the existing the microheterogeneities in the solid bodies. The given question is discussed in the ref [4] and the model of the elementary subsystems (ES) is supposed to use for its decision. Toward this end the system can be divided on the big number of ES with the similar volumes v_0 near PT point. Such system is characterized by the

macroscopic temperature T and macroscopic point $\text{PT}-T_0$. The separate ES have local temperature τ , differed from all T sample. If change of T carries out slowly enough, then the definite distribution of ES on the local temperatures carries out at the each meaning of the temperature. For comfort of the calculations, the local temperature of ES τ is accounted from average T as $\theta = T - \tau$. Designating the being probability of ES through $W(\theta)$ with the local temperature in the limits from θ till $\theta + d\theta$, we obtain

$$dW(\theta) = \varphi(\theta)d\theta, \quad (4)$$

where $\varphi(\theta)$ presents the probability density, the norm of which is equal to one. Knowing the distribution probability of $dW(\theta)$, it is possible to calculate the temperature dependence $\eta(T)$. Designated the order parameter through $\eta^2(\tau, \theta)$ at the macroscopic temperature $t = T - T_0$ of that part of the system, the local temperature of which is in the limits from θ till $\theta + d\theta$, then at t we obtain:

$$\eta^2(t) = \int \eta^2(t, \theta) d\theta = \int \eta^2(t, \theta) \varphi(\theta) d(\theta) \quad (5)$$

As it is seen it is need to know the distribution function of ES on the local temperatures $\varphi(\theta)$ and the order parameter of the separate ES for the calculation of square of order parameter $\eta^2(t)$. It is supposed, that the first from them can be defined on the base of the common introduction of the fluctuation theories, and second one is defined by PT character in the separate ES (PT of I and PT of II type). In the case, when ES consist on the PT of II type, without taking under consideration of effects of anisotropy and elastic stresses on the base of formulae (3), we obtain:

$$\eta^2(T, \theta) = \alpha_0/\beta_0 (\theta - t), \quad (\text{at } t \leq \theta) \quad (6)$$

And consequently

$$\eta^2(t) = \alpha_0/\beta_0 \int_t^\infty \varphi(\theta) \cdot (\theta - t) d\theta. \quad (7)$$

As it was mentioned, it is need to apply the fluctuation theory for the calculation of $\varphi(\theta)$. In [4] the case of small fluctuations, realizing on practices very often is considered, at which

$$dW(\theta) = \frac{1}{v\sqrt{n}} \exp\left(-\frac{\theta^2}{v^2}\right) d\theta, \quad (8)$$

where v parameter characterizes the given distribution. Considering v as the constant value, we obtain:

$$\eta^2(t) = \frac{\alpha_0 \nu}{2\beta_0 \sqrt{\pi}} \exp\left(-\frac{t^2}{y^2}\right) - \frac{t\alpha_0}{2\beta_0} \left[1 + \Phi\left(\frac{\sqrt{2}}{y}|t|\right)\right], \quad (t < 0)$$

$$\eta^2(t) = \frac{\alpha_0 \nu}{2\beta_0 \sqrt{\pi}} \exp\left(-\frac{t^2}{y^2}\right) - \frac{t\alpha_0}{2\beta_0} \left[1 - \Phi\left(\frac{\sqrt{2}}{y}|t|\right)\right], \quad (t > 0) \quad (9)$$

where

$$\Phi(x) = \sqrt{\frac{2}{\pi}} \cdot \int_0^x \exp\left(-\frac{x^2}{2}\right) dx$$

In ref. [4] the calculations $\eta(t)$ for PT of II type had been carried out. For this the definite simplifications and admissions, defensible for the common theoretical evaluation $\eta(t)$ had been carried out. The obtained data are compared with the calculated curves, carried out on Landau classic theory (on formulae 3). It is shown, that the blur of order parameter η has place in the case of the heterogeneity in the solid bodies in region of PT of II type. At the same time, it is observed, that the blur of η can take place at the other PT.

The task in the given ref. leads to the selection method for the definition of the order parameter η and the degree of its blur in PT region of argentums chalcogenides, having the structural PT. In principle, ES model can be applied to the argentums chalcogenides, considering α -phase till phase transition through the ordered system, and the inclusion of germs of β -phase in each PT point through elementary subsystems, having local temperatures $\theta = T - \tau$ and creating the disordering of phase system. However, as it is seen from (9) the ν parameter, characterizing the distribution of small fluctuations, thermodynamic potential $\Phi(x)$, the local temperatures of germs, and other parameters, the values of which in the difference from the theoretical evaluations η is hard to define for the concrete crystal, enter in their expressions. At the same time, it is known, that the differences in the character of the phase transitions is more clear revealed with the help of the physical values, connected with the differential coefficients of parameters, characterizing PT. The $L_0(T)$ and dL_0/dT have been investigated for the argentums chalcogenides in refs [5-8] and it is shown, that PT are strongly blurred in them. That's why the blur of order parameter η in PT region can be considered by the introduction of dL_0/dT in the formulas (3) or (9) in the form:

$$\eta^2(t) = \frac{\alpha_0}{\beta_0} \cdot \left(\frac{dL_0}{dT}\right)^{-1} = \frac{\alpha_0}{\beta_0} \frac{2}{a_0} \{1 + ch[a_0(T - T_0)]\} \quad (10)$$

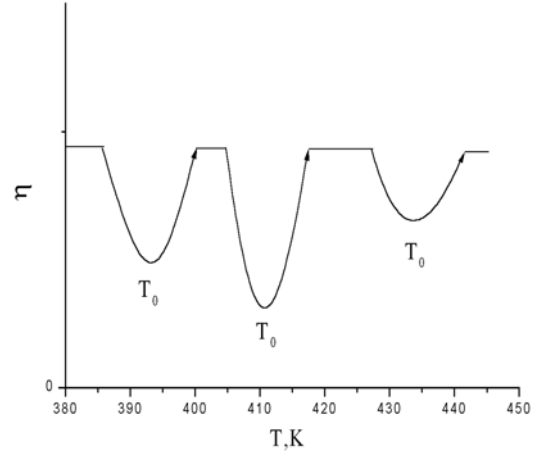


Fig.1. Temperature dependence of order parameter in argentums chalcogenides: a-Ag₂Te, в-Ag₂Se и с-Ag₂S.

where a_0 is temperature constant of PT, characterizing the blur degree of PT. Then the temperature motion $\eta(t)$ in the ordered region is defined by the formula (3), and in PT region is defined by formulae (10). The calculation results, carried out for the Ag₂Te, Ag₂Se and Ag₂S samples (with excess Te ≈ 0.75at.%) in SPT (α' - β') with the use of a_0 and dL_0/dT parameters [5-8], are presented on the fig.1. At the calculations β_0 was considered constant ($\beta_0 > 0$), and α_0 was selected analogically to the theoretical calculations, carried out in ref [4]. The ration α_0/β_0 in PT region didn't influence significantly on $\eta(T)$. As it is seen from the figure, the change of $\eta(T)$ at PT hasn't clearly spasmodic type, has the wide interval ΔT , the curve $\eta(T)$ is strongly blurred near PT- T_0 point and η_0 meaning is more bigger than zero. All this shows on the strongly blur of order parameter. Physically it means that disordering of the phases at PT in the argentums chalcogenides doesn't carry out totally, as it is followed from the classical theory. In Ag₂Te, Ag₂Se and Ag₂S the disordering of phases in PT region achieves only 69%, 62% and 49% correspondingly.

- [1] L.D.Landau, E.M.Lifshis, Statisticheskaya fizika, M. "Nauka", 1964.
- [2] L.D.Landau, JETP, 7, 1937, p.19.
- [3] L.Landau, Phys. Zs. Sowjet., 11, 1937, p.26.
- [4] B.N.Rolov, Razmitiye Fazovie perechodi, Riga, 1972, 311.
- [5] S.A.Aliev, F.F.Aliev, Z.S.Gasanov, FTT, v. 40, №9, 1693 (1998).
- [6] S.A.Aliev, Z.S.Gasanov, Z.F.Agayev, R.K.Guseynov, TRANSACTIONS of NAS of Azerbaijan, phys-mat. And tech.sciences, 5, 81 (2002).
- [7] Prof. Dr.habil Sabir Aliev, Dr. Ziraddin Gasanov, Dr. Zakir Agayev, Dipl-Phys. Rasim Guseynov, Abhandlungen der WGB, Band 3, p.103, Berlin, 2003.
- [8] Prof. Dr.habil Sabir Aliev, Dr. Ziraddin Gasanov, Abhandlungen der WGB, Band 3, p.98, Berlin, 2003.

FAZA KEÇİDİ OBLASTINDA GÜMÜŞ XALKOQENİDLƏRDƏ NİZAMLILIQ PARAMETRİNİN YAYINIQLIĞI

Sıfırıncı yaxınlaşmada daxilolma funksiyasının törəməsinin temperatur asılılığından istifadə edilərək gümüş xalkoqenidlərdə η nizamlılıq parametrinin temperatur asılılığı təyin edilmişdir. Faza keçidi (FK) oblastında η -nin kəskin yayınlıq olması müşahidə edilmişdir. FK oblastında Ag_2Te , Ag_2Se , Ag_2S –də fazaların yayınlıqlığının uyğun olaraq 69%, 52% və 49% olduğu göstərilmişdir.

С.А.Алиев

**РАЗМЫТИЕ ПАРАМЕТРА УПОРЯДОЧЕНИЯ В ХАЛЬКОГЕНИДАХ СЕРЕБРА В ОБЛАСТИ
ФАЗОВОГО ПЕРЕХОДА**

Используя температурную производную функции включения в нулевом приближении определена температурная зависимость параметра неупорядоченности η в халькогенидах серебра. Обнаружено, что в области фазового перехода (ФП) η сильно размыт. Установлено, что разупорядочение фаз, в области ФП Ag_2Te , Ag_2Se и Ag_2S достигает только 69%, 52% и 49% соответственно.

Received: 15.06.05

THE EQUATIONS FOR THE MULTI-QUARK GREEN FUNCTION IN NAMBU-JONA-LAZINIO MODEL

R.G. JAFAROV

Baku State University, AZ1148 Baku, Z.Khalilov, 23

The equations for the multi-quark Green functions have been obtained in the decay of the average field with bilocal source in NJL model.

The equations for many-particle functions play very important role at the description of the connected states, the scattering of connected states on particles, the scattering of the connected states on connected states and e.t.c. The first representative of the family of the many-particle equations is the well-known Bethe-Salpeter (BS) equation [1] for the two-particle Green function. The generalization of BS equation in the case of three or more particles is given in the refs [2-4]. These generalizations are based on the analysis of the Feynman diagrams of the perturbation theory and all statements concerning nucleus structure have clearly perturbative character. The main disadvantage of these diagram methods is that practically all statements can be formulated only as the verbal recipes and they aren't subordinated to the formalization that makes the investigation more difficult.

However, there is natural language for the description of the many-particle equations in the limits of Legendre field theory. Legendre functional transformations allow to obtain the equations for the many-particle Green functions as the direct consequences of the field equations. In the ref [5] Legendre transformations are applied to the study of n -particle equations for fermions.

In the present ref in the limits of Nambu-Jona-Lazinio (NJL) [6,7] the equations for the many pointed functions are obtained. At the obtaining of these equations the iterative scheme (one of the variants of field degradation), supposed in refs [8,9], which is based on the approximation system of Schwinger-Dayson (SD) equations for the functional of Green functions with the exactly solvable equation.

Let's consider NJL model with Lagrangian [7,10]:

$$L = \bar{\psi} (i\hat{\partial} - m_0) \psi + \frac{g}{2} \left[(\bar{\psi} \psi)^2 + (\bar{\psi} i \gamma_5 \tau^a \psi)^2 \right], \quad (1)$$

which we will call SU(2) model of NJL. Here, $g > 0$ is the constant of the connection with the dimension of square of reverse mass. Lagrangian is invariant with respect to the transformations of chiral group $SU(2)_V \times SU(2)_A$.

$\psi \equiv \psi^\alpha(x)_j^c$ and $\alpha = 1, \dots, 4$; $c = 1, \dots, n_c$; $j = 1, 2$. τ_{jk}^α – are generators of SU(2) group (Pauli matrix):

$$\tau^a \tau^b = \delta^{ab} + i \varepsilon^{abc} \tau^c, \quad a = 1, 2, 3; \quad ;$$

which are normed by the following method:

$$tr \tau^a \tau^b = 2 \delta^{ab} \dots$$

The SD equation is defined from the ratio [10]:

$$0 = \int D(\psi, \bar{\psi}) \frac{\delta}{\delta \bar{\psi}^\alpha(x)_j^c} \bar{\psi}^\beta(y)_k^d \times \\ \times \exp i \left[\int dx' L(x') - \int dx' dy' \bar{\psi}(y') \eta(y', x') \psi(x') \right] \quad (2)$$

where η is the bilocal source of the quarks and

$$\bar{\psi}(y) \eta(y, x) \psi(x) \equiv \bar{\psi}^\beta(y)_k^d \eta^{\beta\alpha}(y, x)_{kj}^{dc} \psi^\alpha(x)_j^c, \\ \bar{\psi}^\beta(y)_k^d \psi^\alpha(x)_j^c \rightarrow i \frac{\delta}{\delta \eta^{\beta\alpha}(y, x)_{kj}^{dc}} \dots$$

The transmission invariance of the measure of functional integration in (2) leads to the functionally-differential SD equation for the generating functional:

$$\delta^{\alpha\beta} \delta^{cd} \delta_{jk} \delta(x-y) G + (i\hat{\partial} - m^0)_{ji}^{\alpha\alpha'} \frac{\delta G}{\delta \eta^{\beta\alpha'}(y, x)_{ki}^{dc}} + \\ + i g \left\{ \frac{\delta}{\delta \eta^{\beta\alpha}(y, x)_{kj}^{dc}} tr \left[\frac{\delta G}{\delta \eta(x, x)} \right] - \gamma_5^{\alpha\alpha'} \tau_{ji}^a \frac{\delta}{\delta \eta^{\beta\alpha'}(y, x)_{kj}^{dc}} tr \left[\gamma_5 \cdot \tau^a \cdot \frac{\delta G}{\delta \eta(x, x)} \right] \right\} = \\ = \int dx_1 \eta^{\alpha\beta_1}(x, x_1)_{ji}^{cc_1} \frac{\delta G}{\delta \eta^{\beta\beta_1}(y, x_1)_{ki}^{dc_1}} \dots \quad (3)$$

The solution of this equation we will find by the method, supposed in the refs [8,9]. Further, we will consider the chiral

limit ($m_0=0$). The unique connected function of the main approximation is the free quark propagator. In the first step of

iteration the equations for the two-particle Green function (four-tail) and for the addition to the quark propagator appear [10].

The equation for the functional of n -step $G^{(n)}$ has the form:

$$\begin{aligned} & \delta^{\alpha\beta} \delta^{cd} \delta_{jk} \delta(x-y) G^{(n)} + (i\delta)_{ji}^{\alpha\alpha'} \frac{\delta G^{(n)}}{\delta \eta^{\beta\alpha'}(y, x)_{ki}^{dc}} + \\ & + ig \left\{ \frac{\delta}{\delta \eta^{\beta\alpha}(y, x)_{kj}^{dc}} tr \left[\frac{\delta G^{(n)}}{\delta \eta(x, x)} \right] - \gamma_5^{\alpha\alpha'} \tau_{ji}^a \frac{\delta}{\delta \eta^{\beta\alpha'}(y, x)_{kj_i}^{dc}} tr \left[\gamma_5 \cdot \tau^a \cdot \frac{\delta G^{(n)}}{\delta \eta(x, x)} \right] \right\} = \\ & = \eta * \frac{\delta G^{(n-1)}}{\delta \eta(x, x_1)}. \end{aligned} \quad (4)$$

The solution for the equation (4) we will find in the form $G^{(n)} = P^{(n)} G^{(0)}$, where $P^{(0)} \equiv 1$. The equation for $P^{(n)}$ will have the form

$$\begin{aligned} & - \frac{\delta P^{(n)}}{\delta \eta^{\beta\alpha}(y, x)_{kj}^{dc}} + ig \int dx_1 S^{(0)\alpha\alpha'}(x-x_1)_{ji}^{cc_1} \left\{ \frac{\delta}{\delta \eta^{\beta\alpha'}(y, x_1)_{ki}^{dc_1}} tr \left[\frac{\delta P^{(n)}}{\delta \eta(x_1, x_1)} \right] - \right. \\ & \left. - \gamma_5^{\alpha'\alpha_1} \tau_{il}^a \frac{\delta}{\delta \eta^{\beta\alpha_1}(y, x_1)_{kl}^{dc_1}} tr \left[\gamma_5 \cdot \tau^a \cdot \frac{\delta P^{(n)}}{\delta \eta(x_1, x_1)} \right] + \right. \\ & \left. + S^{(0)\alpha'\beta}(x_1-y)_{ik}^{c_1d} tr \left[\frac{\delta P^{(n1)}}{\delta \eta(x_1, x_1)} \right] - \gamma_5^{\alpha'\alpha_1} \tau_{il}^a S^{(0)\alpha_1\beta}(x_1-y)_{ik}^{c_1d} tr \left[\gamma_5 \cdot \tau^a \cdot \frac{\delta P^{(n1)}}{\delta \eta(x_1, x_1)} \right] \right\} = \\ & = \int dx_1 dx_2 S^{(0)\alpha\alpha'}(x-x_1)_{ji}^{cc_1} \eta^{\alpha'\beta'}(x_1, x_2)_{il}^{c_1c_2} \times \\ & \times \left[P^{(n-1)} S^{(0)\beta'\beta}(x_2-y)_{lk}^{c_2d} + \frac{\delta P^{(n-1)}}{\delta \eta^{\beta\beta'}(y, x_2)_{kl}^{dc_2}} \right]. \end{aligned} \quad (5)$$

According to the equations for $P^{(n)}$ (5) the equation for the second step of iteration will have the form:

$$\begin{aligned} & - \frac{\delta P^{(2)}}{\delta \eta^{\beta\alpha}(y, x)_{kj}^{dc}} + ig \int dx_1 S^{(0)\alpha\alpha_1}(x-x_1)_{ji}^{cc_1} \left\{ \frac{\delta}{\delta \eta^{\beta\alpha_1}(y, x_1)_{ki}^{dc_1}} tr \frac{\delta P^{(2)}}{\delta \eta(x_1, x_1)} - \right. \\ & \left. - \gamma_5^{\alpha_1\alpha_2} \tau_{il}^a \frac{\delta}{\delta \eta^{\beta\alpha_2}(y, x_1)} tr \gamma_5 \tau^a \frac{\delta P^{(2)}}{\delta \eta(x_1, x_1)} + \right. \\ & \left. + S^{(0)\alpha_1\beta}(x_1-y)_{ik}^{c_1d} tr \frac{\delta P^{(2)}}{\delta \eta(x_1, x_1)} - \gamma_5^{\alpha_1\alpha_2} \tau_{il}^a S^{(0)\alpha_2\beta}(x_1-y)_{ik}^{c_1d} tr \gamma_5 \tau^a \frac{\delta P^{(2)}}{\delta \eta(x_1, x_1)} \right\} = \\ & = \int dx_1 dx_2 S^{(0)\alpha\alpha_1}(x-x_1)_{ji}^{cc_1} \eta^{\alpha_1\alpha_2}(x_1, x_2)_{il}^{c_1c_2} \times \\ & \times \left\{ P^{(1)} S^{(0)\alpha_2\beta}(x_2-y)_{lk}^{c_2d} + \frac{\delta P^{(1)}}{\delta \eta^{\beta\alpha_2}(y, x_2)_{kl}^{dc_2}} \right\} \end{aligned} \quad (6)$$

The solution of the equation (6) we will find in the form:

$$P^{(2)} = \frac{1}{4!} Tr(S_4^{(2)} * \eta^4) + \frac{1}{3!} Tr(S_3^{(2)} * \eta^3) + \frac{1}{2} Tr(S_2^{(2)} * \eta^2) + Tr(S^{(2)} * \eta) \quad (7)$$

(here Tr means the step in the operative meaning, and $*$ - means operator multiplication). The solution of the equation of the first step of iteration has been chosen in the form [10].

$$P^{(1)} = \frac{1}{2} Tr(S_2^{(1)} * \eta^2) + Tr(S^{(1)} * \eta) \quad (8)$$

Substituting expressions (7) and (8) in (6), making one differentiation and switching on searches η (i.e. $\eta=0$) we obtain the equation for propagator of second step of iteration

$$S^{(2)\alpha\beta}(x-y)_{jk}^{cd} = ig \int dx_1 S^{(0)\alpha\alpha_1}(x-x_1)_{j_1}^{cc_1} \left\{ S_2^{(2)} \begin{pmatrix} x_1 & y \\ x_1 & x_1 \end{pmatrix}^{\alpha_1\beta, c_1d, j_1k} - \right. \\ \left. - \gamma_5^{\alpha_1\alpha_2} \tau_{j_1k_1}^a S_2^{(2)} \begin{pmatrix} x_1 & y \\ x_1 & x_1 \end{pmatrix}^{\alpha_2\beta, c_1d, k_1k} \gamma_5^{\alpha_3\alpha_4} \tau_{k_2j_2}^a + S^{(0)\alpha_1\beta}(x_1-y)_{j_1k}^{c_1d} tr S^{(2)}(0) \right\}. \quad (9)$$

After analogical procedure we will obtain the equations for the rest functions of the second step ($S_2^{(2)}$ – two-particle, $S_3^{(2)}$ – three-particle and $S_4^{(2)}$ – four-particle functions) of SU (2) of NJL model:

$$S_2^{(2)} \begin{pmatrix} x & y \\ x' & y' \end{pmatrix}^{\alpha\beta, cd, jk} = - S^{(0)\alpha\beta'}(x-y')_{jk'}^{cd'} S_2^{(1)\alpha'\beta}(x'-y)_{j'k'}^{c'd} + \\ + ig \int dx_1 S^{(0)\alpha\alpha_1}(x-x_1)_{j_1}^{cc_1} \cdot \left\{ S_3^{(2)} \begin{pmatrix} x_1 & y \\ x' & y' \end{pmatrix}^{\alpha_1\beta, c_1d, j_1k} - \right. \\ \left. - \gamma_5^{\alpha_1\alpha_2} \cdot \tau_{j_1k_1}^a S_3^{(2)} \begin{pmatrix} x_1 & y \\ x' & y' \end{pmatrix}^{\alpha_2\beta, c_1d, j_1k} \gamma_5^{\alpha_3\alpha_4} \cdot \tau_{j_2k_2}^a + \right. \\ \left. + S^{(0)\alpha_1\beta}(x_1-y)_{j_1k}^{c_1d} S_2^{(2)} \begin{pmatrix} x_1 & x_1 \\ x' & y' \end{pmatrix}^{\alpha_2\alpha_2, c_2c_2, j_2j_2} - \right. \\ \left. - \gamma_5^{\alpha_1\alpha_2} \cdot \tau_{j_1k_1}^a S^{(0)\alpha_2\beta}(x_1-y)_{k_1k}^{c_1d} S_2^{(2)} \begin{pmatrix} x_1 & x_1 \\ x' & y' \end{pmatrix}^{\alpha_4\alpha_3, c_2c_2, j_2k_2} \gamma_5^{\alpha_3\alpha_4} \cdot \tau_{k_2j_2}^a \right\}, \quad (10)$$

$$S_3^{(2)} \begin{pmatrix} x & y \\ x' & y' \\ x'' & y'' \end{pmatrix}^{\alpha\beta, cd, jk} = - S^{(0)\alpha\beta'}(x-y')_{jk'}^{cd'} S^{(0)\alpha'\beta}(x'-y)_{j'k'}^{c'd} S^{(1)\alpha''\beta''}(x''-y'')_{j''k''}^{c''d''} - \\ - S^{(0)\alpha\beta'}(x-y')_{jk'}^{cd'} S_2^{(1)} \begin{pmatrix} x' & y \\ x'' & y'' \end{pmatrix}^{\alpha'\beta, c'd, j'k} - \\ - S^{(0)\alpha\beta''}(x-y'')_{j''k''}^{cd''} S^{(0)\alpha''\beta}(x''-y)_{j''k''}^{c''d} S^{(1)\alpha'\beta'}(x'-y')_{j'k'}^{c'd} - \\ - S^{(0)\alpha\beta''}(x-y'')_{j''k''}^{cd''} S_2^{(1)} \begin{pmatrix} x'' & y \\ x' & y' \end{pmatrix}^{\alpha''\beta, c''d, j''k} -$$

$$\begin{aligned}
& + ig \int dx_1 S^{(0)\alpha\alpha_1} (x - x_1)_{jj_1}^{cc_1} \left\{ S_4^{(2)} \begin{pmatrix} x_1 & y \\ x_1 & x_1 \\ x' & y' \\ x'' & y'' \end{pmatrix} \begin{matrix} \alpha_1\beta, c_1d, j_1k \\ \alpha_2\alpha_2, c_2c_2, j_2j_2 \\ \alpha'\beta', c'd', j'k' \\ \alpha''\beta'', c''d'', j''k'' \end{matrix} - \right. \\
& - \gamma_5^{\alpha_1\alpha_2} \cdot \tau_{j_1k_1}^a S_4^{(2)} \begin{pmatrix} x_1 & y \\ x_1 & x_1 \\ x' & y' \\ x'' & y'' \end{pmatrix} \begin{matrix} \alpha_2\beta, c_1d, k_1k \\ \alpha_4\alpha_3, c_2c_2, j_2k_2 \\ \alpha'\beta', c'd', j'k' \\ \alpha''\beta'', c''d'', j''k'' \end{matrix} \gamma_5^{\alpha_3\alpha_4} \cdot \tau_{k_2j_2}^a + \\
& + S^{(0)\alpha_1\beta} (x_1 - y)_{j_1k}^{c_1d} S_3^{(2)} \begin{pmatrix} x_1 & x_1 \\ x' & y' \\ x'' & y'' \end{pmatrix} \begin{matrix} \alpha_2\alpha_2, c_2c_2, j_2j_2 \\ \alpha'\beta', c'd', j'k' \\ \alpha''\beta'', c''d'', j''k'' \end{matrix} - \\
& \left. - \gamma_5^{\alpha_1\alpha_2} \cdot \tau_{j_1k_1}^a S^{(0)\alpha_2\beta} (x_1 - y)_{k_1k}^{c_1d} S_3^{(2)} \begin{pmatrix} x_1 & x_1 \\ x' & y' \\ x'' & y'' \end{pmatrix} \begin{matrix} \alpha_4\alpha_3, c_2c_2, j_2k_2 \\ \alpha'\beta', c'd', j'k' \\ \alpha''\beta'', c''d'', j''k'' \end{matrix} \gamma_5^{\alpha_3\alpha_4} \cdot \tau_{k_2j_2}^a \right\}, \tag{11}
\end{aligned}$$

$$\begin{aligned}
& S_4^{(2)} \begin{pmatrix} x & y \\ x' & y' \\ x'' & y'' \\ x''' & y''' \end{pmatrix} \begin{matrix} \alpha\beta, cd, jk \\ \alpha'\beta', c'd', j'k' \\ \alpha''\beta'', c''d'', j''k'' \\ \alpha'''\beta''', c'''d''', j'''k''' \end{matrix} = \\
& = -S^{(0)\alpha\beta'} (x - y')_{jk'}^{cd'} S^{(0)\alpha'\beta} (x' - y)_{j'k}^{c'd} S_2^{(1)} \begin{pmatrix} x'' & y'' \\ x''' & y''' \end{pmatrix} \begin{matrix} \alpha''\beta'', c''d'', j''k'' \\ \alpha'''\beta''', c'''d''', j'''k''' \end{matrix} - \\
& - S^{(0)\alpha\beta''} (x - y'')_{jk''}^{cd''} S^{(0)\alpha''\beta} (x'' - y)_{j''k}^{c''d} S_2^{(1)} \begin{pmatrix} x' & y' \\ x''' & y''' \end{pmatrix} \begin{matrix} \alpha'\beta', c'd', j'k' \\ \alpha'''\beta''', c'''d''', j'''k''' \end{matrix} - \\
& - S^{(0)\alpha\beta'''} (x - y''')_{jk'''}^{cd'''} S^{(0)\alpha'''\beta} (x''' - y)_{j'''k}^{c'''d} S_2^{(1)} \begin{pmatrix} x' & y' \\ x'' & y'' \end{pmatrix} \begin{matrix} \alpha'\beta', c'd', j'k' \\ \alpha''\beta'', c''d'', j''k'' \end{matrix} + \\
& + ig \int dx_1 S^{(0)\alpha\alpha_1} (x - x_1)_{jj_1}^{cc_1} \left\{ S^{(0)\alpha_1\beta} (x_1 - y)_{j_1k}^{c_1d} S_4^{(2)} \begin{pmatrix} x_1 & x_1 \\ x' & y' \\ x'' & y'' \\ x''' & y''' \end{pmatrix} \begin{matrix} \alpha_2\alpha_2, c_2c_2, j_2j_2 \\ \alpha'\beta', c'd', j'k' \\ \alpha''\beta'', c''d'', j''k'' \\ \alpha'''\beta''', c'''d''', j'''k''' \end{matrix} - \right. \\
& \left. - \gamma_5^{\alpha_1\alpha_2} \tau_{j_1k_1}^a S^{(0)\alpha_2\beta} (x_1 - y)_{k_1k}^{c_1d} S_4^{(2)} \begin{pmatrix} x_1 & x_1 \\ x' & y' \\ x'' & y'' \\ x''' & y''' \end{pmatrix} \begin{matrix} \alpha_4\alpha_3, c_2c_2, j_2k_2 \\ \alpha'\beta', c'd', j'k' \\ \alpha''\beta'', c''d'', j''k'' \\ \alpha'''\beta''', c'''d''', j'''k''' \end{matrix} \gamma_5^{\alpha_3\alpha_4} \tau_{k_2j_2}^a \right\}, \tag{12}
\end{aligned}$$

The equations (11) and (12) are new in the given iteration scheme, and the equations (9) and (10) for the two-particle function $S_2^{(2)}$ and for propagator $S^{(2)}$ have the same

forms (see [10]), that the equations of the first step have, except of the nonhomogeneous members, in which the four-

particle function $S_4^{(2)}$ and three-particle function $S_3^{(2)}$ of the second step are included.

Here it is need to note, that the third step of iterations leads to the appearance of the equations for the six-particle (twelve-tail), fifth-particle (ten-tail), four-particle (eight-tail), three-particle (six-tail), two-particle (four-tail) one-particle

(propagator) functions. The above obtained equations allow to make the consequent theoretico-field calculation of the characteristics of hadronic decays, and also to investigate the possibilities of the dynamic description in the limits of the supposed approach of the interaction of the nucleons and new exotic baryons of pent quark type.

-
- | | |
|---|---|
| [1] <i>H. Bethe, E. Salpeter.</i> Phys.Rev.,1951,v.32, N1, p.309. | [8] <i>V.E. Rochev:</i> J.Phys. A: Math. Gen. 30 (1997)3671; |
| [2] <i>D.Z. Freedman, C. Lovlace, J.M. Namyslowski.</i> Nuovo Cim., 1966, v.43A, N2, p.258. | <i>V.E. Rochev and P.A. Saponov:</i> Int. J.Mod. Phys., 1998, v.A13, p.3649; <i>V.E. Rochev:</i> J.Phys. A: Math. Gen., 2000, v.33, p. 7379. |
| [3] <i>J.G. Taylor.</i> Phys.Rev., 1966, v.150, N4, p.1321. | [9] <i>V.E. Rochev:</i> in Proc. XIV Int. Workshop on High Energy Physics and Quantum Field Theory (QFTHEP'99, Moscow 1999, eds. <i>B.B. Levchenko and V.I. Savrin</i> , Moscow: MSU-Press, 1999, p.572 (hep-th/9911033). |
| [4] <i>K. Huang, H.A. Weldon.</i> Phys. Rev., 1975, v.D11, N2, p.257. | [10] <i>R.G. Jafarov and V.E. Rochev:</i> Centr. Eur. J. of Phys., 2004, v.2, p.367 (hep-ph/0311339). |
| [5] <i>V.E. Rochev.</i> TMF, 1982, v. 51, N1, p.22. | |
| [6] <i>Y. Nambu and G. Jona-Lasinio.</i> Phys. Rev., 1961, v.122, N1, p.345. | |
| [7] <i>S.P. Klevansky.</i> Rev. Mod. Phys., 1992, v.64, p.649. | |

R.Q. Cəfərov

NAMBU-YONA-LAZINIO MODELİNDƏ ÇOXKVARKLI QRİN FUNKSİYALARI ÜÇÜN TƏNLİKLƏR

Bilokal mənbəli orta sahə paylanması Nambu-Yona-Lazinio modelində çoxkvarklı Qrin funksiyaları üçün tənliklər alınmışdır.

Р.Г. Джафаров

УРАВНЕНИЯ ДЛЯ МНОГОВАРКОВЫХ ФУНКЦИЙ ГРИНА В МОДЕЛИ НАМБУ-ИОНА-ЛАЗИНИО

В разложении среднего поля с биллокальным источником в модели Намбу-Иона-Лазинио получены уравнения для многоварковых функций Грина.

Received: 26.04.05

OPTİK KANALLARDAKI MULTIPLİKATİV MANEƏLƏRİN TƏSİRİNİN AYIRICI PARAMETRLƏ QİYMƏTLƏNDİRİLMƏSİ

R.A. ABDULLAYEV, M. YÜKSƏK
Qafqaz Universiteti, Qars, Türkiyə

Məqalədə informasiya daşıyan faydalı signalın optik kanalda meydana gələn multiplikativ (moduledici) maneələr tərəfindən əlavə bir amplituda modulyasiyasına uğradığı və bunun nəticəsində signalın ortimal qəbulunun pisləşdiyi göstərilir. Burada təklif edilən ayırıcı parametrlə vasitəsilə müxtəlif multiplikativ maneələr yaranan optik kanalın effektivliyi hər bir hal üçün ayrıca statistik xarakteristikaları hesablamadan keyfiyyətə qiymətləndirilə bilirdiyi əsaslandırılır. Hesablamalar hər bir multiplikativ maneənin signalın qəbulunu çətinləşdirdiyini, bu təsirin signalın və maniyənin nisbi dispersiyasına bağlı olduğunu göstərir. Bu nöqtəyi-nəzərdən lazer şüalanmasına multiplikativ maneələrin təsiri daha az olduğundan informasiyanın ötürülməsi üçün daha yararlı olduğu nəticəsinə gəlirik.

Giriş

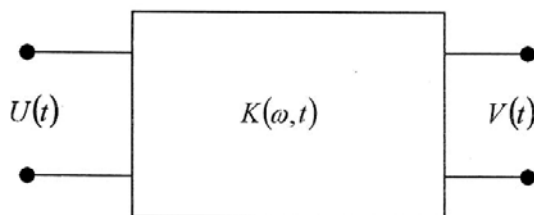
İnformasiyanın optik diapozonda ötürülməsi zamanı bu diapozona bağlı olan yeni xüsusiyyətlər ortaya çıxarır. Optik signalın kiçik intensivliklərində signalın optimal qəbulunda kvant-say metodundan istifadə edilir, yəni hər bir informasiya simvoluna müəyyən bir T zaman müddətində qeyd olunan foton sayı uyğun gəlir. Məlum olduğu kimi optik kanalın informasiya tutumu buradakı daxili və xarici maneələrə (küylərə) bərabər signalın kvant təbiətiylə də məhdudlaşır [1]. Bu zaman optik kanalda yaranan multiplikativ (moduledici) küylərin təsiri daha da artır. Çünki bu maneələr faydalı signalın şəklini dəyişdirdiyi kimi, onun statistik xarakteristikalarını da dəyişdirir [2]. Bu isə signalın qəbulunun orta xətasının artmasına səbəb olur.

Alınan nəticələr

Optik kanalın riyazi araşdırılması zamanı ona dəyişən parametrlə xətti dördqütblü kimi (şəkil 1) baxılır və ötürmə funksiyası $K(\omega, t)$;

$$K(\omega, t) = A(\omega, t) e^{i\varphi(t)} \quad (1)$$

şəklində yazılır [3]. Burada $A(\omega, t)$ dördqütblünün amplituda, $\varphi(t)$ faza xarakteristikasıdır.



Şəkil 1. Dəyişən parametrlə xətti dördqütblü kanalın girişindəki $U(t)$ analitik sinyali;

$$U(t) = x(t) \cdot a(t) \exp\{i[\omega_0 t + \Psi(t)]\} \quad (2)$$

şəklində yazaraq çıxışdakı $V(t)$ analitik signalı Furiye integralının köməyiylə

$$V(t) = \frac{1}{2\pi} \int_{-\infty}^{\infty} S(\omega) K(\omega, t) e^{i\omega t} d\omega \quad (3)$$

şəklində yazıla bilər. Buradakı $S(\omega)$ giriş signalının spektral sıxlığıdır.

Əgər $A(\omega, t)$ və $\varphi(t)$ funksiyalarının ω_0 daşıyıcı tezlik ətrafında ω yə görə Teylor sırasına ayıraraq sıranın iki ilk həddi ilə məhdudlaşdırılacaq (kiçik dispersiyası olan kanalda dar zolaqlı signallar üçün bu mümkündür, çünki bu halda signalın tezlik təhriflərinə uğraması diqqətə alınmayacaq qədər kiçik olur).

Beləliklə ötürmə funksiyası

$$K(\omega, t) \cong K(\omega_0, t) e^{-i(\omega - \omega_0)\tau} \quad (4)$$

şəklində düşür. Bu ifadədə

$$\tau = - \left. \frac{\partial \varphi(\omega, t)}{\partial \omega} \right|_{\omega = \omega_0} \quad (5)$$

olaraq işarə edilmişdir. (2) ifadəsini (3) də yazaraq bəzi sadə çevirmələri apardıqdan sonra dördqütblünün çıxışında alınan analitik signalın

$$V(t) = A(\omega_0, t) \cdot a(t - \tau) \exp\{i[\omega_0 t + \Psi(t - \tau) + \varphi(\omega_0, t)]\} \quad (6)$$

şəklində olduğu görünür. Buradakı $a(t) e^{i\Psi(t)}$ göndərilən informasiyaya uyğun olan və dəyişməyə uğramamış faydalı signalın kompleks amplitudasıdır. Optik kanalın çıxışında alınan analitik signalın (5) ifadəsinin girişindəki (2) analitik signalı ilə müqayisə edək. Burada $a(t)$ və $\Psi(t)$ modulə edilməmiş prosesdə amplituda və faza, $x(t)$ isə amplituda

modulyasiyasını göstərən həddləridir. Müqayisə göstərir ki, optik kanaldan keçən dar zolaqlı signal $A(\omega, t)$ qanunuyla dəyişən amplituda, $\varphi(\omega, t)$ qanunu ilə dəyişən faza modulyasiyasına uğrayır. Faza modulyasiyası heterodin tipli qəbulətilərdə və holografik sistemlərdə böyük əhəmiyyətə malikdir. Bizi maraqlandıran enerji həssasiyyətinə əsaslanan qəbulətilərdə faza modulyasiyasından istifadə olunmadığından

bu modulyasiyanı gələcəkdə diqqətə almayacağıq. (5) ifadəsi eyni zamanda optik kanalın çıxışındakı siqnalın girişindəkinə görə $\tau(t)$ gecikməsinə uğradığını göstərir. Bu hadisə faza-implus tipli optik sistemlərdə xüsusən çox böyük əhəmiyyətə malikdir. Dördqütblünün amplituda xarakteris-

$$a(t-\tau) \approx a(t-\tau_0) + \frac{d[a(t-\tau_0)]}{dt} \delta\tau(t) = a(t-\tau_0)[1 + \xi(\tau)] \quad (7)$$

yazdığımız zaman

$$\xi(\tau) = \frac{\frac{d[a(t-\tau)]}{dt}}{a(t-\tau_0)} \cdot \delta\tau(t) \quad (8)$$

həddinin əlavə küy modulyasiyasının ifadə etdiyi ortaya
ÇIXIR.

Beləliklə, dəyişən parametrlı optik kanaldan keçən faydalı siqnalın burada yaranan multiplikativ (və ya modulə edici) maneələr tərəfindən əlavə amplituda modulyasiyasına uğradığı görünür. Foton-say prinsipinə əsaslanan optik qəbuledicilərdə bu küylərin ilk növbədə verilən T müddətində qeyd olunan fotoelektronların n sayının $P(n)$ paylanma funksiyasının dəyişməsinə səbəb olur. Buna görə optik informasiya kanalını yaradarkən qabaqcıdan burada ortaya çıxacaq multiplikativ maneələrin təsiri nəzərə alınmalıdır.

Optik rabitə və lokasiya sistemlərinin nəzəri araşdırılmasında və mühəndislik layihələndirilməsində optik sahələrin statistik xarakteristikaların bilinməsinə böyük ehtiyac vardır. Bunların içində ən əhəmiyyətli qəbuledicilərin çıxışında alınan fotoelektronların $P(n)$ paylanma funksiyasıdır. Statistik xarakteristikalar məlum olduğu zaman qəbuledici qurğuların optimal quruluşu seçilə bilər, optik signalın funksiyaları müəyyənləşdirilir və istifadə edilən elektron cihazların həssasiyyətinin sərhəd qiymətləri tapılır. Prinsipcə ortaq kA-nalda additiv və multiplikativ maneələr olduğu hər bir hal üçün $P(n, T)$ funksiyaları hesablanaraq qəbuledicinin buna uyğun olan optimal quruluşu seçilir [4].

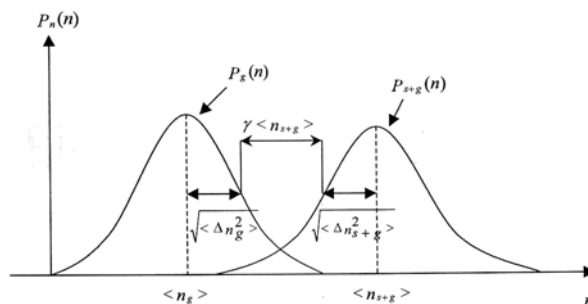
Amma hər bir hal üçün bu xarakteristikalar xüsusi olaraq hesablandıqlarından mürəkkəb və vaxt alan bir prosesdir. Halbuki, aşağıda göstərəcəyimiz kimi qəbul edilən siqnalın flüktüasiya xassələrini nəzərə alan bir kəmiyyətdən istifadə edərək optik rabitə sisteminin effektivliyini tez və asan qiymətləndirmək mümkündür. Optik diapazonda qəbuledicinin girişindəki siqnalların intensivliyi kiçik olduğundan radiodiapozondakı siqnal maneə nisbətinə əsaslanan qiymətləndirmə burada yetərsiz olur. Bu halda siqnal və küy flük-

tikasının mailliyi az olduğu halda $a(t - \tau)$ ifadəsini $(t - \tau_0)$ nöqtəsi ətrafında (burada τ_0 orta gecikmə dəyəridir) Teylor sırasına ayıraraq, bu gecikmə hadisəsinin signalın amplitudasının əlavə bir küy modulyasiysına gətirdiyini görürük. Doğrudan da

tüsiyalarının statistik xarakteristikalarının əhəmiyyəti daha da artacaqdır. Bu durumda optik qəbuledicinin effektivliyinin keyfiyyətə qiymətləndirilməsi qəbul edilən signalın flüktüasiya xassələrini əhatə edən kəmiyyətlərə əsaslanmalıdır. Bu məqsədlə maneə prosesi ilə signal və maneə süperpozisiyasını prosesini bir-birindən ayırmasına əsaslanan

$$\gamma = \frac{\left[\langle n_{s+g} \rangle - \sqrt{\langle \Delta n_{s+g}^2 \rangle} \right] - \left[\langle n_g \rangle + \sqrt{\langle \Delta n_g^2 \rangle} \right]}{\langle n_{s+g} \rangle} \quad (9)$$

kəmiyyəti seçilə bilər. Ayrıçı parametrlər adlandıracağımız bu kəmiyyətin (8) ifadəsindəki $\langle n \rangle$ və $\langle \Delta n^2 \rangle$ kəmiyyətləri indekslərinə uyğun olaraq maneə və signal + maneə proseslərinin orta dəyərləri və dispersiyalarıdır. Ayrıçı parametrlərin fiziki mənası şəkildən aydın olur.



Şəkil 2. Ayırıcı parametrin göstərilməsi

Buradan göründüyü kimi γ artdıqca küylərin və siqnal ilə maneələrin toplamının paylanma funksiyaları bir-birindən o qədər çox ayrılmış olur və bununla siqnalın ayrılma ehtimalı çoxalır. Multiplikativ maneələrin təsiri γ ayrıca parametrinin, bu maneələrin olmadığı γ_0 qiymətindən olan fərqlə qiymətləndirmək daha faydalıdır, çünki bu halda daha sadə ifadələr alınır. Doğrudan da bu zaman

$$\Delta\gamma = \gamma_0 - \gamma = \sigma^2 \left\{ \left[1 + \frac{\langle n_{s+g} \rangle^2}{\langle \Delta n_s^2 \rangle + \langle \Delta n_g^2 \rangle} \cdot \sigma_l^2 (1 + \sigma_w^2) \right]^{\frac{1}{2}} - 1 \right\} \quad (10)$$

olur. Burada σ_w^2 , σ_I^2 , və σ^2 uyğun olaraq siqnalın, multiplikativ maneənin və modulə edici maneə olmadığı halda siqnal və additiv küylərin birgə fotosayı paylanmalarının nisbi dispersiyalarıdır. (10) dan görüldüyü kimi $\Delta\gamma \geq 0$ olur, yəni istənilən multiplikativ maneə siqnalın qəbulunu pisləşdirir və bu, siqnalın σ_w^2 , modul edici maneənin σ_I^2 nisbi dispersiyası ilə artır. Bununla birlikdə

informaiya daşıyan siqnalın flüktüasiyaları böyük olduğu
durumda multiplikativ maneələrin təsiri daha çox olur. Bu
nöqteyi-nəzərdən konkret şüalanma mənbələrinin istənilən
multiplikativ maneə üçün daha çox optimal olduğunu
görürük. Modulə edici maneələrin nisbi dispersiyasının kiçik
olduğu halda, yəni $\sigma_l^2 \ll 1$ olduğundan (10) ifadəsini sıraya
ayırıraq ilk iki hədlə kifaəytlənərək

$$\Delta\gamma \approx \frac{1}{2} \cdot \frac{\sigma_I^2(1 + \sigma_w^2)}{\sqrt{\sigma_I^2 + \sigma_w^2 + \sigma_I^2 \sigma_w^2 + \frac{1}{\langle n_g \rangle \chi} \left(1 + \frac{1}{\chi}\right) + \frac{\sigma_w^2}{\chi^2}}} \quad (11)$$

yaza bilərik. Burada $\chi = \frac{\langle n_s \rangle}{\langle n_g \rangle}$ siqnal maneə nisbətidir.

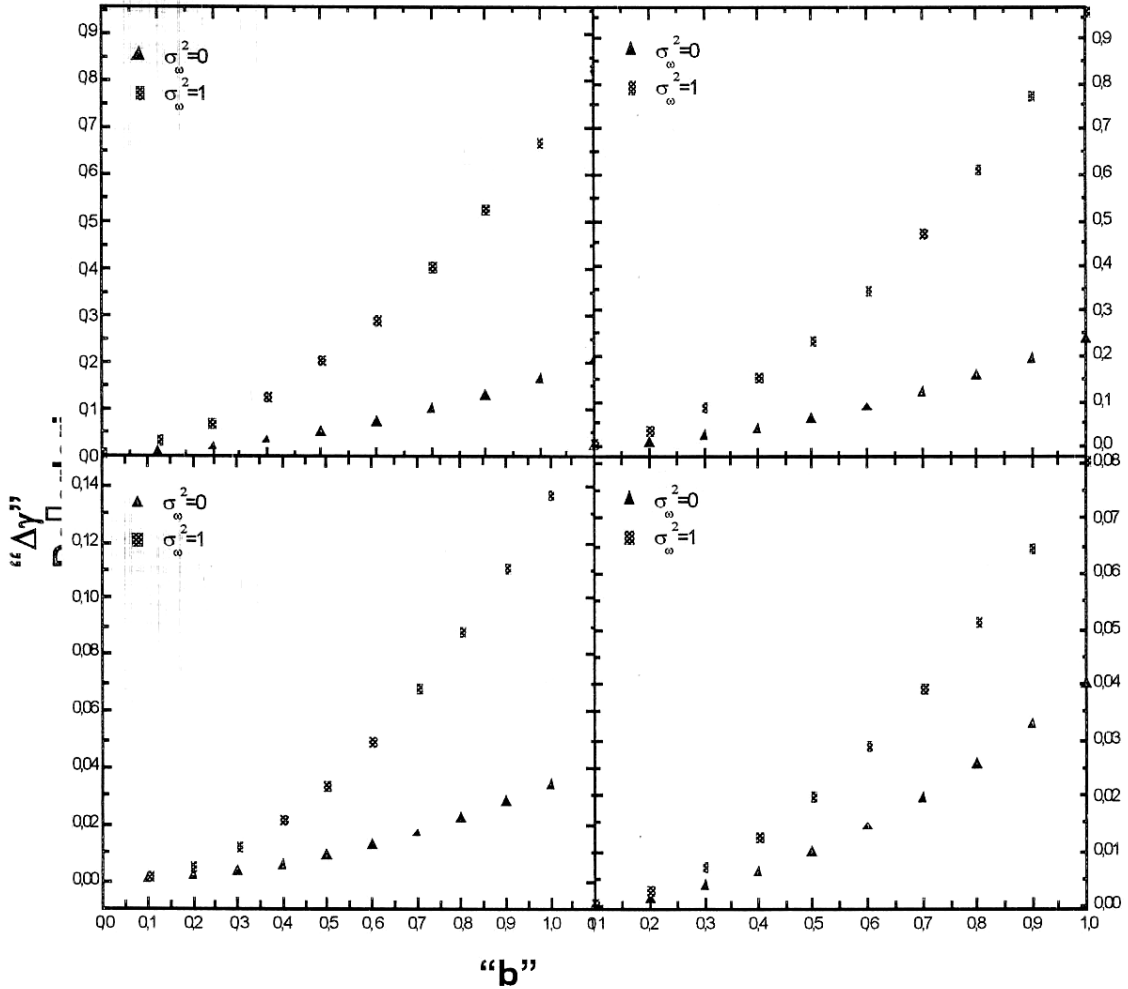
$\chi \gg 1$ olduğu halda bu ifadə daha çox sadələşərək

$$\Delta\gamma = \frac{1}{2} \cdot \frac{\sigma_I^2(1 + \sigma_w^2)}{\sqrt{\sigma_I^2 + \sigma_w^2 + \sigma_I^2 \sigma_w^2}} \quad (12)$$

şəklinə düşər. Bu yaxınlaşmada $\Delta\gamma$ nın additiv küylərdən asılı olmadığı və σ_I^2 və σ_w^2 kəmiyyətləri ilə mütənəsb arttığını görürük. Alınan nəticələri əyani olaraq göstərmək

üçün şəkil 3-də $\langle n_g \rangle = 0,1$, $\chi = 10$ və $\chi = 50$ qiymətləri üçün (10) ifadəsi ilə hesablanmış qiymətlərinin multiplikativ maneələrin modulyasiyası əmsalı b ilə dəyişməsi verilir.

Siqnal mənbəyi olaraq lazer ($\sigma_w^2 = 0$) və darzolaqlı istilik mənbəyi ($\sigma_w^2 = 1$) görürülmüşdür[5]. Multiplikativ maneələr xətti dəyişən ($\sigma_I^2 = \frac{b^2}{12}$) və sinusoidal ($\sigma_I^2 = \frac{b^2}{2}$) siqnallarla appoksimə edilmişdir [6].



Şəkil 3. Ayrıcı parametrin işıq mənbəyinə, multiplikativ maneə növünə və modulyasiya əmsalına bağlılığı. Soldakı qrafiklərdə siqnal maneə nisbəti $\chi = 10$, sağdakılarda isə $\chi = 50$ 'dir. Koherent mənbə üçün üçbucaq nöqtələr ($\sigma_w^2 = 0$), istilik mənbələri

üçün düzbucaq nöqtələr ($\sigma_w^2 = 1$) olaraq hesablanmışdır. Sinusoidal maneələrdə $\sigma_I^2 = \frac{b^2}{2}$; xətti dəyişən maneələrdə

$\sigma_I^2 = \frac{b^2}{12}$ olaraq götürülmüşdür.

Alınan nəticələrin müzakirəsi

Qrafiklərdən göründüyü kimi $\Delta\gamma$ signal maneə nisbəti χ artdıqda artır. Beləliklə additiv küylərin olmadığı ideal sistemlərdə multiplikativ maneələrin təsiri daha çoxdur nəticəsinə gəlirik. Bununla bərabər yuxarıda qeyd etdiyimiz kimi $\Delta\gamma$, istilik mənbələrini şüalanmasında koherent

mənbəyinə görə daha böyük alınır, çünki koherent mənbəyin fotosayı paylanması dispersiyası iki qat azdır. Qrafiklər eyni zamanda xətti dəyişən maneələrin təsirinin sünisoldal şəkildə dəyişən maneələrə görə daha az olduğunu göstərir. Alınan nəticələr binar kodlanmış kvant say sistemləri üçün aparılmış hesablamalara uyğun gəlir [7].

- | | |
|---|---|
| [1] <i>J. Arnaud</i> , Opt. Quant. Elektron. 2002, 34, №4, 393 s. | [5] <i>R.Ya. Abdullayev, M.I. Jenik</i> , Baki Universitetinin khaberleri, fiz –mat.el.ser. 2003, №3, 143 s. |
| [2] <i>A.A.Egorov</i> , Opt. Spekr., 2003, 95, №2, 276 s. | [6] <i>R.A. Abdullaev, I.A. Deryugin, B.N. Kurashov, V.N. Nastich</i> , Uchenie zapiski AGU, ser. fiz.- mat nauk, 1972, №4, 88 s. |
| [3] <i>I.E. Kremer, V.I. Vladimirov, B.I.Karpukhin</i> , Moduli- ruyushie pomekhi i priyom radiosignalov. M., 1972. | [7] <i>I.A. Deryugin, V.N. Kurashov, A.V. Mashenko</i> , Izv. VUZ, Radioelektron, 1980, №5, 98 s. |
| [4] <i>A.Q. Sheremetev</i> , Statisticheskaya teoriya lazernoy svyazi. M., 1971. | |

R.A. Abdullayev, M. Yuksek

THE ESTIMATION OF OPTICAL CHANNEL WITH MULTIPLICATIVE NOISE BY USING OF SEPARATING PARAMETER

It is shown that optical signal carrying information in optical channel with multiplicative (modulated) noise is exposed to additional modulation. The offered separation parameter allows to estimate the efficiency of optical channel in the presence of different multiplicative noise without calculation of statistical characteristics of accepted signal. Our calculations showed out that any modulating noise corrupts of signal acceptance and the corruption degree depends both on relative dispersions of optical signal and multiplicative noise. Thus the coherent signal of laser radiation undergoes to the influence of any multiplicative noise in less degree and because is more acceptional for the information delivery.

Р.А. Абдуллаев, М. Юксек

ОЦЕНКА ОПТИЧЕСКОГО КАНАЛА С МУЛЬТИПЛИКАТИВНЫМИ ПОМЕХАМИ С ПОМОЩЬЮ ПАРАМЕТРА РАЗДЕЛЕНИЯ

В статье показано, что оптический сигнал, носящий информацию в оптическом канале с мультипликативными (модулирующими) помехами подвергается дополнительной амплитудной модуляции. Предложенный параметр разделения позволяет оценить эффективность оптического канала при наличии различных мультипликативных помех без вычисления статистических характеристик принимаемого сигнала. Вычисления показывают, что любая модулирующая помеха ухудшает условия приема, и это зависит от относительных дисперсий, как оптического сигнала, так и мультипликативной помехи. С этой точки зрения когерентный сигнал лазерного излучения подвергается меньшему влиянию любых мультипликативных помех, и он является наиболее оптимальным для передачи информации.

Received: 20.09.05

POSSIBLE CAUSES OF SCREEN BACKGROUND RADIATION OF ELECTRO-OPTICAL TRANSFORMER (EOT)

X.N. VEZIROV, N.I. IBRAGIMOV

*Institute of Physics of NASA,
Baku Az-1143, G. Javid av., 33, Azerbaijan*

The analysis of the possible mechanisms of the appearance of the screen background radiation of (EOT) has been carried out.

As it is known, the electron (ϕ) work function for the effective functioning of the photocathode should be less than the energy of the absorbed photon. The important circumstance is the spectral distribution of the photosensitivity. Nowadays the photocathodes Ag – O – Cs have the biggest photosensitivity in the wave-length region of the spectrum (nearest is infrared). At the same time these photocathodes have the biggest current density of the thermionic emission at the room temperature [1]. However, the thermionic emission of photocathode of EOT is very undesirable, i.e. it leads to the appearance of the parasitical background radiation of the luminescent screen. The big quantity of the investigations on the revealing of the mechanisms, causing this phenomenon has been carried out, but the final answer hasn't been found yet. Thus, in the ref [2] the high density of the thermionic current (as cause – background radiation) connects with presence of the caesium oxide in the photocathode, and in the ref [3] it connects with the existence of the corpuscular caesium in the photocathode. Below we will consider the set of another circumstances, which can cause the screen background radiation of EOT.

The metallic argentine, evaporated in high vacuum ($p < 10^{-6}$ mm of mercury) at the production of Ag – O – Cs photocathode oxidizes [4]. As Ag_2O and Ag have different crystalline structure, and the pressure of the steams of oxygen under Ag_2O is significantly even at the room temperature, so Ag_2O film can't be total and consists from the smallest particles. The photocathode formation carries out in the result of the interaction of the gaseous caesium with the oxidated film of argentine. The caesium oxides, rolling each submicroparticle of argentine are created at Cs evaporation because of the presence of the oxygen around Ag_2O particles [5]. The pressure of the saturated steams of the oxygen under Ag_2O at $400\text{K} \approx 58\text{mm}$ of mercury, and at 450K is 464mm of mercury [2]. Thus, Ag_2O decomposes with the creation of the metallic argentine at the photocathode formation in the evacuated volume, and evaporated Cs transfers into Cs_2O (as in the solid phase because of the diffusion processes, so in the gas phase directly). The creation of the caesium oxide, which as impurity in Cs_2O (semiconductor with forbidden band width is $\approx 2,4\text{eV}$ approximately [4]) influences on the photocathode characteristics, creating the p-type levels in the forbidden band Cs_2O and causes the chemisorption of corpuscular Cs in the evaporation process of the last is possible because of the excess of the oxygen.

For the increase of the emission ability of the cathode it is needed to form thin layer of the metal with the low ionized potential on its surface. The use of Cs is caused by the fact, that it has the less work function ($\phi = 1,87 \div 1,94\text{ eV}$ [6,7]), melting temperature (303K) and high pressure of the saturated steams at the moderate temperatures (for example at

$423\text{K} \approx 10^{-2}$ mm of mercury [7]) among alkali elements. In the result of the thermal ionization the electrons of Cs atoms transfer into the conductivity band of Cs_2O and the negative volume charge forms in the near-surface layer, which is equal to the charge of the positive ions (Cs^+) on the surface. The electric field of the double layer, created by this way leads to the decrease of the cathode work function. The work function of photocathode Ag – O – Cs, defined on the red line ($\approx 1300\text{ nm}$) is $\phi \approx 0,95\text{eV}$, the measures on the method of the contact potential difference give the same value [6].

The integral sensitivity of photocathode Ag – O – Cs achieves $\approx 8 \cdot 10^{-5}\text{ A/Lm}$, and quantum efficiency in the wave-length region of the spectrum $\approx 0,002\text{ el/kv}$. [6].

The semiconductor layer Cs_2O , supplying the photosensitivity in the short-wave region and the colloidal particles of the argentine, covered by caesium, causing the photosensitivity in the wave-length region of the radiation are the main emitters in the photocathode Ag – O – Cs. The spectral sensitivity of the photocathode includes the spectrum region $\approx 300 \div 1300\text{ nm}$ (with maximums ≈ 350 and $\approx 800\text{ nm}$). The typical spectral distribution of the photosensitivity of photocathode Ag – O – Cs is given on the fig.1.

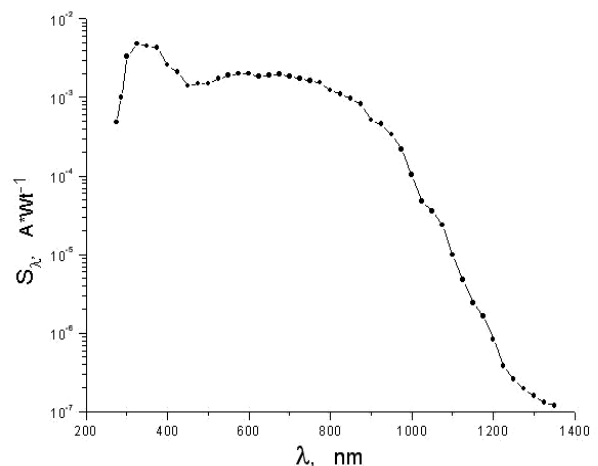


Fig. 1.

In spite of the big quantity of the data the detail structure of photocathode Ag – O – Cs hasn't been established yet. The finally formed cathode is multicomponent and complex system, consisting from Ag, Cs and semiconductors Ag_2O , Cs_2O . The quantitative ratio of the components and technological steps, supplying optimal photoemission and spectral sensitivity, are chosen by the experimental way in the process of photocathode formation, and this can't be reflected on screen background radiation of EOT.

Let's consider the set of the circumstances, causing the appearance of the screen background radiation of EOT. The exclusive purity of the surface as the base (substrate), so photocathode is the important thing, i.e. the absence of the roughnesses and adsorbed alien atoms (molecules) that can cause the filling of the surface levels by the current carriers with all consequences. In spite of the fact, that modern technological methods allow to come to the minimum this circumstance, it is impossible to exclude it totally.

It is widely known, that the islands of the (aggregation) metal form on the substrate at the precipitation (evaporation) of thin layers (≈ 10 nm) of Cs or Ag because of the high mobility of the condensated atoms even at the enough low temperature of the substrate. And this, on the level with the technological fluctuations, is the one of the important reasons of the incomplete repeatability of the properties, produced photocathode. Moreover, the isle structure can cause the significant background radiation. Thus, if we are proceed from theory of Langmuir spots [6], then the local work functions of the separate regions won't be similar because of the irregularity of the cesium distribution on photocathode surface and consequently, the photo- and thermoemission of the electrons will be different from these regions and this will create directly nonhomogeneous distribution of the brightness of screen background radiation on the screen of EOT.

At the isle distribution the interfaces between particles Ag, Cs and Cs₂O present the enough developed surface with the irregulars and microlugs and the effect of the strong field appears at the current chose from the photocathode on the anode because of the known phenomena of the increase of the electric field on the microlugs [8], that leads to the increase of the electron emission from these regions, i.e. to background screen radiation. And indeed, it is established by the electron-microscopic investigations, that sizes of metal particles (Ag, Cs) ≈ 10 nm, sizes of the irregulars on these particles ≈ 1 nm. Thus, the size of the canals, where electrons can tunneled through the barrier in the boundary layer from the metals as into cesium oxide, so into vacuum because of the effect of the strong field.

For the calculation of the gain β we can use the formula [9]:

$$\beta = \frac{1,89 \cdot 10^9 \cdot \varphi_0^{3/2} \cdot \Delta d}{\chi \varepsilon},$$

Where Δd is thickness of semiconductor Cs₂O film (m), ε is its dielectric constant, χ is the energy of the electronic relationship of the semiconductor (external work function in eV), φ_0 is metal work function (eV). Substituting the typical values of the parameters of the semiconductor film and metal ($\Delta d \approx 40$ nm, $\varepsilon \approx 8$, $\chi \approx 0,3$ eV, $\varphi_0 \approx 4,5$ eV [1,10]), we obtain that β can achieve the value ≈ 300 .

Thus, the resistance of the electric field can achieve the value $\approx 3 \cdot 10^5$ V/cm at the usual values of the electric fields for the vacuum volume of EOT ≈ 1000 V/cm in separate regions of the photocathode. At such electric fields the significant current of the autoelectronic emission even from the metals is observed. The density of the dark current of the autoelectronic emission from photocathode Ag – O – Cs achieves the value $\approx 10^{-10}$ A/cm at the room temperature, and isle character of the autoelectronic emission causes the background luminescence of the screen.

The photocathode Ag – O – Cs has the significant second electronic emission because of the electron warming-up, thermoexcited into the conductivity band Cs₂O by the electric field inside the last one (especially at the existence Cs⁺ ions on the photocathode surface). The coefficient of the second electronic emission ≈ 10 at the energy of the primary electrons 600eV and ≈ 4 at 100eV [11]. Finally the current of the photocathode emission even at the constant luminescence isn't strictly constant; it has the statistical fluctuation (shot noise). The second electronic emission and shot effect also are causes of the original background luminescence of the screen of EOT.

All above mentioned factors (each separately and in aggregate) put the definite contribution in the parasitic background radiation of the luminescent screen of the electron-optical transformer.

- | | |
|---|---|
| <p>[1] <i>V.S. Fomenko.</i> Emissionnie svoistva materialov. Spravochnik, Naukova dumka, Kiev, 1981, c.223.</p> <p>[2] <i>B.M. Gugel, A.E. Melamid, B.M. Stepanov.</i> Radiotekhnika i elektronika, 1977, т.22, № 7, c.1466.</p> <p>[3] <i>M.T. Pakhomov, A.E. Melamid.</i> Izv. AN SSSA, ser. fiz., 1971, т.35, № 3, c.612.</p> <p>[4] <i>A.Kh. Sommer.</i> Fotoemissionnie materiali. Energiya, M., 1973 c. 123.</p> <p>[5] <i>B.M. Gugel, A.Ya. Krupenina, A.E. Melamid, B.M. Stepanov.</i> Radiotekhnika i elektronika. 1982, № 3, c. 586.</p> <p>[6] <i>L.N. Dobretsov, M.V. Gomoyunova.</i> Emissionnaya elektronika, Hayka, M., 1966, c.149.</p> | <p>[7] <i>T. Reykhel, M. Iedlichka.</i> Fotoelektronnie katodi. Energiya, M., 1968, c.70.</p> <p>[8] <i>I.N. Slivkov.</i> Protsey pri visokom napryajenii v vakuume. Energo-atomizdat, M., 1986, c.256.</p> <p>[9] <i>R.V. Latham.</i> The origin of prebreakdown electron emission from vacuum-insulated high voltage electrodes. Vacuum, 1982, v.32, № 3, p.137.</p> <p>[10] <i>V.E. Kondrashov.</i> Optika fotokatodov. Nauka, M., 1976, c.121.</p> <p>[11] <i>W. Hartmann u. F. Bernhard.</i> Fotovervielfacher, Berlin, Akad. Verlag, 1957, p.102.</p> |
|---|---|

H.N. Vəzirov, N.İ. İbrahimov

ELEKTRON – OPTİK ÇEVİRİCİ EKRANININ KÜY ŞUALANMASININ SƏBƏBLƏRİ HAQDA

Elektron-optik çevirici ekranının küy şualanmasının səbəbləri araşdırılmışdır.

Х.Н. Везиров, Н.И. Ибрагимов

**О ВОЗМОЖНЫХ ПРИЧИНАХ ФОНОВОГО ИЗЛУЧЕНИЯ ЭКРАНА ЭЛЕКТРОННО-ОПТИЧЕСКОГО
ПРЕОБРАЗОВАТЕЛЯ (ЭОП)**

Проведен анализ возможных механизмов возникновения фоновое излучения экрана ЭОП.

Received: 30.06.05

EDGE STATES IN A KANE TYPE SEMICONDUCTOR QUANTUM WIRE

A.M. BABAYEV^{a,b}, Ş. ÇAKMAKTEPE^b, A. KÖKÇE^b^a*Institute of Physics, Azerbaijan Academy of Sciences, Baku 370143, Azerbaijan*^b*Department of Physics, University of Suleyman Demirel, Isparta 32260, Turkey*

The energy spectra of carriers confined to a cylindrical semiconductor quantum wire in an inhomogeneous magnetic field which is $B = 0$ $r < r_0$ and $B \neq 0$ elsewhere are studied by, taking into account the real band structure of InSb type semiconductors; narrow energy gap and strong spin-orbit interaction. It's found that the eigen energy spectra for the magnetic quantum wire critically depend on the number of missing flux quanta. Since the spin effect is taken into account, each energy curve splits into two curves. The crossover point of energy curves for $m=0$ state with opposite spins is obtained around the value of $S=8$. The magnetic field and the radius dependence of the edge g-factor is also studied.

1. Introduction

Recently there has been a great interest in the behavior of carriers with an inhomogeneous perpendicular magnetic field about low-dimensional systems both theoretically and experimentally [1,2]. On the other hand edge states play an important role in understanding the transport properties of quantum nanostructures [3]. Magnetic edge state in a magnetic quantum wire becomes quite popular, in particular conjunction with a possible candidate for a high density memory device or spintronic materials, so various magnetic nano-quantum structures are reviewed in detail [4]. Advances with respect to growth as well as high-resolution electron-beam lithography techniques allow the novel confined structures called quantum wires or quantum rings. Transport properties of edge states in quantum nanostructures have been discussed by many groups. Peeters, Matulis and İbrahim [5] presented energy levels in the magnetic antidote, while Reijneries, Peeters and Matulis [6] further performed a more detailed and complete study of the bound states of such a system. Solimay and Kroner [7] solved the classical and quantum mechanical equations for a magnetically confined quantum dot and discussed the eigen energies. Badalyan and Peeters have developed a theory for the non-homogeneous magnetic field induced magnetic edge states and their transport in a quantum wire formed by a parabolic confining potential [8]. Ihm et al [9,10] investigated the two dimensional electrons further confined in an inhomogeneous magnetic field. They have found that the eigenstates deviated from Landau levels, due o the non-uniform magnetic field distributions, forming the magnetic edge states which critically depend on the number of missing flux quanta within

the dot or the ring. Recently Young Guo et al [11] investigated the electron spin effect on quantum states and magneto-conductance in a magnetic quantum antidote with inhomogeneous magnetic field results in further splitting of energy levels. In the work of [12] the electron states and circulating probability currents due to the inhomogeneous field distribution formed in a magnetic quantum ring is studied. However, the experimental advantages of using narrow-gap semiconductors for the reduced dimensionality systems make it necessary to account for the real band structure of these materials. The purpose of our work is taking into account the coupling of the conduction and valence bands and the non-parabolicity of the electron dispersion while studying the narrow and medium gap semiconductors. It's also aimed to study the magnetic field and the radius change of edge g-factor. In the present study, using eight band Kane's model including the conduction band, light and spin orbital hole bands, the energy spectrum and edge g-factor of electrons confined to a cylindrical semiconductor quantum wire (InSb) in an inhomogeneous magnetic field which is $B = 0$ $r < r_0$ and $B \neq 0$ elsewhere are investigated. In the eight-band Kane's Hamiltonian the valence and conduction bands interaction is taken into account via the only matrix element P (so called Kane's parameter). We also neglect the free-electron term in the diagonal part and the Pauli spin term as they give small contributions to the effective mass and the spin g-value of electrons in InSb. The system of Kane equations including the non-dispersional heavy hole bands have the form [13,14,15,16]:

$$-EC_1 - \frac{Pk_-}{\sqrt{2}}C_3 + \sqrt{\frac{2}{3}}Pk_zC_4 + \frac{Pk_+}{\sqrt{6}}C_5 + \frac{Pk_z}{\sqrt{3}}C_7 + \frac{Pk_+}{\sqrt{3}}C_8 = 0 \quad (1)$$

$$-EC_2 - \frac{Pk_-}{\sqrt{6}}C_4 + \sqrt{\frac{2}{3}}Pk_zC_5 + \frac{Pk_+}{\sqrt{2}}C_6 + \frac{Pk_-}{\sqrt{3}}C_7 - \frac{Pk_z}{\sqrt{3}}C_8 = 0 \quad (2)$$

$$-\frac{Pk_+}{\sqrt{2}}C_1 - (E + E_g)C_3 = 0 \quad (3)$$

$$\sqrt{\frac{2}{3}}Pk_zC_1 - \frac{Pk_+}{\sqrt{6}}C_2 - (E + E_g)C_4 = 0 \quad (4)$$

$$\sqrt{\frac{2}{3}}Pk_z C_2 + \frac{Pk_-}{\sqrt{6}}C_1 - (E + E_g)C_5 = 0 \quad (5)$$

$$\frac{Pk_-}{\sqrt{2}}C_2 - (E + E_g)C_6 = 0 \quad (6)$$

$$\frac{Pk_z}{\sqrt{3}}C_1 + \frac{Pk_+}{\sqrt{3}}C_2 - (\Delta + E + E_g)C_7 = 0 \quad (7)$$

$$\frac{Pk_-}{\sqrt{3}}C_1 - \frac{Pk_z}{\sqrt{3}}C_2 - (\Delta + E + E_g)C_8 = 0 \quad (8)$$

Here P is the Kane parameter, E_g - the band gap energy, Δ - the value of spin-orbital splitting and $k_{\pm} = k_x \pm ik_y$, $\vec{k} = -i\vec{\nabla}$, C_i are envelope functions.

2. Theory

The model that is considered in the present study is composed of an electron confined to move in a cylindrical semiconductor quantum wire under the influence of a magnetic field in the z -direction, which is non-zero except with a cylinder of radius r_0 . The magnetic field is described by

$$\vec{B}(\vec{r}) = \begin{cases} B\hat{e}_z & (r > r_0) \\ 0 & (r < r_0) \end{cases} \quad (9)$$

Then the vector potential will be as follows;

$$\vec{A} = \frac{1}{2} \left(1 - \frac{r_0^2}{r^2} \right) B(-y, x, 0) \quad (10)$$

k_{\pm} have forms

$$k_{\pm} \rightarrow k_{\pm} \pm i \frac{1}{2} \lambda_H \left(1 - \frac{r_0^2}{r^2} \right) r_{\pm} \quad (11)$$

where

$$r_{\pm} = x \pm iy, \lambda_H = \frac{eH}{\hbar c} \quad (12)$$

One can now express the envelope functions C_3, C_4, \dots, C_8 by the functions C_1 and C_2 respectively, and substitute them into the first and second equations, we finally obtain the following decoupled equations for $C_{1,2}$:

$$\left(-\varepsilon - \frac{P^2}{3} \left(\frac{2}{\varepsilon + \varepsilon_g} + \frac{1}{\varepsilon + \varepsilon_g + \Delta} \right) \Delta_3 \right) C_{1,2} = 0 \quad (r < r_0) \quad (13)$$

where Δ_3 is three dimensional Laplacian.

When there is magnetic field

$$\left\{ \begin{aligned} & -\varepsilon + \frac{P^2}{3} \left(\frac{2}{\varepsilon + \varepsilon_g} + \frac{1}{\varepsilon + \varepsilon_g + \Delta} \right) \left\{ -\nabla^2 + 2\lambda_H \hbar^{-1} (1 - r_0^2 r^{-2}) L_z + \lambda_H^2 (1 - r_0^2 r^{-2})^2 r^2 \right\} \pm \\ & 2\lambda_H \frac{P^2}{3} \left(\frac{1}{\varepsilon + \varepsilon_g} - \frac{1}{\varepsilon + \varepsilon_g + \Delta} \right) \end{aligned} \right\} C_{1,2} = 0 \quad (r > r_0) \quad (14)$$

where L_z , z component of angular momentum operator L and $r^2 = x^2 + y^2$.

The wave functions in cylindrical coordinates are separable;

$$C_{1,2} = e^{im\phi + ik_z z} \phi_{1,2}^1(r) \quad (r < r_0) \quad (15)$$

$$C_{1,2} = e^{im\phi + ik_z z} \phi_{1,2}^2(r) \quad (r > r_0) \quad (16)$$

where m is the angular momentum quantum number. The equation of the radial part is written as;

$$\left[\frac{d^2}{dr^2} + \frac{1}{r} \frac{d}{dr} + \left(\frac{2m_n E_1'}{\hbar^2} - \frac{m^2}{r^2} \right) \right] \phi_{1,2}^{(1)}(r) = 0 \quad r < r_0 \quad (17)$$

$$\left[\frac{d^2}{dr^2} + \frac{1}{r} \frac{d}{dr} + \left(\frac{2m_n E_2'}{\hbar^2} - \frac{(m-s)^2}{r^2} - r^2 - \lambda_H (m-s) - \frac{e^2 H^2}{4\hbar c^2} r^2 \right) \right] \phi_{1,2}^{(2)}(r) = 0 \quad r > r_0 \quad (18)$$

Here $E'_1 = \frac{\hbar^2}{2m_n} \left(\frac{3}{P^2} \frac{\varepsilon(\varepsilon + \varepsilon_g)(\varepsilon + \varepsilon_g + \Delta)}{(3\varepsilon + 3\varepsilon_g + 2\Delta)} - k_z^2 \right)$, and

$$E'_2 = \frac{\hbar^2}{2m_n} \left[\frac{3}{P^2} \frac{\varepsilon(\varepsilon + \varepsilon_g)(\varepsilon + \varepsilon_g + \Delta)}{(3\varepsilon + 3\varepsilon_g + 2\Delta)} \mp \lambda_H \frac{\Delta}{3\varepsilon + 3\varepsilon_g + 2\Delta} \right]$$

$\phi_{1,2}^{(1)}(r)$ is expressed as $\phi_{1,2}^{(1)}(r) = C_1 J_{|m|}(\sqrt{\chi}r)$ where the function J_m is the Bessel function of order m ,

$\phi_{1,2}^{(2)}(r) = C_2 r^{|m-s|/2} e^{-\frac{r^2}{2}} U(a, b, x)$ where $U(a, b, x)$ is the confluent hypergeometric function [17].

In here

$$\chi^2 = \frac{2m_0}{\hbar^2} \frac{3}{\varepsilon_P} \left(\frac{\varepsilon(\varepsilon + \varepsilon_g)(\varepsilon + \varepsilon_g + \Delta)}{(3\varepsilon + 3\varepsilon_g + 2\Delta)} \right) - k_z^2 \quad (19)$$

$$a = \frac{1}{2} + \frac{|m-s| + m-s}{2} - \frac{3\varepsilon(\varepsilon + \varepsilon_g)(\varepsilon + \varepsilon_g + \Delta)}{\hbar\omega_0(3\varepsilon + 3\varepsilon_g + 2\Delta)\varepsilon_P} \pm \frac{\Delta}{2(3\varepsilon + 3\varepsilon_g + 2\Delta)} \quad (20)$$

$$b = |m-s| + 1 \quad (21)$$

where $\varepsilon_P = \frac{2m_0}{\hbar^2} P^2$, $x = \frac{r^2}{2l_H^2}$ and the magnetic

length is $l_H = \sqrt{\frac{\hbar c}{eH}}$.

It's expressed the whole quantities in dimensionless units by letting $\hbar\omega_0(\omega_0 = \frac{eH_0}{2m_0c})$ is the Larmor frequency) and the inverse length $\beta \left(= \sqrt{\frac{m_0\omega_0}{\hbar}} \right)$ be 1.

In these units, $\frac{\hbar^2}{m_0} = \frac{\hbar\omega_0}{\beta^2} \rightarrow 1$ and $r_0 = \sqrt{s}$ so

that $s = H_0\pi r_0^2 / \phi_0$ is the only relevant parameter. Here s is a scale parameter which represents the number of missing flux quanta within the wire [9,10,11] and $\phi_0 (= \frac{hc}{e})$ the flux quantum. Since there is no magnetic field inside the magnetic wire, the magnetic edge states may not enclose the magnetic flux, resulting in missing flux quanta; these are absent in the edge states formed by electrostatic confinements. The energies are easily determined from the continuity of the wave functions and their derivatives at the boundary of the wire.

In the calculations of the electron energy spectra for narrow gap InSb cylindrical wires we choose the semiconductor band structure parameters for InSb: energy gap $E_g = 0.2368$ eV, spin orbit splitting is $\Delta = 0.810$ eV,

$\varepsilon_P = \frac{2m_0}{\hbar^2} P^2 = 23.42$ eV and m_0 is the free-electron mass [18].

The effective edge g-factor can be determined from the Zeeman splitting of subbands:

$$g(\varepsilon) = \frac{\varepsilon \uparrow - \varepsilon \downarrow}{\mu_B H} \quad (22)$$

Here $\varepsilon \uparrow$ and $\varepsilon \downarrow$ are the electron energy for spin $+z$ and $-z$ directions respectively.

3. Results

In this section, it's calculated exactly and discussed the single-electron eigenstates and transport properties of a magnetic quantum wire by taking into account the real band structure of InSb type materials; narrow energy gap and strong spin-orbit interaction. Figure 1 represents the estimated dependence of the energy eigenvalues in the magnetic quantum wire on the angular momentum m . The solid curves correspond to the spin up case $\sigma = +1/2$ and the spin down case $\sigma = -1/2$ respectively for different m values.

To allow comparison with the works of [9,10,11], in this figure and the following one, the energy is in units of $\hbar\omega_0 = 1$ at $r_0 = 500 \text{ \AA}$ and $H_0 = 2.633T$ (corresponding the $s=5$ in references [9,10,11]).

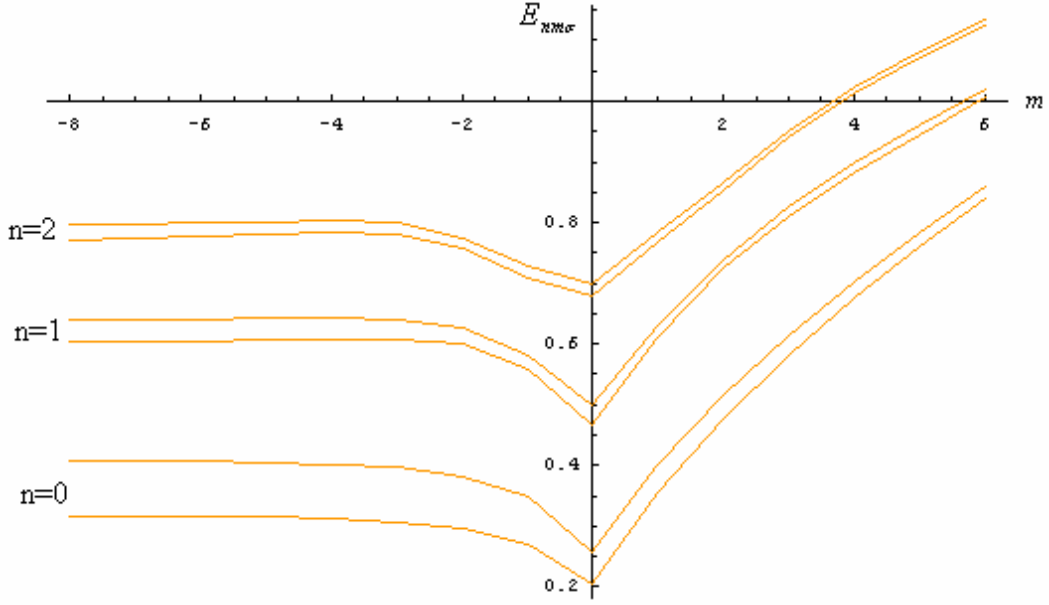


Fig. 1. The dependence of the energy eigenvalues $E_{nm\sigma}$ in the quantum wire on the angular momentum m for $r_0 = 500 \text{ \AA}$, $H_0 = 2.633T$, $k_z = 0$.

At a first look in Figure 1, we notice the Landau level degeneracy is broken. As it can be seen the lowest energy state occurs at $m=0$. This result indicates that the inhomogeneity of the magnetic field perturbs mostly the states near the boundary of the quantum wire, and this perturbation is caused by the missing flux quanta s . The energy levels increase slowly with the decrease of angular

momentum m for $m < 0$, while they increase rapidly with the increasing of m for $m > 0$ as in references [9,10,11]. The splitting, due to the spin between the energy levels are decreased with the increasing of n , which is the main different result in comparison with the ref. [11] and it's because of the interaction between the valence and conduction band.

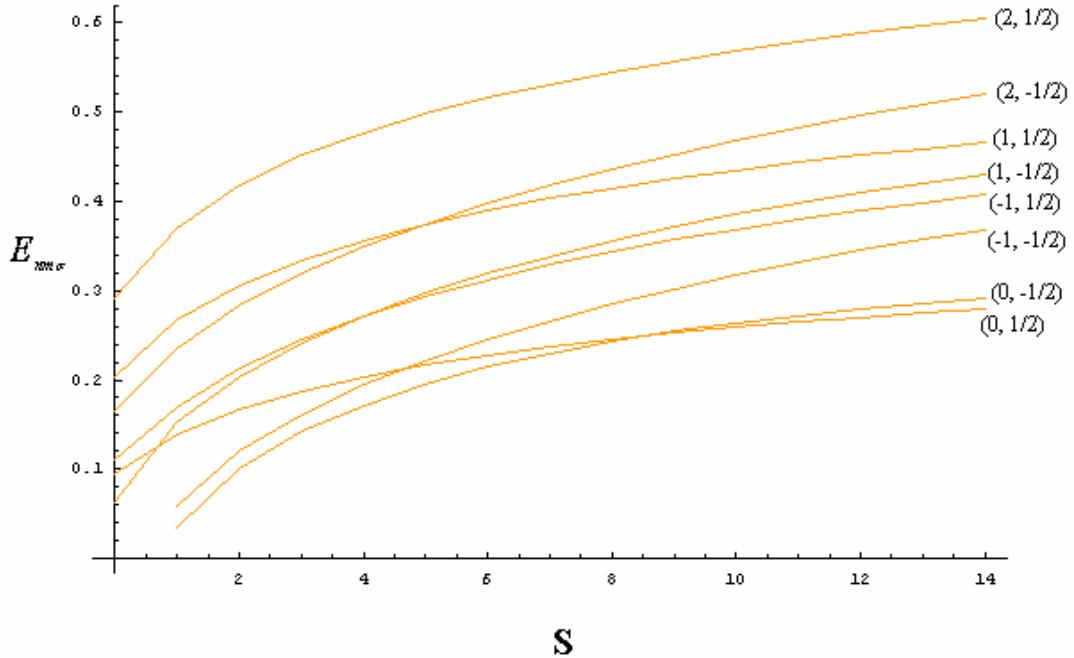


Fig. 2. Energy spectra as a function of S $n=0$ and $m=-1$ to $+2$, where $\pm 1/2$ is spin up and spin down values. $r_0 = 500 \text{ \AA}$, $k_z = 0$.

In Figure 2, we represent the energy spectra as a function of the number of missing magnetic flux quanta S

($S = H\pi r^2 / \phi_0$). In this figure it's shown only $n=0$ and $m=-1$ to $+2$ states to avoid the complexity. The energy units $\hbar\omega_0$

are set to one at $s=5$ and r_0 is fixed. The different energy levels are labeled with the corresponding quantum numbers (m, σ) . Since the spin effect is taken into account, each energy curve splits into two curves. The crossover point of energy curves for $m=0$ state with opposite spins is obtained around the value of $S=8$. It's noted that some of

the crossover points in the same angular quantum number may be located outside the magnetic region presented.

In Figure 3 the magnetic field change of edge g factor for electrons at the ground state ($m=0$) is illustrated. It's seen that edge g-factor increases with the increasing of the magnetic field.

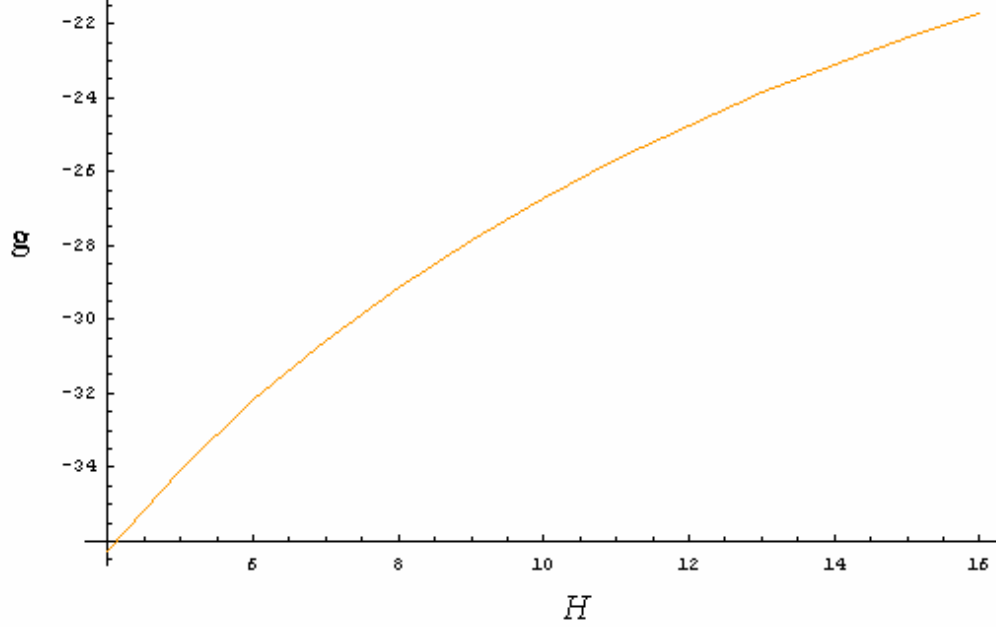


Fig. 3. Edge g-factor versus magnetic field, for electrons of InSb at the ground state. $r_0 = 500 \text{ \AA}$, $k_z = 0$.

Figure 4 represents the radius change of edge g factor for electrons at the ground state ($m=0$). It can be seen that the edge g-factor approaches to the bulk value with the increasing of the radius.

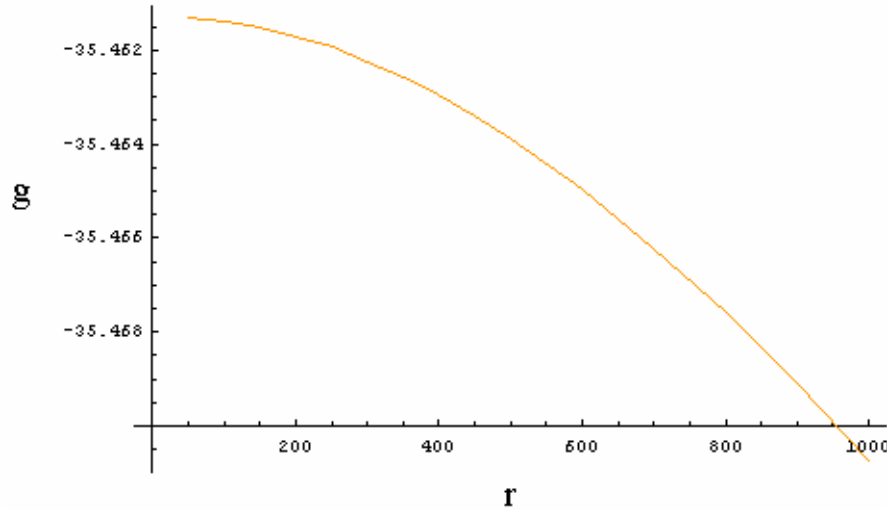


Fig. 4. Edge g factor versus radius for electrons of InSb at the ground state. $H=1 \text{ T}$, $k_z = 0$.

4. Conclusion

We have investigated the energy spectra of a magnetic quantum wire by taking into account the real band structure of InSb type semiconductors. Energy spectra of quantum wire shows deviated structures from the bulk Landau levels. It's shown that the different behaviors of the edge states depend

on the amount of the flux in a magnetic quantum wire. The magnetic field dependence of edge g-factor is also investigated and found that edge g-factor increases with the increasing of the magnetic field. In addition to this, it is shown that the edge g-factor approaches to the bulk value with the increasing of the radius.

- [1] *T. Chakraborty*. Quantum Dots, Elsevier 1999.
- [2] *M.A. McCord and D.D. Awschalom*. 1990 Appl. Phys. Lett. 57 2153.
- [3] *R.K. Willardson, A.C. Beer, E.R. Weber*. Nanostructured systems, Semiconductors and semimetals, vol. 35, Academic Pres, New York, 1992.
- [4] *S.J. Lee, S. Souma, G. Ihm, K.J. Chang*, Physics Reports 394 (2004) 1–40
- [5] *F.M. Peeters, A. Matulis and I.S. Ibrahim*. 1996 Physica B 227 131.
- [6] *J. Reijnders, F.M. Peeters, A. Matulis and I.S. Ibrahim*, 1999 Phys. Rev. B 59 2817.
- [7] *L. Solimany and B. Kramer*. 1995 Solid State Commun. 96, 471.
- [8] *S.M. Badalyan and F.M. Peeters*, Nanotechnology **12** (2001) 570–576.
- [9] *Gukhyung Ihm, Nammee Kim, H.S. Sim, K.H. Ahn, K. J. Chang, S.J. Lee*, Physica B 249-251 (1998), 291-294.
- [10] *Gukhyung Ihm, S.J. Lee, H.S. Sim, K.H. Ahn, K. J. Chang*, Microelectric Engineering 43-44 (1998), 31-36.
- [11] *Yong Guo, Bin Wang, Hui Hu, Jing-Zhi Yu, Bing-Lin Gu and Yoshiyuki Kawazoe*, J. Phys. Condens. Matter 12 (2000), 3359-3367.
- [12] *R. Rosas, R. Riera, J.L. Marin*, J. Phys. Condens. Matter 12 (2000), 6851-6858.
- [13] *E.O. Kane*, J. Phys. Chem. Solids, 1, 4, (1957), 249-261.
- [14] *B.M. Askerov*, Kinetic Effects in Semiconductors (Nauka, Leningrad, 1970).
- [15] *A.I. Anselm*, Introduction to Semiconductor Theory, Nauka, Moscow, 1978.
- [16] *W. Zawadzki, S. Klahn and U. Merkt*, Phys. Rev. B 33 (1996), 6916-6928.
- [17] *V.M. Galitskii, B.M. Karnakov, V.I. Kogan*, A Collection of Problems Quantum mechanics Science, Moscow, 1981 (in Russian).
- [18] *Al. L. Efros, A. Rosen*, Phys. Rev. B 58 (011) (1998) 7120.

A.M. Babayev, Ş. Çakmaktepe, A. Kökçe

KEYN TIPLİ YARIMKEÇİRİCİ KVANT TELLƏRİNDƏ KƏNAR HALLAR

InSb tipli maqnit kvant tellərində elektronların enerji spektrləri yarımkeçiricinin real zona quruluşu nəzərə alınmaqla hesablanmışdır. Elektronların kənar hallarının effektiv g -faktorunun kvant telinin radiusundan və xarici maqnit sahəsindən asılılığı öyrənilmişdir.

A.M. Бабаев, Ш. Чакмактепе, А. Кокче

КРАЕВЫЕ СОСТОЯНИЯ В КВАНТОВОЙ ПРОВОЛОКЕ КЕЙНОВСКОГО ПОЛУПРОВОДНИКА

Исследован энергетический спектр носителей тока в полупроводниковой цилиндрической квантовой проволоке во внешнем, неоднородном магнитном поле, $B = 0$ при $r < r_0$ and $B \neq 0$ в остальном пространстве, с учетом реальной зонной структуры узкощелевых полупроводников типа InSb с сильным спин-орбитальным взаимодействием. Найдено, что энергетический спектр критически зависит от числа квантов магнитного потока. С учетом спина каждая энергетическая кривая расщепляется на две. Для состояния $m=0$ кривые с противоположными значениями спина пересекаются около $S=8$. Изучена зависимость от магнитного поля и радиуса проволоки краевого g - фактора.

Received: 22.09.05

THE GLUONS GREEN FUNCTION IN NLO

L.A. ALIEVA, S.A. GADJIEV

*Baku State University**Acad. Z. Khalilov str., 23, Baku, Az-1145*

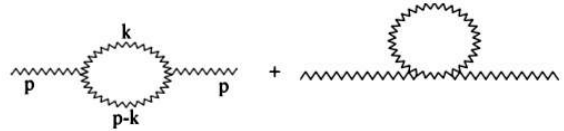
In given article the polarizing operator of $\chi_\mu A_\mu=0$ and $\partial_\mu A_\mu=0$ gauges is calculated. It was shown, that the polarizing operator corresponds to a cross condition for two conditions, only in gauge Landau. Results received in gauges $\chi_\mu A_\mu=0$ and $\partial_\mu A_\mu=0$ strongly differ from each other and in both cases the condition corresponds is not carried out.

The gluons Green function in Yang-Mills gauge theories in a general form can be represented as,

$$G_{\mu\nu}^{ab} = G_{\mu\nu}^{(0)} \delta_{ab} + \sum G_{\mu\mu'}^{(0)} \delta_{aa'} \Pi_{\mu'\nu'}^{a'b'} \delta_{bb'} G_{\nu\nu'}^{(0)} + \dots \quad (1)$$

We shall limited by first two terms, since the second order is determined by the second terms. The sum before the second member means a summation of all diagrams of the second order. There are following two diagrams in our consideration (see fig.1). The ghosts loop, we do not consider, because limited by pure

Yang - Mills theory. The calculation of the Green function



in the second order, leads us to calculated polarization operator, according to formula (1). The polarization operator corresponding to first diagram can be written as follows [1,2]:

$$\Pi_{\mu\nu}^{ab} = -\frac{ig^2}{(2\pi)^4} \int \frac{d^4 k}{k^2 (p-k)^2} f^{aa_1 a_2} f^{bb_1 b_2} \Gamma_{\mu\mu_1 \mu_2} G_{\mu_1 \mu_2}^{(0)} \Gamma_{\nu\nu_1 \nu_2} G_{\nu_1 \nu_2}^{(0)} \delta_{a_1 b_1} \delta_{a_2 b_2} \quad (2)$$

Here g is constant of interaction, $f^{aa_1 a_2} f^{bb_1 b_2}$ - are color indices, $G_{\mu_1 \nu_1}^{(0)}, G_{\mu_2 \nu_2}^{(0)}$ - the free gluons Green function, and $\Gamma_{\mu\mu_1 \mu_2}, \Gamma_{\nu\nu_1 \nu_2}$ - are vertex functions.

We shall calculate eq. (2) in both $\chi_\mu A_\mu=0$ and in Lorenz's gauge. The gluons Green function in $\chi_\mu A_\mu=0$ gauge is determined by us in work [3] and has the following form:

$$G_{\mu\nu}^{(0)} = -\frac{1}{k^2} \left(\delta_{\mu\nu} - \frac{1+\alpha}{k^2} k_\mu k_\nu \right)$$

It is seen from this expression, that it differs from Green functions in Lorenz's gauge by a longitudinal part. Note that Lorenz's gauge corresponds to transverse gauge in momentum space, and gauge $\chi_\mu A_\mu=0$ corresponds to transverse gauge in "x-space". The expression (2) can be written in the following form:

$$\begin{aligned} \Pi_{\mu\nu}^{ab} = & -\frac{ig^2}{(2\pi)^4} \int \frac{d^4 k}{k^2 (p-k)^2} \left(g_{\nu_1 \mu_1} - \frac{1 \pm \alpha}{k^2} k_{\mu_1} k_{\nu_1} \right) \cdot \left(g_{\mu_2 \nu_2} - \frac{1 \pm \alpha}{(p-k)^2} \right) * \\ & * (p-k)_{\mu_2} (p-k)_{\nu_2} \left[(p+k)_{\mu_2} g_{\mu\mu_1} + (p-2k)_\mu g_{\mu_1 \mu_2} + (k-2p)_{\mu_1} g_{\mu\mu_2} \right] * \\ & * \left[(p+k)_{\nu_2} g_{\nu\nu_1} + (k-2p)_{\nu_1} g_{\nu\nu_2} + (p-2k)_\nu g_{\nu_1 \nu_2} \right] \delta^{a_1 b} \delta^{a_2 b_2} \end{aligned} \quad (3)$$

Here the top sign concerns to gauge $\chi_\mu A_\mu=0$, and the bottom sign concerns to Lorenz's gauge. Let to present eq. (3) in more convenient form:

$$\begin{aligned} \Pi_{\mu\nu}^{ab} = & \frac{ig^2}{(2\pi)^4} \left\{ \int \frac{d^4 k}{k^2 (p-k)^2} \Gamma_{\mu\mu_1 \mu_2}^{\nu\nu_1 \nu_2} g_{\mu_1 \nu_1} g_{\mu_2 \nu_2} - \right. \\ & - (1 \pm \alpha) \int \frac{d^4 k}{k^4 (p-k)^2} k_{\mu_1} k_{\nu_1} \Gamma_{\mu\mu_1 \mu_2}^{\nu\nu_1 \nu_2} g_{\mu_2 \nu_2} - \\ & - (1 \pm \alpha) \int \frac{d^4 k}{k^2 (p-k)^4} (p-k)_{\mu_2} (p-k)_{\nu_2} \Gamma_{\mu\mu_1 \mu_2}^{\nu\nu_1 \nu_2} g_{\mu_1 \nu_1} + \\ & \left. + (1 \pm \alpha) \int \frac{d^4 k}{k^4 (p-k)^4} k_{\mu_1} k_{\nu_1} (p-k)_{\mu_2} (p-k)_{\nu_2} \Gamma_{\mu\mu_1 \mu_2}^{\nu\nu_1 \nu_2} \right\} \end{aligned}$$

where

$$\Gamma_{\mu\mu_1\mu_2}^{\nu\nu_1\nu_2} = \left[(p+k)_{\mu_2} g_{\mu_1\mu_2} + (p-2k)_{\mu} + (k-2p)_{\mu_1} g_{\mu\mu_2} \right] * \\ * \left[(p+k)_{\mu_2} g_{\nu\nu_1} + (p-2k)_{\nu} g_{\nu_1\nu_2} + (k-2p)_{\nu_1} g_{\nu\nu_2} \right]$$

The first integral in this expression has been calculated in a number of works (see [1,2]) and looks like:

$$J_1 = \int \frac{d^4 k}{k^2 (p-k)^2} \Gamma_{\mu\mu_1\mu_2}^{\nu\nu_1\nu_2} g_{\mu_1\nu_1} g_{\mu_2\nu_2} = \int \frac{d^4 k}{k^2 (p-k)^2} \left[(2k^2 - 2kp + 5p^2) g_{\mu\nu} - 2p_{\mu} p_{\nu} + 10k_{\mu} k_{\nu} - 5(p_{\mu} k_{\nu} + p_{\nu} k_{\mu}) \right]$$

The second integral after convolution of indices looks like:

$$J_2 = \int \frac{d^4 k}{k^4 (p-k)^2} \Gamma_{\mu\mu_1\mu_2}^{\nu\nu_1\nu_2} k_{\mu_1} k_{\nu_1} g_{\mu_2\nu_2} = \\ = \int \frac{d^4 k}{k^4 (p-k)^2} \left[p_{\mu} p_{\nu} k^2 + k_{\mu} k_{\nu} (p^2 + 2pk - k^2) + (p_{\mu} k_{\nu} + p_{\nu} k_{\mu}) (k^2 - 3pk) + (k^2 - 2pk) g_{\mu\nu} \right]$$

The third and fourth integrals are equal to:

$$J_3 = \int \frac{d^4 k}{k^2 (p-k)^4} (p-k)_{\mu_2} (p-k)_{\nu_2} \Gamma_{\mu\mu_1\mu_2}^{\nu\nu_1\nu_2} g_{\mu_1\nu_1} = \\ = \int \frac{d^4 k}{k^2 (p-k)^4} \left[(p^2 - k^2) g_{\mu\nu} + p_{\mu} p_{\nu} (-p^2 + 2k^2) + k_{\mu} k_{\nu} (-k^2 + 2p^2) - (p_{\mu} k_{\nu} + k_{\mu} p_{\nu}) (pk) \right]$$

and

$$J_4 = \int \frac{d^4 k}{k^4 (p-k)^4} (p-k)_{\mu_2} (p-k)_{\nu_2} \Gamma_{\mu\mu_1\mu_2}^{\nu\nu_1\nu_2} k_{\mu_1} k_{\nu_1} = \int \frac{d^4 k}{k^4 (p-k)^4} \left[k_{\mu} k_{\nu} p^4 + p_{\mu} p_{\nu} (pk)^2 - (p_{\mu} k_{\nu} + k_{\mu} p_{\nu}) p^2 (pk) \right]$$

Now it is necessary to calculate the integrals J_1, J_2, J_3 and J_4 over the momentum and angles variables.

Integration over the k we carry out in n -dimensional space with the further transition $n = 4$ thus we using the following formula [1]:

$$\int \frac{(k^2)^m d^n k}{[k^2 + p^2 x(1-x)]^l} = \frac{i\pi^{\frac{n}{2}}}{\Gamma\left(\frac{n}{2}\right)} (-1)^{m+l} \cdot [-p^2 x(1-x)]^{m+\frac{n}{2}-l} \cdot \frac{\Gamma\left(m+\frac{n}{2}\right) \cdot \Gamma\left(l-\frac{n}{2}-m\right)}{\Gamma(l)}$$

For application of this formula to J_1, J_2, J_3 and J_4 we use Feynman's parameterization:

In this formula it was done in to Euclidean space.

$$\int \frac{d^4 k}{k^2 (p-k)^2} \rightarrow \int_0^1 dx \int \frac{d^n k}{[k^2 - p^2 x(1-x)]^2}$$

$$\int_0^1 x^{\alpha} (1-x)^{\beta} dx = \frac{\Gamma(1+\alpha)\Gamma(1+\beta)}{\Gamma(2+\alpha+\beta)}$$

Having integrated over the k and x we receive the following expression:

And we carry out integration over x by use of formula

$$\begin{aligned}\Pi_{\mu\nu}^{ab} = & -\frac{ig^2}{(2\pi)^4} i\pi^2 \left\{ \left[(p^2 g_{\mu\nu} - p_\mu p_\nu) \frac{19}{6} - \frac{1}{2} p_\mu p_\nu \right] \Gamma\left(2 - \frac{n}{2}\right) \left(-\frac{p^2}{\mu^2}\right)^{\frac{n}{2}-2} - \right. \\ & - (1 \pm \alpha) \left[(p^2 g_{\mu\nu} - p_\mu p_\nu) \frac{11}{12} - \frac{1}{4} (p^2 g_{\mu\nu} - p_\mu p_\nu) \Gamma\left(2 - \frac{n}{2}\right) + \frac{1}{4} p_\mu p_\nu \Gamma\left(2 - \frac{n}{2}\right) \right] \cdot \left(-\frac{p^2}{\mu^2}\right)^{\frac{n}{2}-2} - \\ & - (1 \pm \alpha) \left[(p^2 g_{\mu\nu} - p_\mu p_\nu) \frac{11}{12} - \frac{1}{4} (p^2 g_{\mu\nu} - p_\mu p_\nu) \Gamma\left(2 - \frac{n}{2}\right) + \frac{3}{4} p_\mu p_\nu \Gamma\left(2 - \frac{n}{2}\right) \right] \cdot \left(-\frac{p^2}{\mu^2}\right)^{\frac{n}{2}-2} - \\ & \left. - \frac{(1 \pm \alpha)}{2} (p^2 g_{\mu\nu} - p_\mu p_\nu) \cdot \left(-\frac{p^2}{\mu^2}\right)^{\frac{n}{2}-2} \right\} \delta_{ab}\end{aligned}$$

This expression can be written in a more foreseeable form, separating divergent parts:

$$\begin{aligned}\Pi_{\mu\nu}^{ab} = & -\frac{g_1^2 \delta_{ab}}{16\pi^2} \left\{ (p^2 g_{\mu\nu} - p_\mu p_\nu) \left[\frac{19}{6} + \frac{1}{2} (1 \pm \alpha) \right] \Gamma\left(2 - \frac{n}{2}\right) - \frac{1}{2} p_\mu p_\nu \left[1 - \frac{1}{2} (1 \pm \alpha) \right] \Gamma\left(2 - \frac{n}{2}\right) - \right. \\ & \left. - (1 \pm \alpha) (p^2 g_{\mu\nu} - p_\mu p_\nu) \cdot \left(\frac{11}{6} + \frac{1}{2} (1 \pm \alpha) \right) \right\} \cdot \left(\frac{\mu^2}{-p^2} \right)^{2-\frac{n}{2}}\end{aligned}\quad (4)$$

In order to keep correct dimension of polarization operator, we have used a dimensionless constant of interaction $g_1^2 = g^2 \left(\frac{\mu^2}{-p^2} \right)^{4-n}$

According eq.(4) we can write out expression for the polarization operator in both gauge:
a) Lorentz's gauge:

$$\begin{aligned}\Pi_{\mu\nu}^{ab} = & -\frac{g_1^2 \delta_{ab}}{16\pi^2} \left\{ (p^2 g_{\mu\nu} - p_\mu p_\nu) \cdot \left[\frac{11}{3} - \frac{1}{2} \alpha \right] \Gamma\left(2 - \frac{n}{2}\right) - \frac{1}{4} p_\mu p_\nu (1 \pm \alpha) \Gamma\left(2 - \frac{n}{2}\right) - \right. \\ & \left. - (1 - \alpha) (p^2 g_{\mu\nu} - p_\mu p_\nu) \cdot \left(\frac{7}{3} + \frac{\alpha}{2} \right) \right\} \cdot \left(\frac{\mu^2}{-p^2} \right)^{\frac{n}{2}-2}\end{aligned}\quad (5)$$

b) $\chi_\mu A_\mu = 0$ gauge

$$\begin{aligned}\Pi_{\mu\nu}^{ab} = & -\frac{g_1^2 \delta_{ab}}{16\pi^2} \left\{ (p^2 g_{\mu\nu} - p_\mu p_\nu) \left[\frac{11}{3} + \frac{1}{2} \alpha \right] \Gamma\left(2 - \frac{n}{2}\right) - \frac{1}{4} p_\mu p_\nu (1 - \alpha) \Gamma\left(2 - \frac{n}{2}\right) - \right. \\ & \left. - (1 + \alpha) (p^2 g_{\mu\nu} - p_\mu p_\nu) \cdot \left(\frac{7}{3} + \frac{\alpha}{2} \right) \right\} \cdot \Gamma\left(2 - \frac{n}{2}\right)\end{aligned}\quad (6)$$

The analysis of the formula (5) shows, that in Lorentz's gauge ($\alpha=1$) the polarization operator is not transverse. And in gauge $\chi_\mu A_\mu = 0$ at $\alpha=1$ it has (the formula (6)) the form of transverse polarization operator. Thus, it is possible to obtain the transverse polarization operator not introducing Faddeev-Popov's ghost. It is necessary to choose successful gauge. Let us use the renormalization procedure for expressions (5) and (6).

The preliminary factor $\left(\frac{\mu^2}{-p^2} \right)^{2-\frac{n}{2}}$ we present in the following form:

$$\left(\frac{\mu^2}{-p^2} \right)^{2-\frac{n}{2}} = 1 + (2 - \frac{n}{2}) \ln \frac{\mu^2}{-p^2} + \dots$$

a $\Gamma(2 - \frac{n}{2})$ we represent as,

$$\Gamma(2 - \frac{n}{2}) = \frac{1}{2 - \frac{n}{2}} - \gamma$$

where $\gamma = 0,5772$ - Euler's constant.

Thus:

$$\Gamma\left(2 - \frac{n}{2}\right) \left(\frac{\mu^2}{-p^2}\right)^{2 - \frac{n}{2}} = \left(1 + \left(2 - \frac{n}{2}\right) \ln \frac{\mu^2}{-p^2}\right) \cdot \left(\frac{1}{2 - \frac{n}{2}} - \gamma\right)$$

Carrying out renormalization procedure we shall have:

a) For Lorenz's gauge:

$$\begin{aligned} \Pi_{\mu\nu}^{ab} = & -\frac{g_1^2 \delta_{ab}}{16\pi^2} \left\{ (p^2 g_{\mu\nu} - p_\mu p_\nu) \cdot \left[\frac{11}{3} + \frac{1}{2} \alpha \right] \cdot \left(-\gamma + \ln \frac{\mu^2}{-p^2} \right) - \frac{1}{4} p_\mu p_\nu (1 + \alpha) \left(-\gamma + \ln \frac{\mu^2}{-p^2} \right) - \right. \\ & \left. - (1 - \alpha) (p^2 g_{\mu\nu} - p_\mu p_\nu) \cdot \left(\frac{7}{3} + \frac{\alpha}{2} \right) \right\} \end{aligned}$$

at $\alpha=1$, we have

$$\Pi_{\mu\nu}^{ab} = -\frac{g_1^2 \delta_{ab}}{16\pi^2} \left\{ (p^2 g_{\mu\nu} - p_\mu p_\nu) \frac{19}{6} \left(-\gamma + \ln \frac{\mu^2}{-p^2} \right) - \frac{1}{2} p_\mu p_\nu \left(-\gamma + \ln \frac{\mu^2}{-p^2} \right) \right\} \quad (7)$$

This formula coincides with earlier known formula (see [1,2]).

b) For gauge $\chi_\mu A_\mu = 0$

$$\begin{aligned} \Pi_{\mu\nu}^{ab} = & -\frac{g_1^2 \delta_{ab}}{16\pi^2} \left\{ (p^2 g_{\mu\nu} - p_\mu p_\nu) \left[\frac{11}{3} + \frac{1}{2} \alpha \right] \cdot \left(\ln \frac{\mu^2}{-p^2} - \gamma \right) - \frac{1}{4} p_\mu p_\nu (1 - \alpha) \left(\ln \frac{\mu^2}{-p^2} + \gamma \right) - \right. \\ & \left. - (1 + \alpha) (p^2 g_{\mu\nu} - p_\mu p_\nu) \cdot \left(\frac{7}{3} + \frac{\alpha}{2} \right) \right\} \end{aligned}$$

and at $\alpha=1$

$$\Pi_{\mu\nu}^{ab} = -\frac{g_1^2 \delta_{ab}}{16\pi^2} \left\{ (p^2 g_{\mu\nu} - p_\mu p_\nu) \left[\frac{25}{6} \left(-\gamma + \ln \frac{\mu^2}{-p^2} \right) - \frac{17}{3} \right] \right\} \quad (8)$$

The formula (8) in Feynman gauge is new result and it is transverse. Now we shall consider the second diagram. The second diagram contains the integral:

$$J = \int \frac{d^4 k}{k^2}$$

$$J = \int \frac{(k^2)^{\alpha-1} d^n k}{(2\pi)^n}$$

(Here $\alpha=0, 1, \dots, m$)

And equal to zero.

Thus, the contribution of the second diagram to Green functions in the second order equal to zero.

In the n-dimensionally space the following formula takes place:

- [1] A.A. Slavnov, L.D. Faddeev. Introduction to quantum theory of gauge fields. Moscow: Nauka, 1978
- [2] F. Indurain. The theory of quark and gluon interactions. Springer, 1999

- [3] L.A. Alieva. Bulletin of Sumgait State University, v.3, N2, p.26, 2004.

L.A. Əliyeva, S.A. Hacıyev

ƏSAS YAXINLAŞMADAN SONRAKI TƏRTİBDƏ QLUONUN QRİN FUNKSIYASI

Məqalədə $\chi_\mu A_\mu=0$ və $\partial_\mu A_\mu=0$ kalibrovkalarında polyarizasiya operatoru hesablanıb. Göstərilmişdir ki, yalnız Landau kalibrovkasında hər iki hal üçün polyarizasiya operatoru eninəlik şərtini ödəyir. Feynman kalibrovkasında $\chi_\mu A_\mu=0$ və $\partial_\mu A_\mu=0$ kalibrovkaların verdiyi nəticələr bir-birində jiddi fərqlənir, və eninəlik şərti ödənmir.

Л.А. Алиева, С.А. Гаджиев

ФУНКЦИЯ ГРИНА ГЛЮОНА В СЛЕДУЮЩЕМ ПОРЯДКЕ ЗА ГЛАВНЫМ ПРИБЛИЖЕНИЕМ

В данной статье вычислен поляризационный оператор в калибровке $\chi_\mu A_\mu=0$ и $\partial_\mu A_\mu=0$. Было показано, что в калибровке Ландау поляризационный оператор для обоих состояний является поперечным. В калибровке Феймана полученные значения в калибровках $\chi_\mu A_\mu=0$ и $\partial_\mu A_\mu=0$ сильно отличаются друг от друга и не отвечают условию поперечности.

Received: 19.10.05

THE REACTION OF DISLODGING OF NUCLEONS BY THE PROTONS FROM THE NUCLEUSES

M.M. MIRABUTALIBOV

Azerbaijan State Oil Academy, AZ-1010, Baku, Azadlig av., 20

On the base of the quasi-classical approach the obtained expression for the amplitude of the quasi-elastic dislodging of nucleons by protons from the nucleuses is applied for the study of the membrane structure of light nucleuses. The results of concrete calculations of amplitude of $A(p, 2p)B$ process on ^{16}O and ^{12}C nucleuses are given for the comparison with the experimental data. The calculations have been carried out for the different outlet angles of the slow protons $\theta_1=61^\circ, 64^\circ, 67^\circ, 73^\circ$ at the fixed scattering angle of the quick proton $\theta_2=13.4^\circ$. The analysis of the results shows, that cross-sections of the scattering weakly depends on the angles of dislodging protons.

The quasi-elastic dislodging of nucleons by protons of intermediate energies from nuclears on the base of the quasi-classical approach, described in the ref. [1] is investigation.

Toward this end, the differential cross-section of reaction $A(p, NpP)B$ is written in the form [2].

$$d\sigma = (2\pi)^4 \frac{m_p}{k} \mathbf{dp}_2 \mathbf{dp}_1 \delta(T_p - T_2 - T_1 - E_N - E_R) \frac{1}{2(2J_i + 1)} \sum_{\substack{M_i M_f \\ \sigma_i \sigma_f}} |T_{if}|^2. \quad (1)$$

Here T_p , T_2 and T_1 are energies of the corresponding incident, scattered and dislodging nucleons, E_N is the break energy of the weak connected nucleon.

$$E_R = \frac{P_R^2}{2M_{A-1}} \quad (2)$$

where E_R is the recoil energy of the daughter nucleus.

The matrix element of nucleus transition is presented in the form:

$$T_{if} = \langle J_f M_f | \int d\mathbf{r} d\mathbf{x}_1 \psi^{(-)}(\mathbf{r}) \psi^*(\mathbf{x}_1) V(\mathbf{r}, \mathbf{x}_1) \psi^{(+)}(\mathbf{r}) \psi(\mathbf{x}_1) | J_i M_i \rangle. \quad (3)$$

The wave functions of the relative motion of the rescattered proton are obtained from the solution of the Shroedinger nonrelativistic equation [2].

The wave function of the dislodging nucleon (slow) has the form:

$$\psi(\mathbf{x}_1) = \int \varphi_{A-1}^*(\xi) \varphi_A(\mathbf{x}_1, \xi) d\xi. \quad (4)$$

The nucleus recoil energy is defined with the help of the momentum of recoil nucleus (P_R), which connected with missing mass (M_r) from the reaction, on the base of the law of conservation of energy:

$$M_R = [(M_A - m_p + T_p - T_2 - T_1)^2 - P_R^2]^{1/2} \quad (5)$$

The connection between nucleon divided energy (E_N) and daughter nucleus mass (M_{A-1}), which are known from experiment for missing mass is used by the following form:

$$E_N = M_R - M_{A-1}. \quad (6)$$

Thus, applying the quasi-classical theory on the proton scattering on the nucleuses, described in the ref [1], for the matrix element, we obtain:

$$T_{if} = -\frac{\hbar^2}{(2\pi)^2 \mu_0} \int d\mathbf{r} d\mathbf{x}_1 d\mathbf{q}' e^{i[\mathbf{q}\mathbf{r} + \Phi(\mathbf{r})]} e^{-i\mathbf{k}_1 \mathbf{x}_1} e^{-i\mathbf{q}'(\mathbf{r} - \mathbf{x})} \cdot \psi(\mathbf{x}_1) f_{NN}(\mathbf{q}') \langle J_f M_f | \rho(\mathbf{x}, \xi) | J_i M_i \rangle. \quad (7)$$

After change of variables $u=r-x$ and using the expansion for the ill-wresting member $\Phi(r)$, we obtain:

$$T_{if} = -\frac{\hbar^2}{(2\pi)^2 \mu_0} \sum_{LM} \frac{1}{2L+1} \int e^{i[\mathbf{q}_{\text{ph}} - \mathbf{q}']u} e^{-i\mathbf{k}_1 \mathbf{x}_1} e^{i[\mathbf{q}\mathbf{x} + \Phi(\mathbf{r})]} \times \\ \times \psi(\mathbf{x}_1) f_{NN}(\mathbf{q}') Y_{LM}^*(x) \rho_L(x) d\mathbf{u} d\mathbf{x} d\mathbf{x}_1 d\mathbf{q}' \quad (8)$$

Here $\rho(x, \xi)$ is expressed through radial transition nucleus density $\rho_L(x)$.

The expression for the nucleon-nucleonic amplitude $f_{NN}(\mathbf{q}')$ is considered in the generic form [3].

Integrating the expression (8) on du , further on $d\mathbf{q}'$ and using the property of δ -function, for the cross-section we obtain:

$$\frac{d^3\sigma_{p,Np}}{d\Omega_1 d\Omega_2 dT_2} = \frac{(2\pi)^2 m_p^4 \hbar^2}{k \mu_0^2} T_p^{1/2} (T_p - T_2 - E_N - E_R)^{1/2} \frac{2(J_f + 1)}{2J_i + 1} \sum \frac{1}{2L + 1} |F_{LM}|^2. \quad (9)$$

At the quasi-elastic dislodging of nucleons, the recoil nucleuses have the hole in the casing, from which the proton is radiated, and the separation energy is equal to the energy of this single-particle state. The energy of dislodging nucleon has the value

$$T_1 = T_p - T_2 - E_N - E_R \quad (10)$$

And is defined with the help of the formula (2) and law of conservation of momentum

$$\mathbf{P}_R = \hbar \mathbf{k}_i - \hbar \mathbf{k}_f - \hbar \mathbf{k}_1. \quad (11)$$

The form factor of nucleus is

$$F_{LM}(\mathbf{q}) = \int e^{i[\mathbf{q}\mathbf{x} + \Phi(\mathbf{x})]} f_{NN}(\mathbf{q}_{3\Phi}) Y_{LM}^*(\hat{x}) \rho_L(x) d\mathbf{x}, \quad (12)$$

The mathematic calculation method is given in ref [1].

At the calculation (12) it is need to choose the coordinate system. Toward this end, it is supposed, that axis OZ $\uparrow\uparrow \mathbf{q}$,

where $q = |\mathbf{k}_i - \mathbf{k}_f| = 2k \sin \frac{\theta_2}{2} = 2k\alpha$ is recoil

momentum to the nucleus, $\alpha = \sin \frac{\theta_2}{2}$ and axis OX $\perp \mathbf{q}$,

where θ_2 is scattering angle of the incident particle,

$$\begin{aligned} \cos(\hat{\mathbf{q}} \hat{\mathbf{x}}_1) &= \mu, \quad \mathbf{x}_1 = \{x_1 \mu \varphi\}, \\ \cos(\hat{\mathbf{x}}_1 \hat{\mathbf{k}}_1) &= -\mu \sin(\theta_1 - \frac{\theta_2}{2}) + \cos(\theta_1 - \frac{\theta_2}{2}) \sqrt{1 - \mu^2} \cos \varphi, \end{aligned}$$

where θ_1 is the angle between incident and dislodging particles, which are familiar from the experiment.

Moreover, it is need to choose the function of nucleon density distribution in nucleuses. For the light nucleuses it is advisable to apply the symmetrized Fermi-densities, which well describe experimental cross-sections at the analysis of the elastic scattering of electrons and protons on light nucleuses [4,5].

The supposed approach allows to calculate the differential cross-sections on the dislodging of nucleons by protons with energy $T_p = 1$ GeV without free parameters. The results of the concrete calculations of reactions $A(p, 2p)B$ on nucleuses ^{16}O and ^{12}C in the comparison with the experimental data are given on the fig.1. and 2. The calculations, carried out for the outlet angle of slow protons $\theta_1 = 61^\circ$ and at the fixed scattered angle of the quick proton $\theta_2 = 13.4^\circ$. The analysis of the results shows, that scattering cross-section weakly depends on the angles of the dislodging protons.

The nucleus ^{16}O can radiate the protons from the levels $1 P_{3/2}$, $1 P_{1/2}$, $1 S_{1/2}$ and nucleus ^{12}C can radiate from levels $1 P_{3/2}$ and $1 S_{1/2}$, that's why the differential cross-section is calculated for each of this cases.

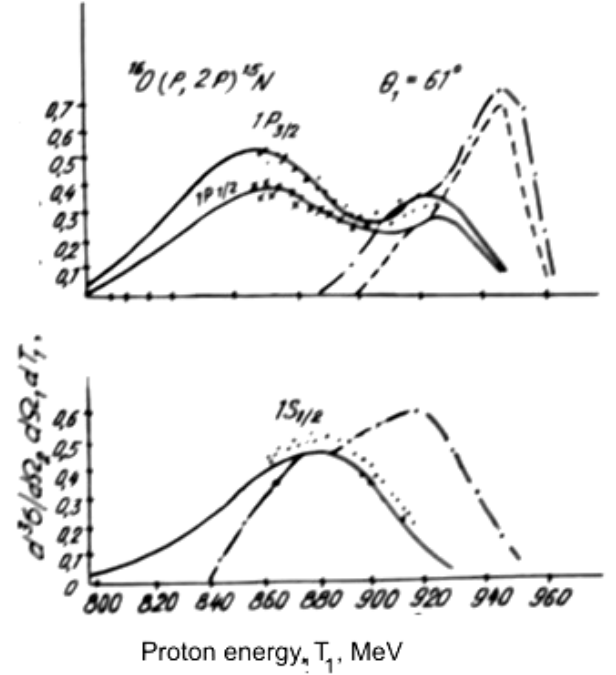


Fig. 1. The experimental (points) and theoretical differential cross-sections of the reactions of quasi-elastic dislodging of protons from the different nucleus membranes ^{16}O (touch dotted line). The cross-sections correspond to $\theta_1 = 61^\circ$, $\theta_2 = 13.4^\circ$. The continuous curve is results of the ref [6].

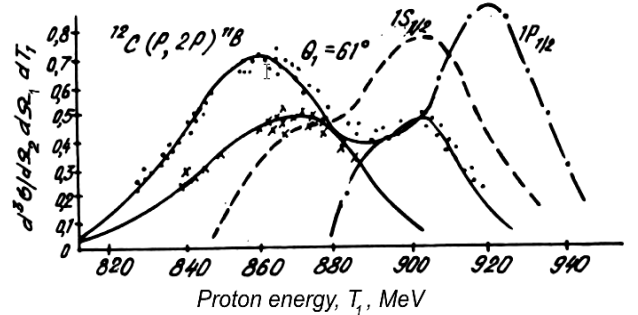


Fig. 2. The same, that on the fig.1., but for $p\text{-}^{12}\text{C}$.

In the experiment the slow protons were registered at energies $T_1 = (60 \div 105) \text{ MeV}$, the agreement of the theoretical cross-section with quick protons, measured on the registration was carrying out at these energy values of slow protons. As it is seen from fig.1., the theoretical curves, obtained in the present work on the dislodging of protons from the levels $1 P_{3/2}$ and $1 P_{1/2}$ in the difference from the experiment have only one maximum. This is the consequence of that in the process the absolute quasi-elastic dislodging of protons is considered, i.e. the residual nucleus doesn't react. The shift of the maximum to the side of the big energies probably connects with that the distortion doesn't take under consideration in the wave function of the dislodging proton.

For the comparison the theoretical curves, calculated in the wave-distorted momentum approximation, where the Hartri-Fock wave functions were used for the nuclear nucleons, are presented on the figures. Moreover, the authors of the work [6] also took under the consideration the excitation of the residual nucleus.

Thus, it is possible to conclude, that such calculations are comfortable for the practical use with the analytic wave functions of nucleus.

The theoretical analysis of dislodging reactions needs more detail consideration of the nuclear-force wave functions, in particular, more detail account of the excitation and distortion in the nucleus wave function.

-
- [1] *M.M. Mirabutalibov*. Fizika NAN, Az. Res., 2, 60, 2002. [4] *V.K. Lukyanov, Yu.S. Pol.* EChAYa, v.5, 955, 1974.
[2] *M.M. Mirabutalibov*. Fizika NAN, Az. Res., 3, 3, 2004. [5] *M.M. Mirabutalibov*. Fizika NAN, Az. Res., 2, 53, 1999.
[3] *M.M. Mirabutalibov*. Yadernaya Fizika, 67, 12, 2171 (2004). [6] *S.L. Belostotskiy i dr.* Pr. LIYaF, 867, 58, 1983.

M.M. Mirabutalibov

PROTONLARIN TƏSİRİLƏ NUKLONLARIN NÜVƏDƏN QOPARILMASI

Protonların təsirilə nüvədən nuklonların kvazielastiki qopma reaksiyasının amplitudunun analitik şəkli kvaziklassik yaxınlaşma əsasında tapılmışdır. A(p,2p)B reaksiyasının differensial kəsiyi ^{16}O və ^{12}C nüvələri üçün hesablanmış və alınan nəticələr təcrübə ilə müqayisə olunmuşdur. Hesablamalar sürətli protonların yalnız $\theta_2 = 13.4^\circ$ səpilmə bucağında, zəif protonların isə $\theta_1 = 61^\circ, 64^\circ, 67^\circ, 73^\circ$ qopma bucaqları üçün aparılmışdır.

Nəticələrin analizi göstərmişdir ki, səpilmənin effektiv kəsiyi, qoparılan protonların uçuş bucağından asılılığı çox zəifdir.

М.М. Мирабута́либов

РЕАКЦИЯ ВЫБИВАНИЯ НУКЛОНОВ ИЗ ЯДЕР ПРОТОНАМИ

На основе квазиклассического подхода полученное выражение для амплитуды квазиупругого выбивания нуклонов из ядер протонами применено для изучения оболочечную структуру легких ядер. Результаты конкретных расчетов амплитуды процесса A(p,2p)B на ядрах ^{16}O и ^{12}C приведены в сопоставлении с экспериментальными данными. Расчеты выполнены для различных углов вылета медленных протонов ($\theta_1 = 61^\circ, 64^\circ, 67^\circ, 73^\circ$) при фиксированном угле рассеяния быстрого протона $\theta_2 = 13.4^\circ$. Анализ результатов показал, что сечение рассеяния слабо зависит от углов выбитых протонов.

Received: 09.06.05

THE ELECTROWEAK ASYMMETRIES IN THE SEMI-INCLUSIVE DEEP-INELASTIC REACTIONS $l^+N \Rightarrow l^-BX$

S.K. ABDULLAYEV, A.I. MUKHTAROV, S.M. RAGIMOVA

Baku State University

Acad. Z. Khalilov str., 23, Baku, Az-1145

The investigation of the degree of longitudinal polarization of Λ -hyperon and electroweak asymmetries in semi-inclusive reactions $l^+N \Rightarrow l^-BX$ was carried out in the frameworks of the standard theory and quark-parton model. The expressions for the degree of longitudinal polarization of Λ -hyperon, left-right, polarized, charge-polarized and charge asymmetries have been obtained.

The standard model (SM) well describes the series of experiments, carried out in the different laboratories of the world. In particular, the one from the most its detailed checking was carried on e^+e^- -colliders SLAC, LEP and TRISTAN, where the agreement with the experimental data is convincing. Along with e^+e^- -annihilations, the processes of the deep-inelastic scattering (DIS) of the leptons on the nucleons play the important role in SM checking and nowadays are experimentally investigated intensively [1-5].

Here the electroweak asymmetries in the semi-inclusive reactions are considered

$$l^+(\lambda) + N(h_N) \Rightarrow (\gamma^*, Z^0) \Rightarrow l^- + B(h_B) + X, \quad (1)$$

in which the lepton and detailed inclusive hadron B are registered on the coincidence, and X is the system of the non-detected hadrons. Here λ is the lepton spirality (antilepton), h_N is longitudinal polarization of nucleon-target, h_B is longitudinal polarization of B baryon.

The differential cross-section of semi-inclusive reaction $l^+N \Rightarrow l^-BX$ in SM frameworks can be written in the following form:

$$\frac{d\sigma^{l^+}}{dx dy dz} = \sum_{q, h_q} f_{q(h_q)}^{N(h_N)}(x, Q^2) \frac{d\hat{\sigma}}{dy} D_{q(h_q)}^{B(h_B)}(z, Q^2), \quad (2)$$

Here $f_{q(h_q)}^{N(h_N)}(x, Q^2)$ is distribution function of polarized quarks in the polarized nucleon, $D_{q(h_q)}^{B(h_B)}(z, Q^2)$ is fragmentation function of polarized quarks into the polarized baryon B; $\frac{d\sigma}{dy}$ is the differential cross-section of the

elementary subprocess $l^+q \rightarrow l^-q$ ($l^+\bar{q} \rightarrow l^-\bar{q}$); x, y, z are common kinematic variables of DIS.

Taking under the consideration the exchange of γ and Z^0 , It is easy to make sure, that the spiralities of quark and lepton should be saved separately in subprocess $l^+ + q \rightarrow l^- + q$. That's why in this process only four spiral amplitudes F_{RR}, F_{LL}, F_{RL} and F_{LR} which describe the following reactions

$$\begin{aligned} l_R^- + q_R &\Rightarrow l_R^- + q_R, & l_L^- + q_L &\Rightarrow l_L^- + q_L, \\ l_R^- + q_L &\Rightarrow l_R^- + q_L, & l_L^- + q_R &\Rightarrow l_L^- + q_R \end{aligned}$$

should be saved.

The spiral amplitudes in SM limits are defined by the expressions

$$F_{\alpha\beta} = \frac{Q_q}{yS} - \frac{g_\alpha^l g_\beta^q}{yS + M_Z^2} \quad (\alpha, \beta = L; R), \quad (3)$$

Where M_Z is mass of Z^0 -boson, is the square of total energy of $l\bar{q}$ -system in c.m.s., Q_q is quark electric charge q , g_R^l and g_L^l (g_R^q and g_L^q are right and left neutral weak charges of lepton (quark):

$$\begin{aligned} g_R^l &= \sqrt{\frac{x_w}{1-x_w}}, & g_L^l &= \frac{-1/2+x_w}{\sqrt{x_w(1-x_w)}}, \\ g_R^q &= -Q_q \sqrt{\frac{x_w}{1-x_w}}, & g_L^q &= \frac{T_3 - Q_q x_w}{\sqrt{x_w(1-x_w)}}. \end{aligned} \quad (4)$$

Here $x_w = \sin^2 \theta_w$ is Weinberg parameter, T_3 is third projection of the weak isospin of q quark.

Let's reduce the subprocess cross-section $l^+q \rightarrow l^-q$ at the definite values of initial and final particles:

$$1. l_R^- + q_R \Rightarrow l_R^- + q_R:$$

$$\frac{d\sigma}{dy} = 4\pi\alpha^2 s F_{RR}^2,$$

$$2. l_L^- + q_L \Rightarrow l_L^- + q_L:$$

$$\frac{d\sigma}{dy} = 4\pi\alpha^2 s F_{LL}^2,$$

$$3. l_R^- + q_L \Rightarrow l_R^- + q_L:$$

$$\frac{d\sigma}{dy} = 4\pi\alpha^2 s (1-y)^2 F_{RL}^2,$$

$$4. l_L^- + q_R \Rightarrow l_L^- + q_R:$$

$$\frac{d\sigma}{dy} = 4\pi\alpha^2 s (1-y)^2 F_{LR}^2. \quad (5)$$

The difference of y -dependencies of the above-mentioned cross-sections (5) connects with the difference of the total spiralities of the system l^+q : for $l_R^-q_R$ and $l_L^-q_L$ -collisions the total system spirality is equal to zero and y -dependence

doesn't appear; for $l_R^- q_L$ and $l_L^- q_R$ -collisions the sum spirality is equal to one that leads to the characteristic y -dependence.

The differential cross-section of the elementary subprocess $l^- q \Rightarrow l^- q$ with taking under the consideration of the spiralities of the initial units can be imagined in the form (the spiralities of the final particles are the same, as of the initial ones, i.e. the spiralities of lepton and quark are saved separately):

$$\frac{d\sigma}{dy} = \pi \alpha^2 s \left\{ (1+\lambda)(1+h_q)F_{RR}^2 + (1-\lambda)(1-h_q)F_{LL}^2 + [(1+\lambda)(1-h_q)F_{RL}^2 + (1-\lambda)(1+h_q)F_{LR}^2](1-y)^2 \right\}, \quad (6)$$

where h_q is spirality of the initial (or final) quark.

The differential cross-section of subprocess $l^- \bar{q} \Rightarrow l^- \bar{q}$ can be obtained from (6) with the help of the elementary changes:

$$F_{RR} \Rightarrow F_{RL}, F_{RL} \Rightarrow F_{RR}, F_{LR} \Rightarrow F_{LL}, F_{LL} \Rightarrow F_{LR}.$$

On the base of formulas (2) and (6), the expression for the differential cross-section of semi-inclusive reactions $l^- N \Rightarrow l^- B X$ has been obtained:

$$\begin{aligned} \frac{d\sigma^{(-)}}{dx dy dz} = & \sum_q \left[f_q^N(x, Q^2) \times D_q^B(z, Q^2) + h_N h_B f_q^N(x, Q^2) \Delta D_q^B(z, Q^2) \right] \times \left[(1+\lambda)(F_{RR}^2 + (1-y)^2 F_{RL}^2) + (1-\lambda)(F_{LL}^2 + (1-y)^2 F_{LR}^2) \right] + \\ & + \left[f_q^N(x, Q^2) D_q^B(z, Q^2) + h_N h_B f_q^N(x, Q^2) \Delta D_q^B(z, Q^2) \right] \times \left[(1+\lambda)(F_{RL}^2 + (1-y)^2 F_{RR}^2) + (1-\lambda)(F_{LR}^2 + (1-y)^2 F_{LL}^2) \right] + \\ & + \left[h_N f_q^N(x, Q^2) D_q^B(z, Q^2) + h_B f_q^N(x, Q^2) \Delta D_q^B(z, Q^2) \right] \times \left[(1+\lambda)(F_{RR}^2 - (1-y)^2 F_{RL}^2) - (1-\lambda)(F_{LL}^2 - (1-y)^2 F_{LR}^2) \right] + \\ & + \left[h_N f_q^N(x, Q^2) D_q^B(z, Q^2) + h_B f_q^N(x, Q^2) \Delta D_q^B(z, Q^2) \right] \times \left[(1+\lambda)(F_{RL}^2 - (1-y)^2 F_{RR}^2) - (1-\lambda)(F_{LR}^2 - (1-y)^2 F_{LL}^2) \right] \end{aligned} \quad (7)$$

where

$$f_q^N(x, Q^2) = f_{q(+)}^{N(+)}(x, Q^2) + f_{q(-)}^{N(+)}(x, Q^2),$$

$$\Delta f_q^N(x, Q^2) = f_{q(+)}^{N(+)}(x, Q^2) - f_{q(-)}^{N(+)}(x, Q^2),$$

$$D_q^B(z, Q^2) = D_{q(+)}^{B(+)}(z, Q^2) + D_{q(-)}^{B(+)}(z, Q^2)$$

$$\Delta D_q^B(z, Q^2) = D_{q(+)}^{B(+)}(z, Q^2) - D_{q(-)}^{B(+)}(z, Q^2),$$

$f_q^N(x, Q^2)$ and $D_q^B(z, Q^2)$ present the usual function of quark distribution in nucleon and quark fragmentation function in baryon B .

The summation over q in (7) extends over all quarks and antiquarks which are in nucleon N .

The differential cross-section of semi-inclusive DIS antilepton on nucleon $l^+ N \Rightarrow l^+ B$ can be obtained from (7) with the help of the following exchanges:

$$\frac{d\sigma^{(+)}}{dx dy dz} = \frac{d\sigma^{(-)}}{dx dy dz} (F_{RR} \Leftrightarrow F_{LR}, F_{RL} \Leftrightarrow F_{LL}). \quad (8)$$

P -odd electroweak asymmetries DIS of longitudinal polarized leptons and antileptons can be defined by the unpolarized target by the following form:

$$A(l_L^- - l_R^-) = [\sigma_L^{(-)} - \sigma_R^{(-)}] / [\sigma_L^{(-)} + \sigma_R^{(-)}], \quad (9)$$

$$A(l_L^+ - l_R^+) = [\sigma_L^{(+)} - \sigma_R^{(+)}] / [\sigma_L^{(+)} + \sigma_R^{(+)}], \quad (10)$$

$$A(l_R^- - l_L^-) = [\sigma_R^{(-)} - \sigma_L^{(-)}] / [\sigma_R^{(-)} + \sigma_L^{(-)}], \quad (11)$$

$$A(l_L^- - l_R^+) = [\sigma_L^{(-)} - \sigma_R^{(+)}] / [\sigma_L^{(-)} + \sigma_R^{(+)}]. \quad (12).$$

$$\text{Here } \sigma_L^{(-)} = \frac{d\sigma_L^{(-)}}{dx dy dz} \text{ and } \sigma_R^{(-)} = \frac{d\sigma_R^{(-)}}{dx dy dz} \text{ and } \sigma_R^{(+)}$$

are differential cross-sections of semi-inclusive DIS right- and left-polarized lepton (antilepton) on nucleons.

At DIS of longitudinal polarized lepton (antilepton) the polarized asymmetries can be defined on the polarized nucleon

$$A_p^{(\mp)} = [\sigma_{RR}^{(\mp)} - \sigma_{LL}^{(\mp)}] / [\sigma_{RR}^{(\mp)} + \sigma_{LL}^{(\mp)}] \quad (13)$$

$$A_a^{(\mp)} = [\sigma_{RL}^{(\mp)} - \sigma_{LR}^{(\mp)}] / [\sigma_{RL}^{(\mp)} + \sigma_{LR}^{(\mp)}] \quad (14)$$

Charge-polarized asymmetries

$$B_p^{(\mp)} = [\sigma_{RR}^{(\mp)} - \sigma_{LL}^{(\pm)}] / [\sigma_{RR}^{(\mp)} + \sigma_{LL}^{(\pm)}] \quad (15)$$

$$B_a^{(\mp)} = [\sigma_{RL}^{(\mp)} - \sigma_{LR}^{(\pm)}] / [\sigma_{RL}^{(\mp)} + \sigma_{LR}^{(\pm)}] \quad (16)$$

and charge asymmetries

$$C_{\alpha\beta} = [\sigma_{\alpha\beta}^{(-)} - \sigma_{\alpha\beta}^{(+)}] / [\sigma_{\alpha\beta}^{(-)} + \sigma_{\alpha\beta}^{(+)}], (\alpha, \beta = R, L). \quad (17)$$

Here $\sigma_{RR}^{(\mp)}$, $\sigma_{LL}^{(\mp)}$, $\sigma_{RL}^{(\mp)}$ and $\sigma_{LR}^{(\mp)}$ are cross-sections of the processes (1) at the polarization of lepton (antilepton) and nucleon $\lambda = 1, h_N = 1; \lambda = -1, h_N = -1, \lambda = 1, h_N = -1$ and $\lambda = -1, h_N = 1$.

The study of the longitudinal polarization of baryon B , which can be measured on angle distribution of decay products in processes $B \Rightarrow N + \pi$ presents the special interest.

$$P_B^{(\mp)} = [\sigma^{(\mp)}(h_B = 1) - \sigma^{(\mp)}(h_B = -1)] / [\sigma^{(\mp)}(h_B = 1) + \sigma^{(\mp)}(h_B = -1)] \quad (18)$$

$$P_B^{(\mp)}(\lambda) = [\sigma^{(\mp)}(\lambda, h_B = 1) - \sigma^{(\mp)}(\lambda, h_B = -1)] / [\sigma^{(\mp)}(\lambda, h_B = 1) + \sigma^{(\mp)}(\lambda, h_B = -1)] \quad (19)$$

$$P_B^{(1)}(h_L) = \frac{\sigma^B(h_L, h_B=1) - \sigma^B(h_L, h_B=-1)}{\sigma^B(h_L, h_B=1) + \sigma^B(h_L, h_B=-1)}. \quad (20)$$

The electroweak asymmetries (9)-(17) and also the

degree of longitudinal polarization of baryon (18)-(20) are expressed through spiral amplitudes $F_{\alpha\beta}$ and quark distribution and fragmentation functions. For example, the left-right asymmetry $A(l_L^- - l_R^-)$ and the degree of longitudinal polarization of baryon $P_B^{(1)}(\lambda=1)$ are defined by the expressions:

$$A(l_L^- - l_R^-) = \frac{1 - (1-y)^2}{1 + (1-y)^2} \left[\sum_q (F_{LL}^2 - F_{LR}^2) \times [f_q^N(x, Q^2) D_q^B(z, Q^2) - f_{\bar{q}}^N(x, Q^2) \times D_{\bar{q}}^B(z, Q^2)] \right] \left[\sum_q (F_{LL}^2 + F_{LR}^2) [f_q^N(x, Q^2) \times D_q^B(z, Q^2) + f_{\bar{q}}^N(x, Q^2) D_{\bar{q}}^B(z, Q^2)] \right]^{-1} \quad (21)$$

$$P_B^{(1)}(\lambda=1) = \left[\sum_q f_q^N(x, Q^2) \Delta D_q^B(z, Q^2) (F_{RR}^2 - (1-y)^2 F_{RL}^2) + \sum_{\bar{q}} f_{\bar{q}}^N(x, Q^2) \Delta D_{\bar{q}}^B(z, Q^2) (F_{RL}^2 - (1-y)^2 F_{RR}^2) \right] \left[\sum_q f_q^N(x, Q^2) D_q^B(z, Q^2) (F_{RR}^2 + (1-y)^2 F_{RL}^2) + \sum_{\bar{q}} f_{\bar{q}}^N(x, Q^2) D_{\bar{q}}^B(z, Q^2) (F_{RL}^2 + (1-y)^2 F_{RR}^2) \right]^{-1} \quad (22)$$

In the expressions of the observed values the phenomenological parameters - distribution functions of quarks and antiquarks in polarized nucleons and fragmentation function of polarized quark (antiquark) into polarized baryon B, the values of which are defined from the experiment are present. In the literature there are set of distribution functions of quarks in nucleons [5-7]. The distribution functions of valence and sea polarized quarks (antiquarks) in nucleons, given in [6] have been considered by us for the numeral evaluations of asymmetries and polarizations.

The numeral calculations of the electroweak asymmetries and degree of longitudinal polarization of Λ^0 -hyperons in semi-inclusive reactions $e^+ p \rightarrow e^+ \Lambda^0 X$ at energy $\sqrt{s} = 300 \text{ GeV}$ (ep - collider HERA), Weinberg parameter $\sin^2 \theta_W = 0.232$ are given by us.

According to the refs [9,10], the spin functions of quark fragmentation into Λ^0 -hyperon are parameterized in the form

$$\begin{aligned} \Delta D_S^{\Lambda}(z, Q^2) &= z^\alpha D_S^{\Lambda}(z, Q^2), \\ \Delta D_L^{\Lambda}(z, Q^2) &= \Delta D_d^{\Lambda}(z, Q^2) = N_L \Delta D_S^{\Lambda}(z, Q^2), \end{aligned} \quad (23)$$

α and N_L parameters are chosen in three variants

Parameter	Variant 1	Variant 2	Variant 3
α	0.62	0.27	1.66
N_L	0	-0.2	1

The dependency of electroweak asymmetries $A(e_R^- - e_L^-)$, $A(e_L^- - e_R^-)$, $A(e_L^- - e_R^-)$, $A(e_L^+ - e_R^+)$ on x variable at the fixed value $y=0.5$ and on y variable at the fixed value $x=0.7$ is given on the figures 1. a) and b).

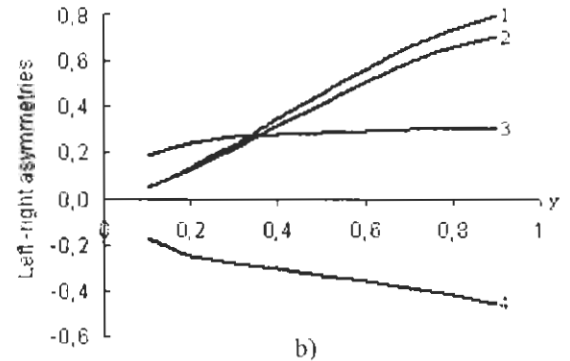
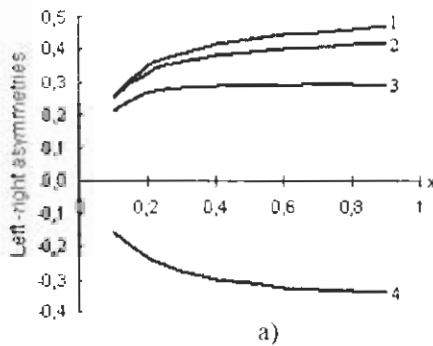


Fig 1. The dependence of the asymmetries $A(e_R^- - e_L^-)$, $A(e_L^- - e_R^-)$, and $A(e_L^- - e_R^-)$ and $A(e_L^+ - e_R^+)$ (curves 1, 2, 3 and 4 correspondingly) on x at $y=0.5$ and on y at $x=0.7$.

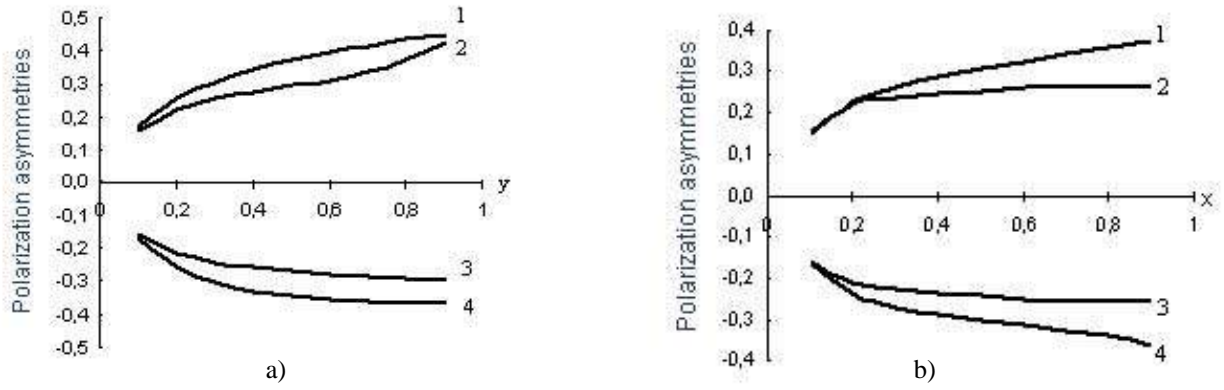


Fig.2. The dependence of the asymmetries $A_p^{(+)}$, $A_u^{(+)}$, $A_p^{(-)}$ and $A_u^{(-)}$ (curves 1, 2, 3 and 4 correspondingly) on x at $y=0,3$ and on y at $x=0,5$.

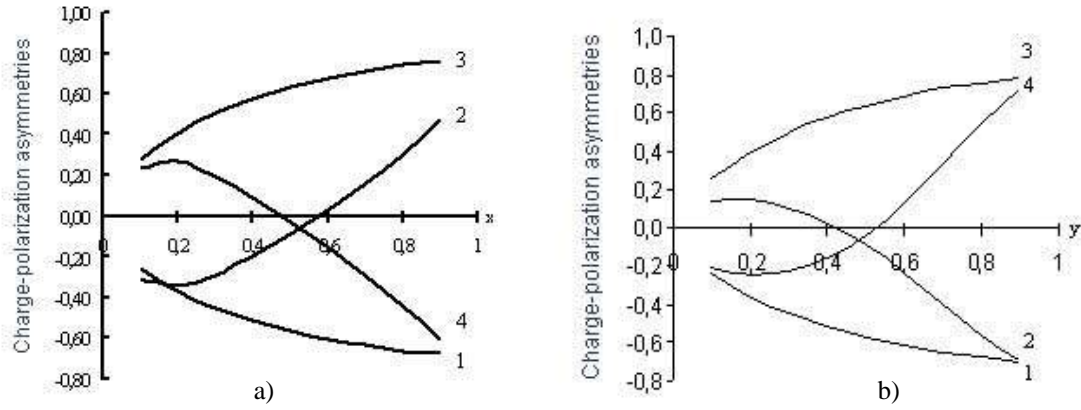


Fig.3. The dependence of the asymmetries $B_p^{(+)}$, $B_u^{(+)}$, $B_p^{(-)}$ and $B_u^{(-)}$ (curves 1, 2, 3 and 4 correspondingly) on x at $y=0,5$ and on y at $x=0,5$.

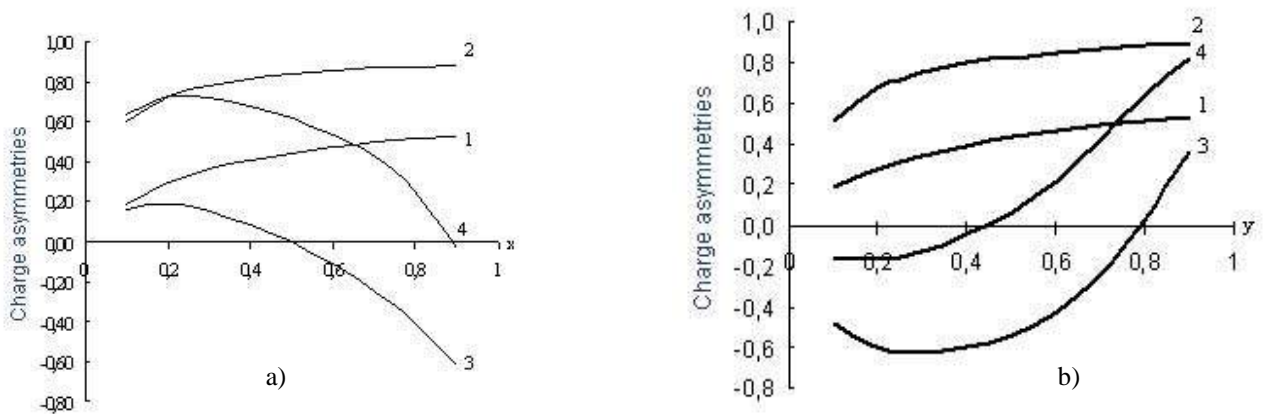


Fig.4. The dependence of the asymmetries C_{RR} , C_{LL} , C_{RL} and C_{LR} (curves 1, 2, 3 and 4 correspondingly) on x at $y=0,7$ and on y at $x=0,7$.

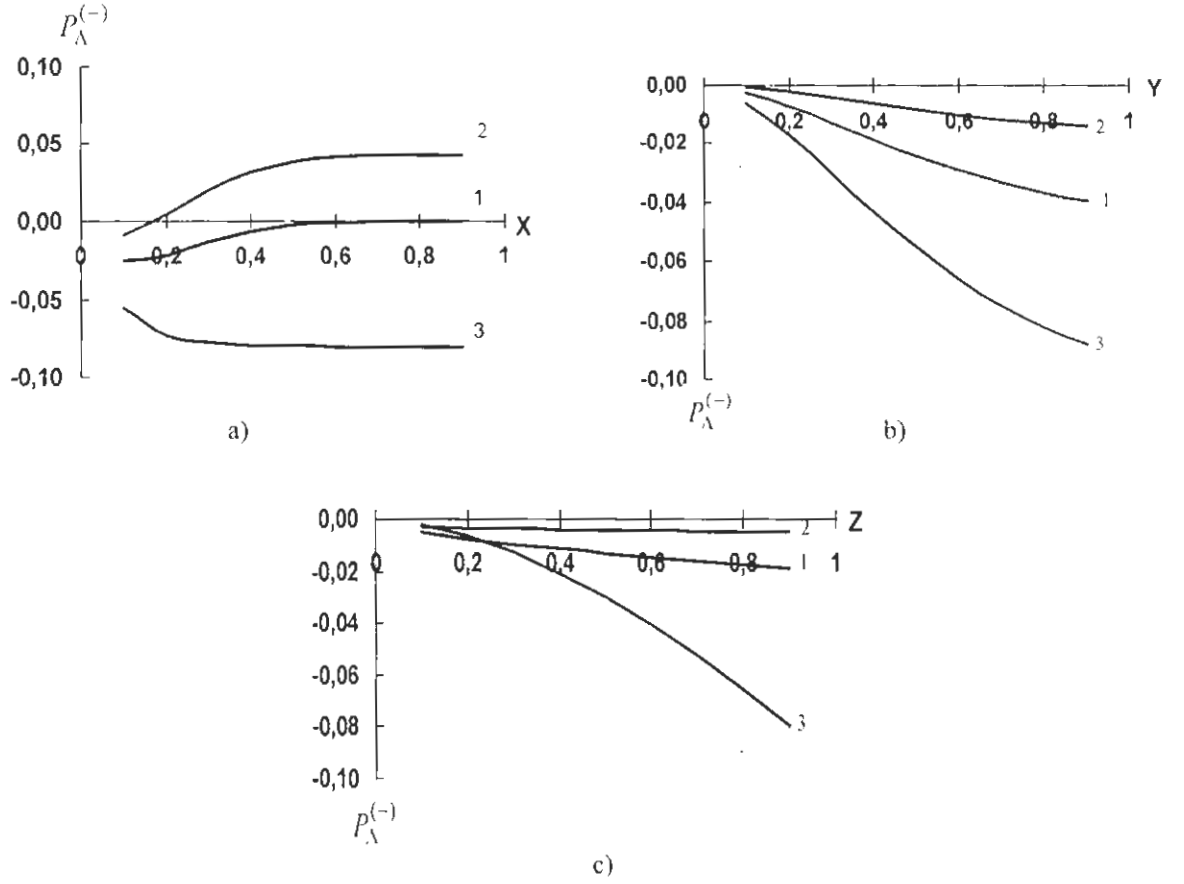


Fig.5. The dependence of $P_A^{(-)}$ on x at $y=0,5, z=0,5$ (a); on y at $x=0,1, z=0,5$ (b) and on z at $x=0,1, y=0,3$ (c).

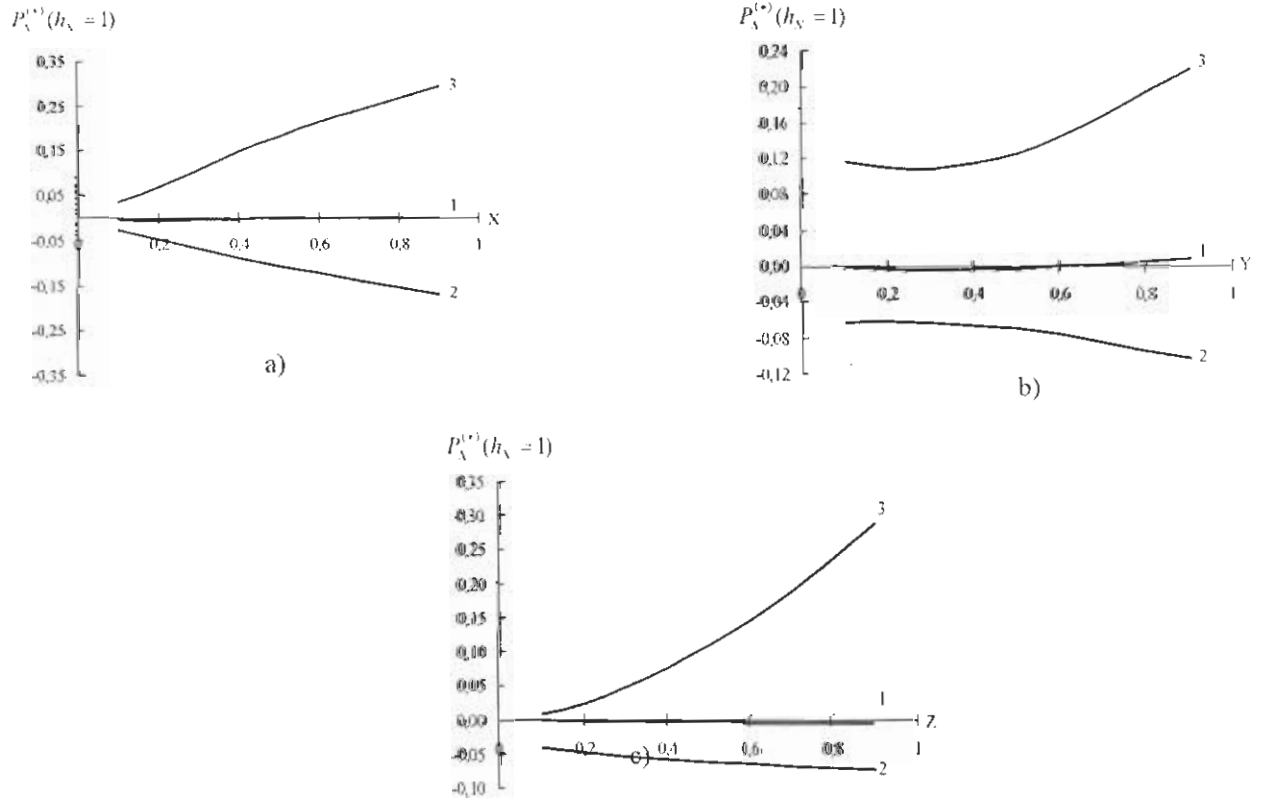


Fig.6. The dependence of the degree of longitudinal polarization $P_A^{(+)}(h_N = 1)$ on x at $y=0,3, z=0,5$ (a); on y at $x=0,3, z=0,5$ (b) and on z at $x=0,3, y=0,3$ (c).

The analogical behavior is observed for x - and y -dependencies of electroweak asymmetries $A_p^{(*)}, A_a^{(*)}, B_p^{(*)}, B_a^{(*)}, C_{RR}, C_{LL}, C_{RL}$ and C_{LR} (see fig.2-4. a) and b)). It is need to note, that the electroweak asymmetries don't depend on z variable at the choice of quark fragmentation function into Λ^0 -hyperon in the form (23).

The dependence of degree of longitudinal polarization of Λ^0 -hyperon $P_\Lambda^{(-)}$ in reactions $e^+p \rightarrow e^+\Lambda^0 X$ on x, y, z variables is given on the fig.5. As it is seen in 1 and 2 variants

the degree of longitudinal polarization of Λ -hyperon is small and weakly depends on x, y, z variables. In 3 variant polarization is negative and with the decrease of x, y or z , it weakly increase on module. The figure 6 illustrates the dependence of longitudinal polarization of Λ^0 -hyperon $e^+p \rightarrow e^+\Lambda^0 X$ with polarized nucleon $h_N = +1$. In 1 model the polarization is almost zero, and in 2 and 3 models it achieves to several percents.

-
- | | |
|---|--|
| [1] C. Adloff et al. Z.Phys., 1997, c. 74, 191. | [7] A.D. Martin, W.I. Stirling. Phys.Rev., 1995, D51, 4756. |
| [2] B. Lampe, E. Reya. Phys. Reports, 2000, 332, 1. | [8] M. Gluck et al. Phys. Rev, 1996, D53, 4775. |
| [3] K. Abe et al. Phys. Rev. Lett., 1997, 79, 26. | [9] D. De Florian, M. Stratmann, W. Vogelsang. Phys Rev., 1998, D57, 5811. |
| [4] K. Ackerstaff et al. Phys. Lett., 1997, B 404, 383. | [10] M. Anselmino et al. hep-ph/0106055, v1, 2001. |
| [5] Hermes Collab. Phys. Lett., 1998, B 442, 1484. | |
| [6] H.Y.Cheng, S.N.Lai, C.Y.Wu. Phys.Rev., 1996, D53, 2380. | |

S.K. Abdullayev, A.I. Muxtarov, S.M. Rəhimova

$I^+N \Rightarrow I^+BX$ YARIMİNKLYUZİV DƏRİN QEYRİ ELASTİKİ REAKSİYALARDA ELEKTROZƏİF PROSESLƏR

Standart nəzəriyyə çərçivəsində və kvark-parton modelində Λ -heperonun uzununa polyarizasiyası və yarıminklyuziv $I^+N \Rightarrow I^+\Lambda X$ reaksiyalarda elektrozəif asimetriyalar tədqiq edilmişdir. Λ -heperonun uzununa polyarizasiya dərəcəsinin, sol-sağ polyarizasiyalarının, yük polyarizasiyasının və yük asimetriyasının analitik ifadələri hesablanmış və analizi verilmişdir.

С.К. Абдуллаев, А.И. Мухтаров, С.М. Рагимова

ЭЛЕКТРОСЛАБЫЕ АСИММЕТРИИ В ПОЛУИНКЛЮЗИВНЫХ ГЛУБОКОНЕУПРУГИХ РЕАКЦИЯХ $I^+N \Rightarrow I^+BX$

В рамках стандартной теории и в кварк-партонной модели проведено исследование степени продольной поляризации Λ -гиперона и электрослабых асимметрий в полуинклюзивных реакциях $I^+N \Rightarrow I^+\Lambda X$. Получены выражения для степени продольной поляризации Λ -гиперона, лево-правых, поляризационных, зарядово-поляризационных и зарядовых асимметрий.

Received: 06.09.05

THE DOPING OF Cu_{2-x}S MAGNETOSENSITIVE AND COMPONENT (Sm) FILMS IN ELECTROSYNTHESIS PROCESS

**E.N. ZAMANOVA, L.A. ALIYEVA, S.M. BAGIROVA,
M.N. YOLCHIEV, G.G. GUSEYNOV**

*Institute of Physics of NAS of Azerbaijan,
Baku, Az-1143, H. Javid av., 3.*

The technology of electrosynthesis and doping in electrosynthesis process of Cu_{2-x}S magnetosensitive and component (Sm) films has been developed. It is established, that the electrolytic sediments and films, precipitated on nickel, platinum planes have monocline syngony, correspond to CuSmS_2 composition, p-type conductivity and are the magnetosensitive material, can be applied in the magneto optic devices.

The wide use of the semiconductor films with big square in earth sun energy has made the problem of the obtaining of the semiconductor layers on simple and chip technology, actual at the saving of optical, electric and photoelectric properties of the films on high enough level. In this respect, the method of the chemical precipitation from the solution (OR) presents interest, i.e. the films with big range of electric and optical properties [1-4] can be obtained by this method, regulating the ion composition of solution and precipitation mode.

The doping technology of Cu_{2-x}S of magnetosensitive and component (Sm) films during electrosynthesis has been developed by us.

The electrodeposition was carried out from the electrolyte solution by the composition:

Cuprum sulfate – $0,4 \div 0,5$ mol/l,

Sulfuric acid – $0,15 \div 0,20$ mol/l,

Sodium thiosulfate – $0,15 \div 0,20$ mol/l,

Samarium oxide – $0,015 \div 0,02$ mol/l.

The electrolysis was carried out at the current density $10 \div 60$ mA/sm², temperature $20 \div 22^\circ\text{C}$ and precipitation time 5-10 min. In the capacity of the cathode the polished planes from nickel, platinum and stainless steel were used and in the capacity of anode the plane from the platinum was used in all cases.

The concrete samples of the electrolytic obtaining of CuSmS_2 compound at the different electrolyte compositions, current densities and electrolysis time, and results of chemical analysis are given in the table 1.

Table1

The samples of the obtaining of Cu-Sm-S alloy, electrolysis modes and results of chemical analysis

	The composition of main components of electrolyte, mol/l	Current density, mA/sm ²	Temperature °C	Alloy composition, weight, %			Alloy composition	Electrolysis duration, min	Thickness of covering, mcm
				Sm	Cu	S			
1	$\text{CuSO}_4 - 0,40$ $\text{Na}_2\text{S}_2\text{O}_3 - 0,15$ $\text{H}_2\text{SO}_4 - 0,50$ $\text{SmO} - 0,015$	10	20	23,8	27,5	46,6	CuSmS_2	5	3,2
2	$\text{CuSO}_4 - 0,40$ $\text{Na}_2\text{S}_2\text{O}_3 - 0,18$ $\text{H}_2\text{SO}_4 - 0,53$ $\text{SmO} - 0,016$	20	20	26	20,8	53	CuSmS_2	5	3,4
3	$\text{CuSO}_4 - 0,48$ $\text{Na}_2\text{S}_2\text{O}_3 - 0,18$ $\text{H}_2\text{SO}_4 - 0,57$ $\text{SmO} - 0,018$	40	22	26,1	24,3	49,48	CuSmS_2	10	3,6
4	$\text{CuSO}_4 - 0,50$ $\text{Na}_2\text{S}_2\text{O}_3 - 0,20$ $\text{H}_2\text{SO}_4 - 0,80$ $\text{SmO} - 0,019$	50	22	26	24	49,8	CuSmS_2	8	3,8
5	$\text{CuSO}_4 - 0,50$ $\text{Na}_2\text{S}_2\text{O}_3 - 0,20$ $\text{H}_2\text{SO}_4 - 1,0$ $\text{SmO} - 0,020$	60	22	27,7	23,7	48,5	CuSmS_2	8	3,8

The films CuSmS_2 were subjected to the spectral analysis for the establishment of the film purity (table 2). As it is seen from the table 2, the obtained film CuSmS_2 has the purity 99,99%. The samples, obtained at the current density

40 mA/cm², electrolysis duration 10 minutes are subjected to the roentgen-phase analysis on the substrate from nickel. The crystallographic constants have been defined and they are compared with the analogical parameters of monocystal, the

composition of which corresponds to CuSmS_2 . The given data in the table 3 allow to suppose, that electrolytic sediments have monoclinic syngony and are correspond to CuSmS_2 composition.

Table 2
The results of spectral analysis of Cu-Sm-S films, obtained by the electrochemical method at the different current densities

Electrolyte, mol/l	Current density, mA/sm^2	Impurities, %			
		Fe	Si	Mg	CuSmS_2
$\text{CuSO}_4 - 0,50$	10	0,0001	0,01	0,001	99,99
$\text{Na}_2\text{S}_2\text{O}_3 - 0,20$	20	0,0001	0,01	0,001	99,99
$\text{H}_2\text{SO}_4 - 1,0$	40	0,0001	0,01	0,001	99,99
$\text{SmO} - 0,020$	50	0,0001	0,01	0,001	99,99
	60	0,0001	0,01	0,001	99,99

Table 3
The results of roentgen-phase analysis of electrochemically precipitated film CuSmS_2
Mode: 40kV, 6mA, $\text{CuK}_\alpha(\lambda=1,5418\text{\AA})$, eks 15 hour. Ni is filter

NN	Interplanar spaces from the single crystal [1,3]		Experimental data from electrochemically precipitated film CuSmS_2	
	D	I	d	I
1	4,109	7	4,166	6
2	3,691	7	3,721	1
3	3,233	1	3,265	1
4	2,924	6	2,942	5
5	2,834	6	2,820	1
6	2,560	7	2,566	4
7	2,337	7	2,327	9
8	2,127	6	2,117	10
9	2,036	1	2,012	1
10	1,954	1	1,977	1
11	1,897	3	1,893	9
12	1,730	2	1,707	6
13	1,545	2	1,580	1

The results of roentgen-phase analysis are given in table 3. The calculated of interplanar spacings of the monoclinic lattice are turned out identical with data, obtained from monocrystal of the analogical composition [1,3] with parameters of lattice: $a=6,496$; $b=7,13$; $c=6,799\text{\AA}$, $\beta=98^\circ 21'$, $P2/C'$, $Z=4$.

The influence of the samarium ions on the process of the combined precipitation sulfur and cuprum have been studied

by us. For the precipitation the platinum plane was used in the capacity of the cathode, and the polished nickel electrodes were used in the capacity of the anode. The polarized measures were carried out in the dependence of the samarium concentration in electrolyte and medium temperature. As it is seen from the table 4 the potential shifts to the negative side with the increase of the temperature and decrease of the samarium concentration in electrolyte.

Table 4
The shifting of the potential from electrolyte temperature and samarium concentration in the electrolyte

Temperature, $^\circ\text{C}$	The potential shifting, volt			
	$C_{\text{Sm}}=0,02 \text{ mol/l}$	$C_{\text{Sm}}=0,04 \text{ mol/l}$	$C_{\text{Sm}}=0,06 \text{ mol/l}$	$C_{\text{Sm}}=0,08 \text{ mol/l}$
25	+0,05	+0,15	+0,15	0
50	-0,05	0	0	0
70	0	0	0	-
90	0	-0,13	-0,3	-

It is known, that reconstruction potential is defined by that energy, which is needed to spend on the destruction of the crystalline lattice. The perfect the crystalline structure is the more energy is needed to spend on its destruction. It is consequent that reconstruction potential will shift to the negative side in the case of the samples with the perfect structure.

The velocity of the electrochemical reaction increases with the temperature increase that is seen from the increase of values of the limiting current and decrease of the region of its existence.

Thus, at the high temperatures the most favourable conditions for the combined precipitation of the components are created, i.e. the rapprochement of their potential separation because of the energy of mixing carries out. However, the best adhesion of the precipitating alloy with base is achieved at the temperature 25°C. The part of the precipitated alloy crumbles from electrode surface with the increase of the temperature and increase of the crystallization velocity, the covering is obtained irregular by the thickness. That's why, from the practical point of view the most interest are samples, obtained at the temperature 25°C. The microscopic photos of the transversal sections, fixed on microscope MIM-7 show, that samples are one-phase.

The use of the proposed technology for the coating of the triple alloy CuSmS_2 supplies the following advantages in the

comparison with the known ones:

a) the possibility of the coating of the semiconductor high-resistance covering with the magnetosensitive component electrolyte composition in practically allowed variation intervals, current density and synthesis temperature

$\text{CuSO}_4 - 0,4-0,5 \text{ mol/l}$,

$\text{Na}_2\text{S}_2\text{O}_3 - 0,15-0,20 \text{ mol/l}$,

$\text{H}_2\text{SO}_4 - 0,5-1,0 \text{ mol/l}$.

$\text{SmO} - 0,015-0,02 \text{ mol/l}$.

$I_k = 10 \div 60 \text{ mA/cm}^2$; $t = 20 \div 22^\circ\text{C}$, precipitation time $\tau = 5 \div 10 \text{ min}$,

b) quick decrease of the power inputs,

c) the simplicity and cheapness of the synthesis technology, the absence of the necessity of pressings, heat treatments and cooling.

Thus, this method allows to obtain the films of the triple alloy, consisting from the cuprum, samarium and sulfur-rare-earth semiconductor (RES) of p-type with $\rho = 2 \cdot 10^3 \div 10^{10} \text{ Ohm}\cdot\text{cm}$ at the room temperature, which are the paramagnetic material; in the temperature interval (77÷373)K and can be applied at the recording and transformation of the optical information in the magneto-optical devices by the method of the electrochemical precipitation as the analysis results show [4].

- [1] E.N. Zamanova, A.A. Mirzoeva, Z.A. Aliyarova Tekhnologiya izgotovleniya poluprovodnikovikh preobrazovateley metodom elektrosinteza. Tezisi XII Mendelevskogo cyezda po obshey i prikladnoy khimii. g. Baku, 1981, v. 3, p. 300. (in Russian)
- [2] E.N. Zamanova, M.A. Jafarov, H.M. Mamedov. Effect of Heattreatment on Electrophysical and Photoelectrical properties of P-type Cds Polycrystals. Semiconductor Science and Technology. Ins. of Phys. Publishing, Bristol, London, Philadelp, Paris, 12SST/ABC, (1999) 1234,1239.

- [3] E.N. Zamanova, A.A. Mirzoeva, G.G. Guseinov, S.M. Bagirova, F.G. Aliev. A.S. №1248326, SSSR .Elektrolit dlya naneseniya visokoomnikh pokritiy CuSmS_2 , 1986. (in Russian)
- [4] A.Sh. Abidinov, E.N. Zamanova, M.A. Jafarov, E.F. Nasirov. Geteropexodi na osnove plynok $\text{A}^2\text{B}^2\text{C}^6$, osajdenikh iz rastvora, IV Mejdunarodnaya konferentsiya "Amorfnye i mikrokristallicheskiye poluprovodniki" Sankt-Peterburg, 5-7 iyulya 2004 g. (in Russian).

E.N. Zamanova, L.A. Əliyeva, S.M. Bağirova, M.N. Elçiyev, Q.Q. Hüseyinov

ELEKTROSİNTEZ PROSESİNDƏ Cu_{2-x}S TƏBƏQƏLƏRİNİN MAQNİTOHƏSSAS KOMPONENT İLƏ (Sm) AŞQARLANMASI

Cu_{2-x}S təbəqələrinin elektrosintez yolu ilə alınması və maqnitohəssas komponent ilə (Sm) aşqarlanması texnologiyası işlənib. Təyin edilib ki, elektrolitik çöküntü və təbəqələr nikel, platin altlıqlar üzərində monoklin sinqoniyaya, CuSmS_2 –tərkibə, p-tip keçiriciliyə malik olan, maqnitohəssas materiallardır.

Э.Н. Заманова, Л.А. Алиева, С.М. Багирова, М.Н. Елчиев Г.Г. Гусейнов

ЛЕГИРОВАНИЕ ПЛЕНОК Cu_{2-x}S МАГНИТОЧУВСТВИТЕЛЬНОЙ КОМПОНЕНТОЙ (Sm) В ПРОЦЕССЕ ЭЛЕКТРОСИНТЕЗА

Разработана технология электросинтеза и легирования в процессе электросинтеза пленок Cu_{2-x}S магниточувствительной компонентой (Sm). Установлено, что электролитические осадки и пленки, осажденные на никелевые и платиновые пластинки, имеют моноклинную сингонию, соответствуют составу CuSmS_2 , р-типу проводимости, являются магниточувствительным материалом, могут найти применение в магнитооптических приборах.

Received: 14.06.05

THE FREQUENCY CHARACTERISTICS OF THE REFLECTION OF THE ELECTROMAGNETIC RADIATION IN THE LAYERED SYSTEMS

M.A. SADIKHOV, S.T. AZIZOV, A.S. ZEYNALOVA

*Institute of Physics of NASA,
Baku-1143, G. Javid av., 33*

In the ref the results of the investigation of the frequency characteristics of the layered systems, obtained by the way of the coating of the dielectric-metal of the quarter-wave-length layers from the non-absorptive material on the two-layered system.

The effect of the non-reflective absorption of the electromagnetic radiation in the two-layered systems of polar dielectric-metal, which is predicted and experimentally proved, appears in the dispersion region of the dielectric covering at the discrete values of the wave length of the incident radiation λ_0 , the thickness l_0 of the reflective layer of the covering and the substance of the polar molecules in it [1]. This effect has resonance character and taking this under consideration, the investigations of the frequency characteristics of the reflection of the electromagnetic waves from such two-layered system, near resonance values λ_0 and l_0 present the definite interest.

The results of the investigations show the bandlimitedness of the frequency spectrum, at which the effect of total absorption carries out. For the increase of the frequency band of the non-reflective absorption it was supposed to use the quarter-wave-length layers from the non-absorptive material, coated on the two-layered system of dielectric-metal. The investigation of the frequency characteristics of such layered system has been showed, that the use of the quarter-wave-layers significantly changes the frequency range, at which the partial or total absorption of the electromagnetic waves in these systems is carried out.

For the calculation of the frequency characteristics of the reflection of such system the following expression for the module of standing-wave ratio was used near chosen values λ_0 , l_0 [1,2]

$$\rho = \left| \frac{Z_{enm} - Z_0}{Z_{enm} + Z_0} \right| \quad (1)$$

where

$$M = \frac{1}{n(1 + y^2)} \frac{\operatorname{sh} 4\pi\bar{x}\bar{y} - y \sin 4\pi\bar{x}}{\operatorname{ch} 4\pi\bar{x}\bar{y} + \cos 4\pi\bar{x}};$$

$$N = \frac{1}{n(1 + y^2)} \frac{\bar{y} \operatorname{sh} 4\pi\bar{x}\bar{y} + \sin 4\pi\bar{x}}{\operatorname{ch} 4\pi\bar{x}\bar{y} + \cos 4\pi\bar{x}}.$$

For the creation of the simple automatized calculation of the reflection frequency characteristics of the absorbent coverings with one or two quarter-wave-length additional layers from the lossless materials, coated on them, the investigated algorithm was applied. It allows to evaluate the influence of the matched layers on the behavior of the frequency characteristics, in particularly, wave absorption band, near the spectral values l_0 , λ_0 in the dependence on the

where Z_{enm} is the input resistance of the multi-layer system depending on the frequency, substance properties and geometric dimensions of the directed system.

Taking under the consideration such approach the input resistance of the system at the connection to it the i -additional layer of the covering is equal:

$$Z_{eni} = \frac{Z_{eni-1} + Z_i \operatorname{th} \gamma_i l}{1 + \frac{Z_{eni-1}}{Z_i} \operatorname{th} \gamma_i l}, \quad (2)$$

where Z_{eni} , Z_{eni-1} are input resistances of the system at the existence of the i and $i-1$ layers; Z_i is wave resistance of i -layer; γ_i is distribution constant in the substance of i -layer in it [3,4].

From the equation (2) it is followed, that the input resistance of the multi-layer system, consisting from the absorptive layer and one additional layer will have the form

$$Z_{en1} = \frac{Z_{en} + Z_1 \operatorname{th} \gamma_1 l}{1 + \frac{Z_{en}}{Z_1} \operatorname{th} \gamma_1 l} \quad (3)$$

where Z_{en} is the input resistance of the absorptive layer.

According to the definition $Z_{en} = Z \operatorname{th} \gamma l$. Using the expression for Z and γ , we obtain:

$$Z_{en} = M + iN, \quad (4)$$

concerning substance properties and additional layers. The algorithm is constructed by the principle of the consistent calculations of the input resistances consisting the layer system during of their connection to the main layer.

The investigations of the frequency characteristics were carried out in the range of wave lengths 0,5-5 cm, moreover, it was considered, that dielectric properties of the adsorbent covering were described by Debye equation at the value

$\varepsilon_\infty=2$. The values, ε_0, τ of the substance of the absorbent layer varied in the interval 5-20 units and $5\text{-}20 \cdot 10^{-12}\text{c}$ correspondingly.

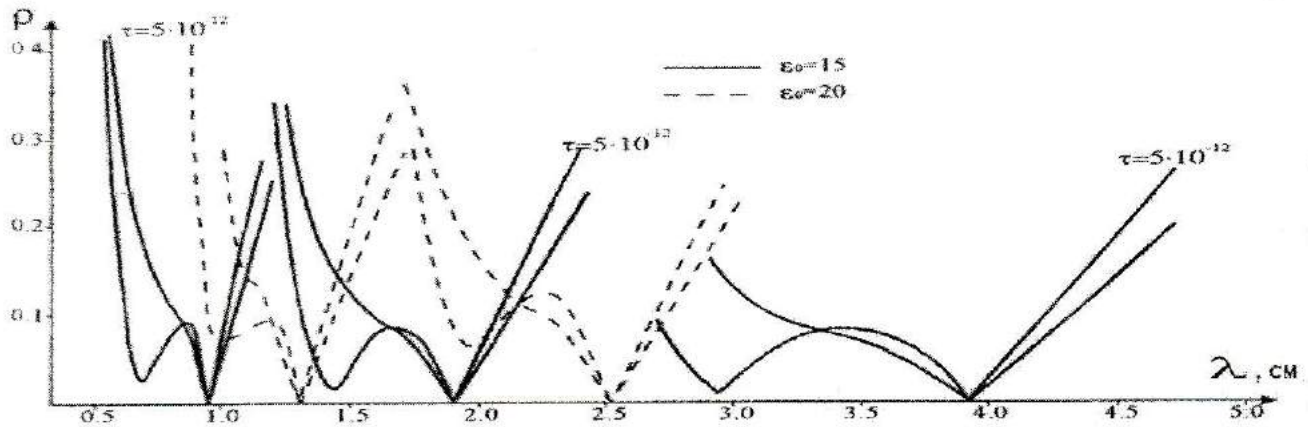


Fig. 1. The reflection frequency characteristics of the three-layered system with the values of the dielectric constant ε_l , which are equal to 2(a,c) and 1,5 (b).

The reflection frequency characteristics of the three-layered system with the value of the dielectric constants ε of the additional quarter-wave-length layer, which are equal to 1,5 and 2,0, are presented on the fig.1. As in the case of the two-layered system dielectric-metal, ε_0 of the absorbent layer of the given system at the constancy of the τ value leads to the decrease of the relative band of the wave selective absorption for the low-frequency spectrum arm and some its stabilization for the high-frequency spectrum arm (see table 1). Moreover, the increase of the N number of zero minimum of ρ value relatively the bans is decreased. However, in the difference from the system dielectric-metal in the given three-layered system the input of the additional quarter-wave-length layer causes to the expansion of the relative band of the selective wave absorption. The variety of the value τ at the constancy ε_0 influences on the absorption band insignificantly.

Table 1.

The values of the statistical dielectric constant ε_0 , relaxation time τ , thickness l_0 , the covering layer, wave length λ_0 , relative absorption band $\Delta\lambda/\lambda_0$ on the level $\rho_l=0,1$ of the three-layered absorbent system at ε_∞ and different values of the dielectric constants of the additional layer ε_l , N is number of dependence minimum of ρ on l .

$\tau 10^{-12}$	ε_0	λ_0	Low-frequency branch $N=1$ $k=2$	
			$\Delta\lambda/\lambda$ at $\varepsilon_l=4; \varepsilon_2=2$	$\Delta\lambda/\lambda$ at $\varepsilon_l=3; \varepsilon_2=1,5$
5	15	0,97	0,37	0,31
	20	1,28	0,37	0,21
10	15	1,93	0,35	0,33
	20	2,55	0,14	0,18
20	15	3,87	0,37	0,32

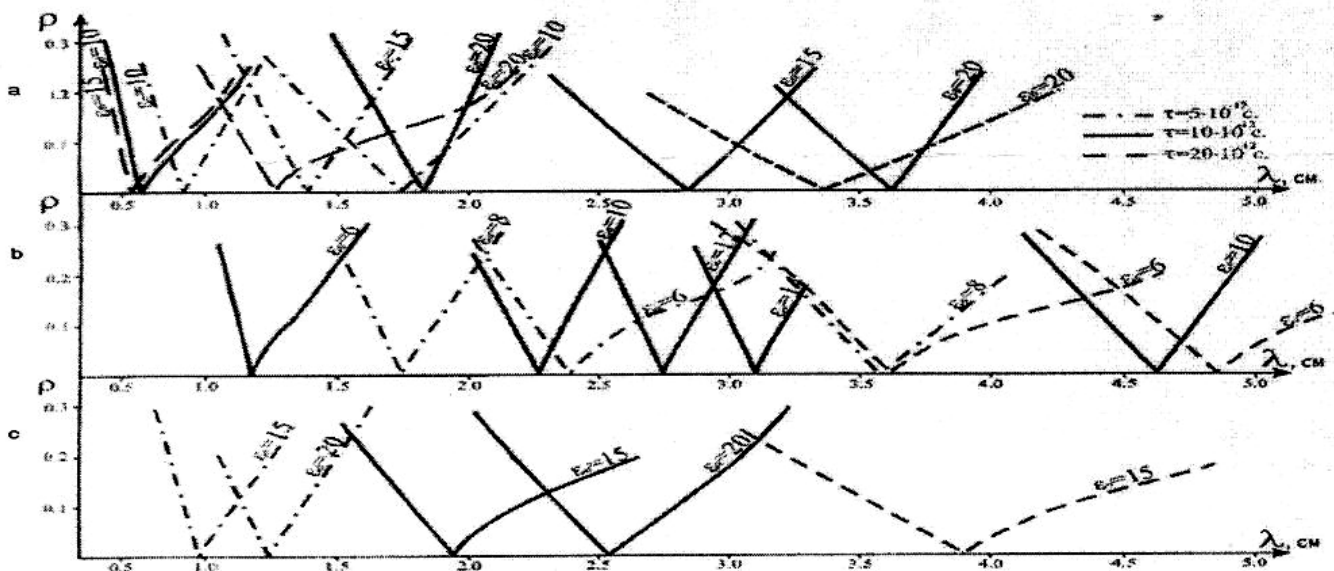


Fig. 2. The reflection frequency characteristics of the four-layered system with the values of the dielectric constant ε_0 , which are equal to 20 and 15 and values of the dielectric constants of the additional layers.

The input of the second additional quarter-wave-length layer significantly changes the frequency characteristic of the

wave reflection from such four-layered absorbent system. The families of the reflection frequency characteristics for the

four-layered systems, consisting the additional layers with the value $\varepsilon_1=4$; $\varepsilon_2=2$ and $\varepsilon_1=3$; $\varepsilon_2=1,5$ correspondingly are given on the fig.2.

The resistance transformer of these systems, appearing because of the two additional layers has the one and the same value of the transformation ratio $k=2$.

At the wave distribution in the waveguide and other direction system, the structure of the given algorithm of the calculation of the reflection frequency characteristics of the

multi-layered system is saved. In this case it is need to make the change of the used values $\varepsilon_0, \varepsilon_\infty, \tau, \varepsilon_1, \varepsilon_2, \dots, \varepsilon_m, \lambda$ on their

reduced values $\frac{\varepsilon_0 - p}{1 - p}$; $\frac{\varepsilon_\infty - p}{1 - p}$; $\tau \sqrt{1 - p}$; $\frac{\varepsilon_1 - p}{1 - p}$;

$\frac{\varepsilon_2 - p}{1 - p}$; $\frac{\varepsilon_n - p}{1 - p}$.

- [1] R.M. Kasimov. Injenerno-fizicheskiy lurnal. 1994, v. 66, №5-6. (in Russian).
 [2] R.M. Kasimov, M.A. Kalafi, E.R. Kasimov, Ch.O. Kajar, E.Yu. Salayev. Jurnal tekhnicheskoy fiziki, 1996, v.67, 2. p.167. (in Russian).

- [3] M.A. Sadikhov, E.R. Kasimov, R.M. Kasimov, Ch.O. Kajar. Fizika, v.4, №4, 1998, pp. 63-66. (in Russian).
 [4] M.A. Sadikhov, E.R. Kasimov. Preprint, №001, 1999, 49 s. (in Russian).

M.A. Sadıxov, S.T. Əzizov, A.S. Zeynalova

LAYLI SİSTEMLƏRDƏ ELEKTROMAQNİT ŞÜALANMANIN ƏKSÖLUNMASININ TEZLİKLİ XÜSUSİYYƏTLƏRİ

Məqalədə laylı sistemlərin, dielektrik-metal iki laylı sistemlərin dördəbirdəlgəli udmayan materialdan layları üstünə çəkilməmiş, tezliklərin xarakteristikalarının tədqiqinin nəticələri verilib.

М.А. Садыхов, С.Т. Азизов, А.С. Зейналова

ЧАСТОТНЫЕ ХАРАКТЕРИСТИКИ ОТРАЖЕНИЯ ЭЛЕКТРОМАГНИТНОГО ИЗЛУЧЕНИЯ В СЛОИСТЫХ СИСТЕМАХ

В статье представлены результаты исследования частотных характеристик слоистых систем, полученных путем нанесения на двухслойную систему диэлектрик-металл четвертьволновых слоев из непоглощающего материала.

Received: 17.06.06

THE INVESTIGATION OF THE STATES OF Cr, Co, Ni, Bi AND K IONS, DEPOSITED ON γ -Al₂O₃ IN THE COMPOSITION OF THE DEHYDROGENATION CATALYST BY ESDO AND RENTGENOGRAPHY METHODS

N.A. ALIYEV, S.A. JAMALOVA, R.B. AKHVERDIYEV, S.G. FARADJEVA,
T.F. ALLAHYAROVA, A.A. KASIMOV

*Institute of Oil-Chemical Processes of NAS of Azerbaijan,
370025, Baku, Hodjali av, 30*

The use of the deposited catalysts, which have more high mechanical strength, thermostability and relatively low inputs on their synthesis are the most suitable in the comparison with massive dehydrogenation catalysts. The data on the states of Cr, Ni, Bi, Co and K ions, deposited on γ -Al₂O₃, including in the composition of the catalysts of the paraffin hydrocarbons C₃-C₄ are presented in the given paper. The catalysts prepared in the atmospheric conditions and in the conditions of the low pressure were used. It is established, that valency and coordinative states of ions of transitive metals (Cr, Ni, Co) depend on the conditions of the catalyst preparation. The metal ions in the oxidated form are present in the samples of the catalysts, prepared in the atmospheric conditions. As oxidate forms of metal ions, so the restored ones are presented in the catalysts, prepared in the vacuum conditions. It is supposed, that high activity of the catalysts, obtained in the vacuum conditions, is caused by the presence of the oxidated and restored forms of the active components in the system.

The processes of the catalytic dehydrogenation of the paraffin hydrocarbons are included in the number of most big-volume processes of the world oil-chemical industry. This is connected firstly with the increase of the demand on the olefinic hydrocarbons, which are used for the obtaining: of the synthetic rubbers, plastics, the components of the automotive fuel (meliltretbutyl ether) and other valuable chemical products. The constant high quantity of the investigations, carried out on the perfection already existed and the working of the new dehydrogenation catalysts is caused by this [1-3].

The one of the perspective direction of the perfection of already existed dehydrogenation catalysts is their promotion by the oxides of the rare-earth elements [1-3].

The process of the dehydrogenation of propane on Cr, Co, Ni, Bi and K/ γ -Al₂O₃ catalysts has been worked in the IOCP of NAS of Azerbaijan.

The results of the states of ion metals (Cr, Ni, Bi, Co and K) in the composition of single-, double-, three-component samples of massive catalysts, prepared in the conditions of the lowered and atmospheric pressure were presented in the previous ref [4].

It is established, that catalysts of the samples, prepared in the atmospheric conditions have only oxidated forms of the given metals. In the difference from it, the samples of the catalysts, prepared in the vacuum conditions have as oxidated (Cr⁵⁺, Cr³⁺(O_h), Ni²⁺(O_h) and Co³⁺, Co²⁺), so the restored forms of the given metals (Cr⁰, Ni⁰, Co⁰).

It is established, that the coexistence of the oxidated and restored ions of these metals causes the relatively high catalytic activity of catalyst samples, synthesized in the vacuum conditions.

However, the use of the massive catalysts connects with set of defects, such as: the difficulties at the formation of catalyst granules in the stage of its preparation, relatively low thermal and mechanical stability, high capital inputs, connected with the use of the big quantity of metal salts.

Taking under the consideration the above mentioned, the use of the deposited catalysts on the base of the relatively cheap carrier - γ -Al₂O₃, which supplies the high enough mechanical strength and thermostability, low capital inputs on catalyst synthesis is the more suitable. Moreover, γ -Al₂O₃

is well connecting component, which supplies the quality and easy-to use formation of catalyst granule of its preparation.

Starting from the above mentioned suppositions, the subject of the given paper is the investigation of the states of Cr, Co, Ni, Bi and K, deposited on γ -Al₂O₃.

Experiment system

The definition of the catalyst activity was carried out in quartz reactor with stationary layer of catalyst, at volume advance speed of raw 400h⁻¹ and temperature in reactive band 590°C. The output of propylene on the passed raw was 49,5% at the selectivity 90,03% (mol).

The catalyst was prepared by the way of the marking of nitrates of the salts of corresponding metals on формула, previously treated by the drying at the temperature 400°C, with the aim of the release of catalyst pores from the air and water steams. The calcinations were carried out in the conditions as the lowered, so the atmospheric pressure at the temperature 600-620°C during eight hours.

The electronic spectrums of diffusion reflection (ESDR) have been fixed on the spectrophotometer "Specord M40" in the region 50000-10000 cm⁻¹.

The experiment results

Let's consider the results of spectral investigation of ion states in the composition of studied catalysts (electronic spectroscopy of diffusion reflection).

The oxide systems Ni (5;10;25 and 86,8%)- γ -Al₂O₃ (95;90;75 and 13,2%)

The well-released absorption bands (a.b.) in the region 13000, 15800, 16700 and 27500 cm⁻¹ are observed in the catalyst spectrum, consisting on 5% Ni (fig.1, c.1). The sample has blue color. The observable a.b. can be interpreted by the following way, taking under the consideration from [5, 6]:

- a.b. at 13000 and 27500 cm⁻¹ are registered to the absorption of Ni²⁺ ions, stabilized in the fields of octahedral

coordination (transfers ${}^3A_{2g} \rightarrow {}^3T_{2g}$ and ${}^3A_{2g} \rightarrow {}^3T_{1g}$ correspondingly);

- a.b. in the regions 15800 and 16700 cm^{-1} show on the existence of the tetrahedrally coordinated ions of $\text{Ni}^{2+}(\text{T}_d)$ in the system [(transfers ${}^3T_1(\text{F}) \rightarrow {}^3T_1(\text{P})$ and ${}^3T_1(\text{F}) \rightarrow {}^3E_1(\text{D})$ correspondingly].

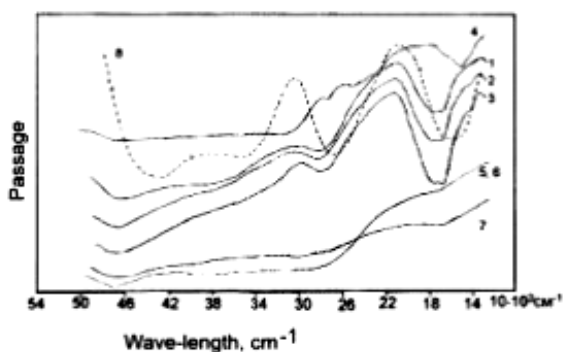


Fig.1. The spectrums of diffusion reflection of catalysts:

1. Ni (5%)- $\gamma\text{-Al}_2\text{O}_3$ (95%) - obtained at the atmospheric pressure
2. Ni (10%)- $\gamma\text{-Al}_2\text{O}_3$ (90%) - obtained at the atmospheric pressure
3. Ni (25%)- $\gamma\text{-Al}_2\text{O}_3$ (75%) - obtained at the atmospheric pressure
4. Ni (86,8%)- $\gamma\text{-Al}_2\text{O}_3$ (13,2%) - obtained at the atmospheric pressure
5. Ni (5%)- $\gamma\text{-Al}_2\text{O}_3$ (95%) - obtained in the vacuum conditions
6. Ni (10%)- $\gamma\text{-Al}_2\text{O}_3$ (90%) - obtained at the vacuum conditions
7. Ni (25%)- $\gamma\text{-Al}_2\text{O}_3$ (75%) - obtained at the vacuum conditions
8. Ni (86,8%)- $\gamma\text{-Al}_2\text{O}_3$ (13,2%) - obtained at the vacuum conditions

It is known, that nickel ions are presented as in octahedral, so in the tetrahedral coordination in the NiAl_2O_4 spinel, which is mixed. The formula of this spinel can be presented as $\text{Ni}_{1/4}\text{Al}_{3/4}[\text{Ni}_{3/4}\text{Al}_{5/4}]\text{O}_4$. It can be proposed, that the surface mixed spinel NiAl_2O_4 creates in our conditions also.

The increase of intensity of a.b. from ions of $\text{Ni}^{2+}(\text{O}_h)$ and $\text{Ni}^{2+}(\text{T}_d)$ is observed with the increase of the nickel concentration till 10 and 25% (fig.1, c. 2 and 3). The spectrum of the sample, consisting 86,8% of Ni significantly differs from the previously spectrums. Thus, the set of a.b. at 14000, 15500, 21700, 23900, 26400 cm^{-1} , characteristic for Ni^{2+} ions is observed in the composition of NiO phase, that explain the green color of the sample (fig.1,c.4).

The given conclusion doesn't exclude the presence of NiAl_2O_4 spinel in the system. From it the another important conclusion is obtained, firstly at the high concentrations of nickel on $\gamma\text{-Al}_2\text{O}_3$ surface the octahedral and tetrahedral vacancies are filled by nickel ions with the creation of NiAl_2O_4 spinel, later the process of formation of NiO phase is carried out.

The spectrums of the samples, consisting 10, 15 and 25% of nickel, obtained in the vacuum conditions significantly differ from the spectrums of the samples of analogical compositions, obtained in the conditions of the air atmosphere. Thus, the strong decrease of the intensity of a.b. from ions of $\text{Ni}^{2+}(\text{O}_h)$ and $\text{Ni}^{2+}(\text{T}_d)$ (fig. 1, c.5, 6 and 7) is

observed. Probably, the process of the partial reconstruction of $\text{Ni}^{2+}(\text{O}_h)$ and $\text{Ni}^{2+}(\text{T}_d)$ ions till Ni^0 carries out in the vacuum conditions.

Thus, at the relative low concentrations (5,10 and 25%) as the oxidated [$\text{Ni}^{2+}(\text{O}_h)$ and $\text{Ni}^{2+}(\text{T}_d)$], so the restored (Ni^0) forms of nickel are stabilized in the system.

The catalyst, consisting 86,8% of Ni and has obtained in the vacuum conditions, has the spectrum, which differs from spectrums of the systems, consisting the relatively less quantity of nickel (fig. 1, c.8). In this case the increase of intensity of a.b. from the ions of Ni^{2+} in NiO phase and their significant expansion is observed. Probably this effect connects with the processes of agglomeration and enlargement of NiO particles, where the strong spin-spin interaction leads to the increase of the intensity and widening of a.b.

The oxide system Cr(10 and 25%)- $\gamma\text{-Al}_2\text{O}_3$ (90 and 75%)

The a.b. are observed in the catalyst spectrum, consisting 10% of Cr and obtained in the atmospheric air in the regions 14400, 17000, 22000, 23000 and 27000 cm^{-1} (fig.2, c.1). The sample has the green-yellow color. The bands in the regions 14400, 22000 and 27000 cm^{-1} can be registered to the Cr^{5+} ions, and at 17000 and 23000 cm^{-1} to the $\text{Cr}^{3+}(\text{O}_h)$ ions (the transfers ${}^4A_{2g} \rightarrow {}^4T_{2g}$ and ${}^4A_{2g} \rightarrow {}^4T_{1g}$ correspondingly). Probably, the surface of the sample has two types of Cr ions: Cr^{5+} and $\text{Cr}^{3+}(\text{O}_h)$.

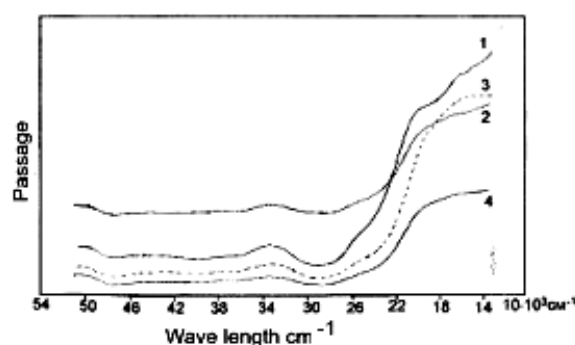


Fig.2. The spectrums of diffusion reflection of catalysts:

1. Cr (5%)- $\gamma\text{-Al}_2\text{O}_3$ (95%) - obtained at the atmospheric pressure
2. Cr (25%)- $\gamma\text{-Al}_2\text{O}_3$ (75%) - obtained at the atmospheric pressure
3. Cr (5%)- $\gamma\text{-Al}_2\text{O}_3$ (95%) - obtained in the vacuum conditions
4. Cr (25%)- $\gamma\text{-Al}_2\text{O}_3$ (75%) - obtained in the vacuum conditions

The increase of the Cr content in the system till 25% leads to the increase of the common absorption background and some degradation of a.b. from Cr^{5+} and $\text{Cr}^{3+}(\text{O}_h)$ ions (fig.2, c.2). The sample has the biscuit color that shows on the increase of the content of Cr_2O_3 phase in the system (in the pure form the Cr_2O_3 phase has the brown color).

The significant decrease of the intensity of a.b. from $\text{Cr}^{3+}(\text{O}_h)$ and Cr^{5+} ions is observed in the catalyst spectrums, obtained in the vacuum conditions. Probably the process of partial reconstruction of $\text{Cr}^{3+}(\text{O}_h)$ and Cr^{5+} ions till Cr^0 carries out in the conditions of the lowered pressure. In the given case the oxidated (Cr^{3+} and Cr^{5+}) and restored forms of Cr (Cr^0) coexist on the catalyst surface.

The oxide systems Cr(50;25;50%)-Ni(16,7;50;25%)- γ -Al₂O₃ (33,3; 25; 25%)

The a.b. in the regions 13000, 14000, 15500, 22000, 23000 and 26000 cm⁻¹ are observed in the sample spectrums, obtained in the air atmosphere (fig.3, c.1).

The observable a.b. can be explained by the following method:

- a.b. at 23000 and 26000 cm⁻¹ can be registered to Cr⁵⁺ ions;

- a.b. at 22000 cm⁻¹ can be registered to Cr³⁺(O_h) ions (transfer ⁴A_{2g}→⁴T_{2g}).

The rest a.b. from Cr³⁺(O_h) ions are masked by the more intensive background absorption.

- a.b. at 13000, 15500 cm⁻¹ are characteristics for Ni²⁺ ions in the composition of NiO phase. The green color of the sample also shows on this fact. The given conclusion also doesn't exclude the presence of NiAl₂O₄ spinel in the system, where probably a.b. from Ni²⁺(O_h) and Ni²⁺(T_d) ions are masked by a.b. from Cr⁵⁺(Cr³⁺)ions and NiO phase.

Thus, Cr⁵⁺, Cr³⁺ ions and NiO, NiAl₂O₄ phases are stabilized on the catalyst surface.

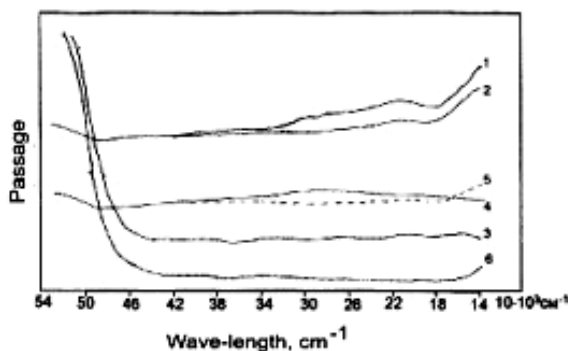


Fig.3. The spectrums of diffusion reflection of catalysts:

1. Cr (25%)-Ni (50%)- γ -Al₂O₃ (25%) – obtained at the atmospheric pressure
2. Cr (50%)-Ni (25%)- γ -Al₂O₃ (25%) – obtained at the atmospheric pressure
3. Cr (50%)-Ni (16,7%)- γ -Al₂O₃ (33,3%) – obtained at the atmospheric pressure
4. Cr (25%)-Ni (50%)- γ -Al₂O₃ (25%) – obtained in the vacuum conditions
5. Cr (50%)-Ni (25%)- γ -Al₂O₃ (25%) – obtained in the vacuum conditions
6. Cr (50%)-Ni (16,7%)- γ -Al₂O₃ (33,3%) – obtained in the vacuum conditions

The disappearance of a.b. at 14000 and 26000 cm⁻¹ is observed in the spectrum at the increase of the Cr concentration till 50% (at the simultaneous decrease of Ni concentration till 25%). Moreover, the intensity of the other a.b. with simultaneous their widening is observed (fig.3, c.2). The sample has brown-green color. Probably the quantity of the surface phase Cr₂O₅ increases at the high concentrations of Cr. The brown constituent of the sample color (in pure form Cr₂O₅ has the brown color) shows on this fact and this leads to the increase of the absorption background and widening of some a.b. Moreover, the part of a.b. from Cr³⁺(O_h) and Ni²⁺(O_h) ions is masked by strong background absorption.

Thus, the catalyst surface is enriched by Cr₂O₅ and NiO phases at relative high Cr concentration.

The decrease of Ni concentration till 16,7% significantly doesn't influence on the spectrum character (at the saving of Cr concentration 50%) (fig.3, c.3). The spectrums of all three catalysts, obtained in the vacuum are characterized by the spectrums, where the total absorption is observed, covering practically all investigated area (fig.3, c.4,5 and 6). Moreover, the samples have gray-black color with bluish shine. The processes of partial reconstruction of Cr⁵⁺, Cr³⁺(O_h) and Ni²⁺(O_h) ions till Cr⁰ and Ni⁰ rather carry out in the samples. It is followed, that the oxidated [Cr⁵⁺, Cr³⁺(O_h) and Ni²⁺(O_h) (in NiO phase)] and restored forms of Cr and Ni (Cr⁰ and Ni⁰) coexist on the surface of the catalyst.

The oxide system Cr(54,1%)-Bi(13,5%)- γ -Al₂O₃ (32,4%)

The total structureless intensive absorption, covering all area is observed in the catalyst spectrum, obtained in the air atmosphere (fig.4, c.1). The sample has black color. On account on this the spectrum interpretation is impossible, but it can be supposed about the presence Cr₂O₅, Cr₂O₃ in the phase system and Bi³⁺ in phase.

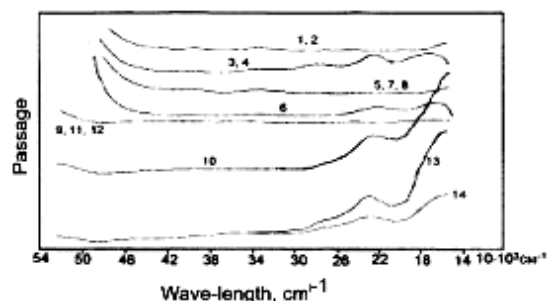


Fig.4. The spectrums of diffusion reflection of catalysts:

1. Cr (54,1%)-Bi (13,5%)- γ -Al₂O₃ (32,4%) – obtained at the atmospheric pressure
2. Cr (54,1%)-Bi (13,5%)- γ -Al₂O₃ (32,4%) – obtained in the vacuum conditions
3. Cr (87,7%)-Bi (7,4%)- γ -Al₂O₃ (4,9%) – obtained at the atmospheric pressure
4. Cr (87,7%)-Bi (7,4%)- γ -Al₂O₃ (4,9%) – obtained in the vacuum conditions
5. Cr (60%)-Bi (20%)- γ -Al₂O₃ (20%) – obtained at the atmospheric pressure
6. Cr (60%)-Bi (20%)- γ -Al₂O₃ (20%) – obtained in the vacuum conditions
7. Cr (67,1%)-Ni (22,4%)-K (5,6%)- γ -Al₂O₃ (4,9%) – obtained at the atmospheric pressure
8. Cr (67,1%)-Ni (22,4%)-K (5,6%)- γ -Al₂O₃ (4,9%) – obtained in the vacuum conditions
9. Cr (57%)-Ni (19%)-Bi (14,3%)- γ -Al₂O₃ (9,7%) – obtained at the atmospheric pressure
10. Cr (10,2%)-Ni (4,3%)-Bi (16%)- γ -Al₂O₃ (69,5%) – obtained at the atmospheric pressure
11. Cr (57%)-Ni (19%)-K (14,3%)- γ -Al₂O₃ (9,7%) – obtained in the vacuum conditions
12. Cr (10,2%)-Ni (4,3%)-Bi (16%)- γ -Al₂O₃ (69,5%) – obtained in the vacuum conditions
13. Cr (10,2%)-Ni (4,3%)-K (1%)-Co(1,6%)- γ -Al₂O₃ - (82,9%) – obtained at the atmospheric pressure
14. Cr (10,2%)-Ni (4,3%)-K (1%)-Co(1,6%)- γ -Al₂O₃ - (82,9%) – obtained in the vacuum conditions.

The quite another picture is observed for the catalyst, obtained in the vacuum. Thus, the wide a.b. are observed in region 17000,22000 and 27000 cm⁻¹ (fig.4, c.2). The bands in

the region 22000 and 27000 cm^{-1} can be registered to the absorption of Cr^{5+} ions, and a.b. at 17000 cm^{-1} can be registered to $\text{Cr}^{3+}(\text{O}_h)$ ions. Probably, Cr^0 particles also present in the system. Probably, bismuth has the doping influence on $\text{Cr}^{3+}(\text{O}_h)$ ions, that leads to their stabilization and stability to the reconstruction processes in the vacuum conditions. In the result of this, the catalyst surface is enriched by Cr_2O_3 phase. The green color of the sample also shows on this fact (in the pure form Cr_2O_3 phase has dark-green color). In the given case mainly Cr^{5+} ions are treated by the reconstruction process. This effect doesn't reveal in the case of the catalyst, prepared in the air atmosphere.

Probably the oxidative medium causes to the enrichment of the surface of Cr_2O_5 and Bi_2O_3 phases that leads to the darkening of the sample and appearance of the wide structureless absorption in the spectrum.

The carried out investigations allow to conclude the set of the important things:

- the surface in the catalyst, obtained in the air atmosphere, is enriched by Cr_2O_5 and Bi_2O_3 oxides in the result of the oxidative processes;
- the Bi^0 particles, having the doping influence on $\text{Cr}^{3+}(\text{O}_h)$ ions stabilize in the result of the reconstruction processes in the catalyst, obtained in the vacuum condition. In the result of this, mainly the Cr_2O_5 phase is treated by the reconstruction. In the given case the Cr^{5+} , $\text{Cr}^{3+}(\text{O}_h)$, Cr^0 and Bi^0 ions coexist in the system.

The oxide system (87,7%)-K(7,4%)- γ - Al_2O_3 (4,9%)

The catalyst spectrums, obtained in the air atmosphere and vacuum are analogical to the spectrums of the system $\text{Cr}(54,1\%)\text{-Bi}(13,5\%)\text{-}\gamma\text{-Al}_2\text{O}_3$ (fig.4, c.3 and 4) and all conclusions, made on the analysis results of this system can be registered to the system $\text{Cr-K-}\gamma\text{-Al}_2\text{O}_3$.

The oxide system Cr(60%)-Ni(20%)-Bi(15%)- γ - Al_2O_3 (5%)

The catalyst, obtained in the conditions of air atmosphere and vacuum has the spectrum, which is identical to the spectrums of the samples $\text{Cr-Bi-}\gamma\text{-Al}_2\text{O}_3$ and $\text{Cr-K-}\gamma\text{-Al}_2\text{O}_3$ (fig.4, c.5 and 6). It is followed, that introduction of Ni in the catalyst doesn't influence significantly on valency and coordination state of Cr and bismuth ions.

On the assumption of the investigation results of $\text{Ni-}\gamma\text{-Al}_2\text{O}_3$ system, it is possible to suppose, that NiO , Cr_2O_5 , Cr_2O_3 , Bi_2O_3 phases form on the catalyst surface, obtained in the air atmosphere.

On the assumption of the investigation results of the previous catalysts, it is possible to suppose, that the surface composition of the catalyst, obtained in the vacuum, consists as on the oxidated forms of Cr (Cr_2O_5 and Cr_2O_3) and Ni (NiO), so on the restored forms Cr^0 and Ni^0 .

The oxide system Cr(67,1%)-Ni(22,4%)-K(5,6%)- γ - Al_2O_3 (4,9%)

The catalyst spectrums, obtained in the air atmosphere and vacuum, are identical and characterized by the total structureless absorption, covering all spectral area (fig.4, c.7 and 8). The both samples have black color. Though spectrum identification in this case is difficult, but it's possible to propose the following:

- the Cr_2O_5 , Cr_2O_3 , NiO , NiAl_2O_4 , K_2O phases are present in the catalysts, obtained in the air atmosphere;
- the phase composition of the catalysts, obtained in the vacuum consists as on oxidated form of Cr (Cr_2O_5 , Cr_2O_3) and Ni (NiAl_2O_4), so on restored forms Cr^0 and Ni^0 . In this case the doping influence of K on Cr ions is absent.

The oxide systems Cr(57 и 10,2%)-Ni(19 и 4,3%)-Bi(14,3 и 16%) and (9,7 и 69,5%)- γ - Al_2O_3

The total structureless absorption, covering practically all area is observed in the catalyst spectrum of $\text{Cr}(57\%)\text{-Ni}(19\%)\text{-Bi}(14,3\%)\text{-K}(9,7\%)\text{-}\gamma\text{-Al}_2\text{O}_3$ composition (fig.4, c.9). The decrease of Cr and Ni concentrations till 10,2 and 4,3% leads to the significant changes in the spectrum. Thus, a.b. are observed in the regions 13000, 14000 (weak a.b. in the form of the shoulder), 15900, 16900, 22000, 26000 cm^{-1} and 27300 cm^{-1} (fig.3, c.10). The observable a.b. can be registered to the following way:

- a.b. at 13000 and 27300 cm^{-1} are registered to $\text{Ni}^{2+}(\text{O}_h)$ ions [transfers ${}^3\text{A}_{2g} \rightarrow {}^3\text{T}_{2g}$ and ${}^3\text{A}_{2g} \rightarrow {}^3\text{T}_{1g}(\text{P})$ correspondingly];
- the absorption in the regions 15900 and 16900 cm^{-1} are characteristic for the systems, consisting $\text{Ni}^{2+}(\text{T}_d)$ ions [transfers ${}^3\text{T}_1(\text{F}) \rightarrow {}^3\text{T}_1(\text{P})$ и ${}^3\text{T}_1(\text{F}) \rightarrow {}^1\text{E}(\text{D})$, correspondingly];
- a.b. at 22000 and 26000 cm^{-1} are characteristic for $\text{Cr}^{3+}(\text{O}_h)$ ions correspondingly (transfer ${}^4\text{A}_{2g} \rightarrow {}^4\text{T}_{1g}$) and Cr^{5+} .
- the presence $\text{Ni}^{2+}(\text{O}_h)$ and $\text{Ni}^{2+}(\text{T}_d)$ simultaneously in the system shows on the creation of the mixed spinel NiAl_2O_4 in the system.

Thus, the catalysts, obtained in the conditions of air atmosphere at relative high Cr and Ni concentrations (57 and 19%) create Cr_2O_5 , Cr_2O_3 , NiAl_2O_4 , NiO phases, probably Bi_2O_3 and K_2O phases, and at relative low concentrations – Cr_2O_5 , Cr_2O_3 , NiAl_2O_4 .

Let's consider the catalysts, obtained in the vacuum conditions:

The both catalysts give total, practically structureless absorption, covering all investigated spectral region (fig.4, c.11 and 12).

In all probability, as in all previous cases, the reconstruction processes, carry out in the vacuum conditions, leading to the appearance of the restored forms of Cr and Ni in the systems (Cr^0 and Ni^0 correspondingly). It is followed the important conclusions:

- as the oxide phases Cr_2O_5 , Cr_2O_3 , NiAl_2O_4 , NiO , so the restored particles Cr^0 and Ni^0 coexist at the high concentrations of Cr and Ni
- the system has the Cr_2O_5 , Cr_2O_3 , NiAl_2O_4 phases and Cr^0 and Ni^0 particles at relative low concentrations.

The oxide system Cr(10,2%)-Ni(4,3%)-K(1%)-Co(1,6%)- γ - Al_2O_3 (82,9%)

The a.b. are observed in the catalyst spectrum, obtained in the air atmosphere in the regions 15800, 17000, 18600, 12000, 23000 and 27500 cm^{-1} (fig. 4, c.13), which can be registered to the following way:

- a.b. in the regions 15800 and 17000 cm^{-1} , as the above mentioned ones can be registered to the absorption of $\text{Ni}^{2+}(\text{T}_d)$ ions [transfers ${}^3\text{T}_1(\text{F}) \rightarrow {}^3\text{T}_1(\text{P})$ and ${}^3\text{T}_1(\text{F}) \rightarrow {}^1\text{E}(\text{D})$, correspondingly];
- a.b. in the regions 17000 and 18600 cm^{-1} can be registered to Co^{2+} ions, stabilized in the fields of tetrahedral

coordination. It is possible to suppose, that state of Co²⁺(T_d) ion is caused by the creation of the normal surface spinel CoAl₂O₄ [5,6];

- the absorption in the regions 22000 and 23000 cm⁻¹ as in all other cases, is registered to Cr³⁺ and Cr⁵⁺ ions correspondingly.

Thus, the investigated four-component catalyst is the complex multicomponent system, consisting Cr₂O₅, Cr₂O₃, NiAl₂O₄, NiO, CoAl₂O₄ and probably K₂O.

The catalyst, obtained in the vacuum conditions, is characterized by the spectrum, in which the same a.b. are observed, that the above mentioned ones, but with lower intensity (fig.3, c.14). This fact shows on the carrying out of the restored processes, leading to the partial transfer Cr⁵⁺(Cr³⁺), Ni²⁺(O_h, T_d), Co²⁺(T_d) → till Cr⁰, Ni⁰ and Co⁰ correspondingly.

Thus, on the base of the carried out spectral investigations of valency and coordination state of Cr, Co,

Ni, Bi and K ions, deposited on γ -Al₂O₃ it is possible to make the following conclusions:

1. The conditions of catalyst synthesis (air atmosphere or vacuum) significantly influence on the high energetic state (valency and coordination) of Cr, Co, Ni, Bi and K ions; the catalysts, obtained in the conditions of air atmosphere have only oxidated forms of deposited elements [Cr³⁺(O_h), Cr⁵⁺, Ni²⁺(O_h), Ni²⁺(T_d), Co²⁺(T_d), Bi³⁺, K⁺], whereas, in the systems, obtained in the vacuum conditions, the oxidated and restored forms of deposited elements coexist.

2. The creation processes of chemical compositions by the type of surface compositions NiAl₂O₄ and CoAl₂O₄ carry out at the marking of the given elements γ -Al₂O₃ in the comparison with massive systems.

3. The relative high catalytic activity of four-component systems, obtained in the vacuum conditions is connected by the presence as oxidative, so restored forms of deposited elements in the system.

- [1] V.B.Loshkina, V.V.Balashova, L.Z. Doroqochinskiy. Degidrirovaniye propana i butana v kipyashem sloe alyumoxromovoqo katalizatora, promotirovyanno-qo okislyami redkozemelnix elementov. NTIS Neftepererabotka i nefteximiya, 1984, № 11, S.19. (in Russian).
- [2] R.A. Buyanov, N.A. Paxomova. Katalizatori i protsessi degidrirovaniya parafinov i olefinov. Kinetika i kataliz, 2001, t.42, № 1, S.72-85. (in Russian).
- [3] S.A. Jamalova, A.A. Kasimov, X.A. Qarabagli, G.S. Geydarova, N.A. Aliev, Z.R. Ismaylova. Izuchenie nekotoryx zakonmernostey reaktsii degidrirovaniya parafinov S₃-S₄ na Ni, Cr, Bi(Sb), Na / γ -Al₂O₃ katalizatore. AXJ, 2003, № 4. (in Russian).
- [4] Aliyev N.A., Jamalova S.A., Akhverdiyev R.B., Faradjeva S.G., Gadjizade S.M., Heydarova G.S., Kasimov A.A. The investigation of states of ions of Ni, Cr, Co, Bi and K in the composition of dehydrogenation catalysts. Fizika, 2004, v.10, № 4, 21-24.
- [5] A.S. Marfunin. Vvedenie v fiziku mineralov. M., Nedra, 1974, 324 s. (in Russian).
- [6] D.T. Sviridov, R.K. Sviridova, Yu.F. Smirnov. Opticheskie spektri ionov perekhodnikh metallov v kristallakh. M., Nauka, 1976, 268 s. (in Russian).

N.A. Əliyev, S.Ə. Camalova, R.B. Haqverdiyev, S.G. Fəracova, T.F. Allahyarova, A.Ə. Qasimov

DEHİDROGENLƏSMƏ KATALİZATORLARININ TƏRKİBİNDƏKİ γ -AL₂O₃ ÜZƏRİNƏ HOPDURULMUŞ Cr, Co, Ni, Bi VƏ K İONLARININ HALININ DƏS VƏ RENTGENOQRAFİYA METODLARI İLƏ TƏDQIQI

Massiv dehidrogenləşmə katalizatorları ilə müqayisədə daha yüksək mexaniki davamlığa, termostabilliyə malik olan hopdurulmuş katalizatorlara üstünlük verilir. Məqalədə γ -Al₂O₃ üzərinə hopdurulmuş və dehidrogenləşmə katalizatorlarının tərkibinə daxil olan Sr, So, Ni, Bi və K ionlarının halı haqqında məlumat təqdim olunub. Atmosfer və vakuum şəraitində hazırlanmış katalizatorlar istifadə olunub. Məlum oldu ki, Sr, So, Ni metallarının valent və koordinasiya halı katalizatorun hazırlanma şəraitindən asılıdır. Atmosfer şəraitində hazırlanmış katalizatorların tərkibində metalların oksidləşmiş ion formaları mövcuddur. Vakuum şəraitində hazırlanmış katalizatorlarda isə həm oksidləşmiş, həm də bərpa olunmuş metalların ion formaları mövcuddur. Ehtimal olunur ki, vakuum şəraitində hazırlanmış katalizatorun yüksək aktivliyini sistemdə metalların oksidləşmiş və bərpa olunmuş ion formalarının mövcudluğu ilə izah etmək olar.

Н.А. Алиев, С.А. Джамалова, Р.Б. Ахвердиев, С.Г. Фараджева, Т.Ф. Аллахъярова, А.А. Касимов

ИССЛЕДОВАНИЕ СОСТОЯНИЯ ИОНОВ Cr, Co, Ni, Bi И K, НАНЕСЕННЫХ НА γ -Al₂O₃ В СОСТАВЕ КАТАЛИЗАТОРА ДЕГИДРИРОВАНИЯ, МЕТОДАМИ ЭСДО И РЕНТГЕНОГРАФИИ

По сравнению с массивными катализаторами дегидрирования предпочтительным является использование нанесенных катализаторов, которые обладают более высокой механической прочностью, термостабильностью и относительно низкими затратами на их синтез. В статье представлены данные по состоянию ионов Cr, Ni, Bi, Co и K, нанесенных на γ -Al₂O₃, входящих в состав катализаторов дегидрирования парафиновых углеводородов C₃-C₄. Были использованы катализаторы, приготовленные в атмосферных условиях и в условиях пониженного давления. Установлено, что валентное и координационное состояние ионов переходных металлов (Cr, Ni, Co) зависят от условий приготовления катализатора. В образцах катализаторов, приготовленных в условиях атмосферы, присутствуют ионы металлов в окисленной форме. А в катализаторах, приготовленных в условиях вакуума, сосуществуют как окисленные, так и восстановленные формы ионов металлов. Предполагается, что высокая активность катализаторов, полученных в условиях вакуума, обусловлена присутствием в системе окисленных и восстановленных форм активных компонентов.

Received: 16.05.05

THE EXPERIMENTAL INVESTIGATION OF P - ρ - T DEPENDENCE OF METHANOL-WATER SOLUTIONS IN THE TEMPERATURE INTERVALS FROM -30°C TILL 30°C AND PRESSURE 1-200 BAR

F.G. ABDULLAYEV, O.A. AGAYEVA, U.A. JABIYEV, D.A. JAFAROVA

Azerbaijan State Oil Academy

370012, Baku, Azadlig av., 20

The experimental investigation of P - ρ - T dependence of the three binary solutions methanol-water with the molar compositions 75-25%, 50-50% and 25-75% in the temperature intervals from -30°C till 30°C and the pressure 1-200 bar. For the density measurement the good treated technique of the piezometer of the constant volume was used. The error of the obtained data doesn't exceed $\pm 0,1\%$.

For the carrying out of experimental investigation of P - ρ - T dependence of methanol-water solution the experimental installation, earlier created by us, working by the method of the piezometer of the constant volume, was used [1]. The main element of the installation is thick-walled piezometer of the spherical form from the stainless steel 1X18H9T, which has the external diameter 140 mm, internal diameter 62 mm and volume $\sim 123 \text{ cm}^3$ at $t=20^{\circ}\text{C}$ and $P=1$ bar. The two thin capillaries from the same stainless steel by the internal diameter 0,4 mm and wall thickness 0,8 mm are soldered in the lower connecting pipe of piezometer. With the help of the central capillary, the piezometer connects with fixing device and the system of the creation and measurement of the pressure, and the second capillary is used for the filling of the piezometer by the liquid and output of the last.

The use of the capillaries of the small diameter (0,4 mm) and the gate of the special construction allows us to lead the ballast volume to the very small value ($0,2 \text{ cm}^3$), which is near 0,15% from the total piezometer volume, moreover, the capillary volume, situated in the band of the transitional temperatures (from thermostat temperature till room one) is equal $0,06 \text{ cm}^3$, i.e. 0.04% from piezometer volume.

All installation nodes, with which the investigated liquid and mercury connect, are produced from the stainless steel 1X18H9T. The choice of this steel is caused by its high anticorrosive properties. Moreover, nowadays its physical properties have been investigated in detail that allows us to calculate the corrections on piezometer deformation with exactness in the dependence on the temperature and pressure.

The piezometer thermostating is carried out in the liquid thermostat, supplied by the axial pump, providing the intensive circulation of the thermostating liquid on the contour, created by the small cylinder, where the pump is situated, by the big cylinder, where the piezometer is situated and the corresponding jet. For the improvement of the thermostating the liquid is given through the lower jet from the small cylinder to the big one tangentially. The intensive motion of the liquid provides the homogeneous temperature field on all thermostat volume and moreover, the regulation of the thermostat temperature and piezometer, consequently, with the investigated substance is carried out on the control for the temperature in the one point of the thermostat. The well heat transfer from the liquid to the piezometer accelerates the transition process from the one measurement mode to another one.

For the obtaining and maintenance of needed temperatures in tests constantly we pass the water from ultrathermostat through copper coil, being in thermostat at $t=15^{\circ}\text{C}$. The vapour of liquid nitrogen, the expenditure of

which was regulated thinly with the help of vacuum pump and needle valves of special constructions, were passed through coil at $t<15^{\circ}\text{C}$.

The pressure in the installation was created by the nitrogen supply into the autoclave and oil multiplier. The pressure though the mercury was passed to the investigated liquid. For the creation of the more high pressure the press of the deadweight ianometer MP-600 was used. Pressing by the press the nitrogen, situating in the oil multiplier and under the mercury in the autoclave, the pressure in the system with the initial pressure 80-100 bar can be reduce till 1000 bar.

In this paper the main attention is given to the assurance of high measurement accuracy of the experimental values: temperature, pressure and specific volumes (density).

For the measurement of the temperature two platinum thermometers of the resistance were used. One of them is

exemplary one with coefficient $\frac{R_{100}}{R_0} = 1.39259$ and

$R_0=9.9980 \text{ Om}$ of VNIIFTRI construction and another (long) thermometer is produced also in VNIIFTRI taking under the consideration the demands to the exemplary resistance thermometers. The sensitive element of the second thermometer is carried out from the plane of PL-1 type with

coefficient $\frac{R_{100}}{R_0} = 1.39245$ and has the resistance

$R_0=10.9251 \text{ Om}$.

The reading of both resistance thermometers coincided to 0.01°C , that's why in experiments only one thermometer was used often, and another one was used for the periodic control of the stability of thermometers in time.

The excess pressures in the installation were measured by the deadweight ianometer MP-600 (class 0,01) and MP-60 (class 0,05). The total maximal error of the pressure measurement practically corresponds to the class of the exactness of the piston manometer.

It is need to note, that before the main experiment the special experiments on the pressure measurement of the saturated vapour of the simple water in the temperature interval from 200°C till critic one, were carried out on the installation. The obtained data are compared with the given ones of International constructional table [2]. The divergence on the pressure in all investigated temperature interval doesn't exceed $\pm 0,02$ bar that proves good agreement degree of the above mentioned measurement accuracy of the temperature and pressure.

The specific volume of the investigated liquid is defined as partial from the division of piezometer volume of the

investigated liquid, filling the piezometer at the measured temperature and pressure.

By analysis, of the measurement error of the main experimental values – temperatures, pressures, piezometer volume and mass of the investigated substance, it is established, that maximal sum relative fault of the density definition is equal $\approx \pm 0,05-0,10\%$, which has been proved in the previous experiments with the simple water and toluol.

After checking experiments, the density investigations of binary solutions methanol-water in the temperature interval

from -30°C till 30°C and pressures from 1,0 till 200 bar had been begun. Toward this end three two-component solutions methanol-water with molar compound: 75-25%, 50-50% and 25-75% had been prepared. The solutions were prepared by the weighing ADB-200 on the analytical scales with the error $\pm 0,01\%$ on mol. Moreover, the methanol by “ch.d.a.” type was used, which repeatedly was treated detail purification and the distilled water.

Table 1. Density values of methanol-water solution of 25-75% molar composition

P , bar	ρ , $\frac{\text{kg}}{\text{m}^3}$	P , bar	ρ , $\frac{\text{kg}}{\text{m}^3}$	P , bar	ρ , $\frac{\text{kg}}{\text{m}^3}$	P , bar	ρ , $\frac{\text{kg}}{\text{m}^3}$	P , bar	ρ , $\frac{\text{kg}}{\text{m}^3}$	P , bar	ρ , $\frac{\text{kg}}{\text{m}^3}$	P , bar	ρ , $\frac{\text{kg}}{\text{m}^3}$
$t = -30^{\circ}\text{C}$		$t = -20^{\circ}\text{C}$		$t = -10^{\circ}\text{C}$		$t = 0^{\circ}\text{C}$		$t = 10^{\circ}\text{C}$		$t = 20^{\circ}\text{C}$		$t = 30^{\circ}\text{C}$	
4,025	965,51	5,107	961,01	2,173	955,50	1,348	950,89	3,245	946,01	6,112	941,52	1,007	936,50
19,153	966,50	22,543	961,52	15,995	956,50	22,349	952,01	19,001	946,89	14,146	941,89	21,094	937,44
50,005	968,01	48,891	962,85	53,763	958,53	57,009	953,81	55,122	948,75	49,217	943,50	57,199	939,41
79,149	969,52	83,504	964,63	89,730	960,51	77,943	954,89	80,245	950,02	79,014	945,18	84,990	940,55
120,845	971,25	130,941	967,52	128,546	962,52	115,240	956,562	118,907	952,01	117,394	947,00	119,044	942,45
157,213	973,52	155,848	968,62	162,005	963,72	160,017	959,01	158,799	954,01	157,205	949,01	161,217	944,33

Table 2. Density values of methanol-water solution of 50-50% molar composition

P , bar	ρ , $\frac{\text{kg}}{\text{m}^3}$	P , bar	ρ , $\frac{\text{kg}}{\text{m}^3}$	P , bar	ρ , $\frac{\text{kg}}{\text{m}^3}$	P , bar	ρ , $\frac{\text{kg}}{\text{m}^3}$	P , bar	ρ , $\frac{\text{kg}}{\text{m}^3}$	P , bar	ρ , $\frac{\text{kg}}{\text{m}^3}$	P , bar	ρ , $\frac{\text{kg}}{\text{m}^3}$
$t = -30^{\circ}\text{C}$		$t = -20^{\circ}\text{C}$		$t = -10^{\circ}\text{C}$		$t = 0^{\circ}\text{C}$		$t = 10^{\circ}\text{C}$		$t = 20^{\circ}\text{C}$		$t = 30^{\circ}\text{C}$	
3,125	925,21	2,115	917,62	1,653	910,04	2,145	902,71	1,128	895,08	3,005	887,73	2,065	880,21
17,413	926,03	16,525	918,41	13,343	910,50	15,123	903,35	18,175	895,82	13,245	888,21	19,153	881,24
53,248	927,30	56,253	920,25	51,245	912,53	53,158	905,27	50,245	897,55	52,125	890,45	48,058	882,72
85,198	929,02	79,135	921,31	81,375	913,89	118,128	908,61	76,343	899,01	77,605	891,70	80,035	884,63
122,051	930,75	123,075	923,51	119,023	915,84	161,062	910,65	124,050	901,52	123,041	894,16	125,148	887,15
160,130	932,30	159,980	925,10	150,085	917,88			159,990	903,33	160,015	896,11	159,980	888,79

Table 3. Density values of methanol-water solution of 75-25% molar composition

P , bar	ρ , $\frac{\text{kg}}{\text{m}^3}$	P , bar	ρ , $\frac{\text{kg}}{\text{m}^3}$	P , bar	ρ , $\frac{\text{kg}}{\text{m}^3}$	P , bar	ρ , $\frac{\text{kg}}{\text{m}^3}$	P , bar	ρ , $\frac{\text{kg}}{\text{m}^3}$	P , bar	ρ , $\frac{\text{kg}}{\text{m}^3}$	P , bar	ρ , $\frac{\text{kg}}{\text{m}^3}$
$t = -30^{\circ}\text{C}$		$t = -20^{\circ}\text{C}$		$t = -10^{\circ}\text{C}$		$t = 0^{\circ}\text{C}$		$t = 10^{\circ}\text{C}$		$t = 20^{\circ}\text{C}$		$t = 30^{\circ}\text{C}$	
1,941	882,54	3,007	873,15	4,543	864,52	2,322	855,51	2,778	847,03	1,004	838,02	6,192	829,75
17,427	883,21	23,483	874,44	19,817	865,53	22,841	857,02	25,993	848,51	19,752	839,49	23,714	831,11
37,546	884,15	49,527	876,00	45,713	867,36	54,724	859,24	55,778	850,52	43,845	841,23	47,512	832,66
79,841	886,12	85,841	878,03	75,841	869,12	81,941	860,76	94,507	853,04	88,392	844,44	81,341	835,31
118,241	888,10	120,712	880,01	112,541	871,13	130,330	863,53	133,118	885,47	140,211	847,50	124,214	838,00
157,844	890,11	161,214	882,02	158,347	873,66	159,971	865,40	161,079	857,28	160,785	849,01	159,973	840,75

The density measurements of each from the mentioned binary solutions were carried out on five quasi-isochore. On each quasi-isochore the measures were carried out with step 10°C and 7 pressure values and densities had been obtained. In sum 126 experimental values of densities, which are given in the tables 1, 2 and 3 were obtained. The internal agreement of the obtained data was checked by the construction of the different isothermal and isobaric cross sections. The divergence of the experimental points relatively smoothing curves doesn't exceed $\pm 0,01\%$.

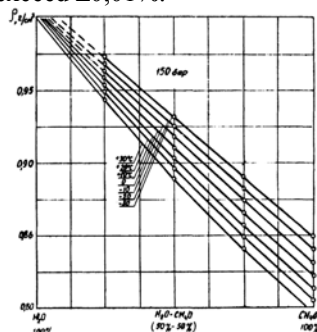


Fig. 1. The dependence of the density of the binary solutions methanol-water on the concentration at $P=50$ bar.

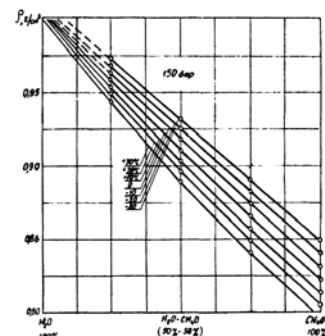


Fig. 2. The dependence of the density of binary solutions methanol-water on concentration at $P=150$ bar.

Such data for the given solution is absent in literature and have been obtained firstly at the given temperatures.

Conclusions

The measurements of P - ρ - T dependence of binary solutions of methanol-water with molar compounds 75-25%, 50-50% and 25-75% in the temperature intervals from -30°C till 30°C and pressures 1-200 bar were carried out on the experimental installation, working on the method of piezometer of the constant volume. In installation construction and technique of the measure carrying out the corresponding changes, taking under consideration the specific properties of the investigated substance and material

and temperature region had been included. Firstly, the P - ρ - T dependences of three binary solutions methanol-water were measured on the given installation and the new density values had been obtained. The maximal relative error of the experimental data doesn't exceed $\pm 0,01\%$.

The graph analytical treatment is established, that in the investigated temperature and density interval, the density of solution methanol-water doesn't obey simple additivity law, and is inclined to the side of the density decrease. The maximal inclination corresponds to molar compound 50-50% and is equal 4,6 and 5,0% at positive temperatures. With the temperature decrease this inclination decreases and changes the sign.

- [1]. V.A. Kirillin, A.E. Sheykhdlin. Issledovaniye termodinamicheskikh svoystv veshchestv. Gosenergoizdat, 1963. (in Russian).
[2]. V.N. Zubarev, P.G. Prusakov, L.B. Sergeyeva. Teplo

- phizicheskiye svoystva metilovogo spirta. 1973. (in Russian).
[3]. Mejdunarodniye skeletniye tablitsy termodinamicheskikh svoystv void i vodyanogo para, 1963. (in Russian).

F.Q. ABDULLAYEV, O.A. AGAYEVA, Y.A. CƏBİYEV, D.A. CƏFƏROVA

METANOL – SU QARIŞIĞI R - p - T ASILILIĞININ -30°S – $DƏN$ 30°S – $YƏDƏK$ TEMPERATUR VƏ 1-200 BAR TƏZYİQ İNTERVALINDA TƏCRÜBİ TƏDQIQI

30°S -dən 30°S –yədək temperatur və 1-200 bar təzyiq intervalında 75-25%, 50-50% və 25-75% mol tərkibli üç binar metanol-su qarışığının R - p - T asılılığı təcrübi tədqiq olunmuşdur. Ölçülər yüksək dərəcədə təkmilləşdirilmiş sabit həcmli pyezometr üsulu ilə yerinə yetirilmişdir. Alınan nəticələrin nisbi xətası $\pm 0,1\%$ -dən çox deyil.

Ф.Г. АБДУЛЛАЕВ, О.А. АГАЕВА, Ю.А. ДЖАБИЕВ, Д.А. ДЖАФАРОВА

ЭКСПЕРИМЕНТАЛЬНОЕ ИССЛЕДОВАНИЕ P - p - T ЗАВИСИМОСТИ РАСТВОРОВ МЕТАНОЛ-ВОДА В ПРЕДЕЛАХ ТЕМПЕРАТУР ОТ -30°C ДО 30°C И ДАВЛЕНИЙ 1-200 БАР

Проведено экспериментальное исследование P - p - T зависимости трех бинарных растворов метанол-вода с мольными составами 75-25%, 50-50% и 25-75% в пределах температур от -30°C до 30°C и давлений 1-200 бар. Для измерения плотности использована хорошо отработанная методика пьезометра постоянного объема. Погрешность полученных данных не превышает $\pm 0,1\%$.

Received: 20.07.05

THE DISTRIBUTION OF INDIUM IMPURITY IN THE Ge-Si HOMOGENEOUS CRYSTALS OF THE SOLID SOLUTIONS, GROWN UP BY BRIDGMAN METHOD IN THE MODE OF THE CONTINUOUS REPLENISHMENT OF THE MELT BY THE SILICON

V.K.KAZIMOVA, Z.M.ZEYNALOV*, G.H. AJDAROV

Institute of Physics of NAS of Azerbaijan, AZ-1143, Baku, H.Javid av., 33

**Gandja State University, Gandja, Azerbaijan*

The problem of the distribution of the indium impurity in the homogeneous single crystals Ge-Si, grown up by Bridgman method with the use of the fuse and feeding ingot of the silicon has been solved in Pfann approximation. The concentrational profiles of the indium impurity along the crystallization axis of ingots with the different compositions, demonstrating the considerable influence of the change of the melt volume on these characteristics, connected with replenishment of the melt and dependence of the segregation coefficient of the impurity on the crystal composition.

The actuality of the investigations, directed on the study of the impurity centers in the semiconductors is defined by the fact, that work of the numerous devices, lying in the base of the modern micro-optoelectronics, is defined in many cases by the impurities of the different types, introduced into the crystal. The indium is the one of the most usable impurity for the doping of the crystals of the silicon, germanium and their solid solutions. Because of the big enough solubility and small activation energy the indium impurity defines the electronic properties of these semiconductors in the wide interval of the temperatures [1,2]. The balanced segregation coefficient of indium impurity is $K_{In}=0,0004$ in Si and $K_{In}=0,001$ in Ge at the melting temperature of the silicon and germanium [3-5]. The small values of K_{In} in Si and Ge lead to the significant axial gradient of the impurity gradient in the semiconductor, grown up from the melt by the traditional methods of Bridgman or Chokhralsky. The questions, connected with the regularities of the distribution of the impurity centers in the simple semiconductors, doped in the process of the growing up from the melt, have been solved in the different approximations enough totally [1,4].

coefficient on the composition of the growing crystal. The task was solving in Pfann approximation and in the frameworks of the model of the virtual crystal for the solid solutions.

The scheme put in the base of the mathematic modeling of the concentration profile of the indium impurity in Ge-Si ingot, grown up in the mode, supplying the homogeneity of the distribution of the matrix atoms in the crystals is given on the fig.1. Initially, the feeding rod of silicon is contacted with the melt surface after the melting of the charging under the fuse from Ge, Si and In impurities with the corresponding ratio of the components and establishment of the temperature of the liquids of the given composition. Further, when the stabilized time is up, the mechanisms of the crystal drawing out and putting of the replenishment in the melt are engaged simultaneously. The growth of the homogeneous crystal with the given ratio of the concentrations of Ge and Si atoms is carried out by the way of the maintenance of the achieved temperature on the crystallization front because of the balancing of the melt composition by the corresponding ratio of the velocities of its crystallization and feeding. In this case the following ratio is correct [6-8]:

$$C_l^{Si} = \frac{\alpha}{K_{Si} - 1 + \alpha} \quad \text{or} \quad C_c^{Si} = \frac{K_{Si}\alpha}{K_{Si} - 1 + \alpha} \quad (1)$$

Here C_l^{Si} and C_c^{Si} are concentrations of the silicon in the melt and growing up homogeneous crystal correspondingly; α is the ratio of the volume of the feeding of the ingot of the silicon, entered into melt to the volume of the crystallizing melt in time unit; K_{Si} is segregation coefficient of silicon in the given composition. The equation (1) gives the possibility to define the value of α for any given C_l^{Si} or C_c^{Si} . Moreover, the corresponding value of K_{Si} is calculated from the phase diagram of the system state Ge-Si [1]. The dependence K_{Si} on the composition of the growing crystal, calculated by such way, is presented on the fig.2.

The task of the distribution of the indium impurity in Ge-Si crystals was solved under the following conditions: the crystallization front is plane; the equilibrium between solid and liquid phases exists on the crystallization front; the diffusion of indium impurity and convection in the melt supply the homogeneity of the liquid phase on all volume; the diffusion of the impurity atoms in the solid phase is approximately small. It is noted, that these conditions are

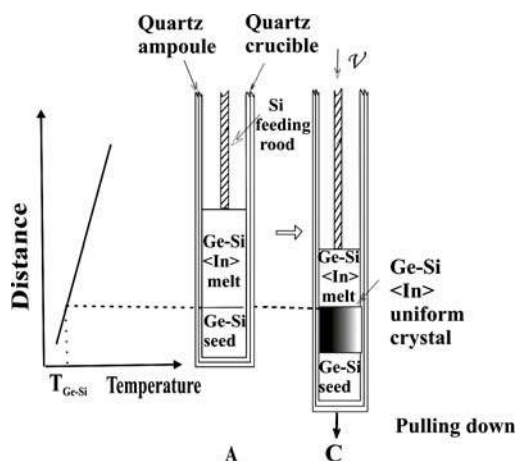


Fig.1. The schematic image of the growth of the homogeneous Ge-Si single crystal with indium impurity by the modernized Bridgman method.

The aim of the present paper is the solution of the task of the distribution of the indium impurity in the homogeneous crystals of the solid solutions Ge-Si, grown up by the modernized method of Bridgman in the mode of the constant replenishment of the melt by the silicon with taking under the consideration of the dependence of the distribution

realized at the growth velocities of crystal, which are less than $1 \times 10^{-6} \text{ m/c}$ [6].

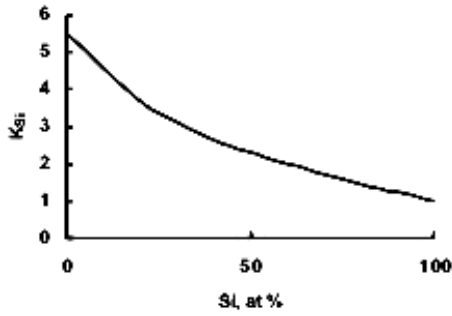


Fig.2. The dependence of the equilibrium segregation coefficient of silicon on the composition of the solid phase of Ge-Si system, calculated from phase state diagram [1].

Let's introduce the following designations: V_l^0, V_l are volumes of the melt in the crucible in the initial and current moments of time; V_c, V_{Si} are the volumes of the crystallizing melt and dissolving silicon rod in time unit; $C_{In,l}^0, C_{In,l}$ are concentrations of indium impurities in the melt in the initial and current moments on time; $C_{In,s}$ is concentration of indium impurities in the solid phase; C is common quantity of indium atoms in the melt; $K_{In} = C_{In,s}/C_{In,l}$ is equilibrium segregation coefficient of indium; t is time.

We have with the above mentioned designations:

$$C_{In,l} = \frac{C}{V_l} \text{ and } \frac{dC_{In,l}}{dt} = \frac{\dot{C}V_l - \dot{V}_l C}{V_l^2} = \frac{\dot{C} - \dot{V}_l C}{V_l}. \quad (2)$$

Taking into the consideration, that V_c and V_{Si} don't depend on time in the considerable period, we have:

$$V_l = V_l^0 - (V_c - V_{Si})t, \\ \dot{V}_l = -V_c + V_{Si} \text{ and } \dot{C} = -V_c C_{In,l} K_{In}. \quad (3)$$

Substituting the data (2) in (1), after the separation of variables and integration, we find

$$\frac{V_c - V_{Si}}{V_c - V_c K_{Al} - V_{Si}} \int \frac{C_{In,l}}{C_{In,l}^0} \frac{dC_{In,l}}{C_{In,l}} = \int_0^t \frac{\frac{V_l^0}{V_l^0} dt}{1 - \frac{(V_c - V_{Si})t}{V_l^0}}. \quad (4)$$

Introducing designations $V_{Si}/V_c = \alpha$; $V_c t/V_l^0 = \gamma$ in (3) after integration, we obtain:

$$C_{In,s} = C_{In,l} K_{In} = C_{In,l}^0 K_{In} [1 - \gamma(1 - \alpha)]^{\frac{(K_{In} + \alpha - 1)}{(1 - \alpha)}}. \quad (5)$$

The equation (5) gives possibility to define the concentration of indium impurity in the dependence on γ , i.e. on crystal length at the known values K_{In} and α . The [1]

coefficient of the separation of K_{In} impurity in Ge-Si crystal with given composition can be defined in the limits of the model of virtual crystal for the solid solutions on the known data K_{In} in germanium and silicon, taking under the consideration, that K_{In} depends linearly on the silicon concentration in the crystal. The experimental data of the ref [3] on the definition K_{In} in the one of the compositions Ge-Si prove the correctness of the mentioned by us approximation. The value $V_{Si}/V_c = \alpha$; in the equation (5), is defined from the condition of the growth totally homogeneous crystals of the solid solutions Ge-Si with the help of the equation (1).

The fig.3 illustrates the calculated curves of the concentration profile of indium impurity along Ge-Si crystals with silicon content 5, 10, 20, 40 and 80 at.% Si, calculated from the equation (5) with the use of the corresponding values α and K_{Si} on data (1) and fig.2. For all crystals the initial concentration of the impurity in the melt is equal to $C_{In,l}^0 = 1 \times 10^{18} \text{ cm}^{-3}$.

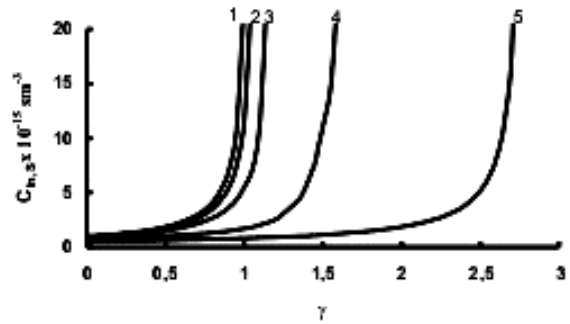


Fig.3. The dependences of the concentration of the indium impurity on γ in homogeneous Ge-Si crystals, grown up by modernized Bridgman method with the use of the feeding silicon ingot. The curves 1, 2, 3, 4 and 5 are related to the crystals with the silicon content 5, 10, 20, 40 and 80 at.% correspondingly.

As it is seen from the fig.3, the velocity of the concentration growth of the impurity on the crystal length decreases with the increase of the silicon content in matrix. Such behavior is explained by the decrease of the segregation coefficient of indium with increase of silicon concentration in melt from one side, and with the increase of the melt volume, caused by its constant feeding from another side. It is need to pay attention on the practical constant of impurity concentration in enough extensive region in melts with big content of silicon. Such distribution character opens the possibility of the Ge-Si crystal obtaining with practically equal concentrational profile of indium impurity.

On the base of the above mentioned material, it is possible to make following conclusion. The dependence of segregation coefficient of the impurity on Ge-Si composition and change of the melt volume, connected with its feeding significantly influences on the velocity change of the concentration of the indium impurity along crystallization axis in homogeneous single crystals of the solid solutions Ge-Si, grown up by Bridgman method on the fuse with the given composition in the mode of the constant feeding of the melt by the second component.

- [2] *V.M. Glazov, V.S. Zemskov*, Physico-khimicheskie osnovi legirovaniya poluprovodnikov, M.: Nauka, (1967) 371.
- [3] *B.I. Shklovskiy, A.L. Efros*, Elektronnie svoistva legirovannikh poluprovodnikov, M.: Nauka, (1979) 416.
- [4] *Barz, P. Dold, U. Kerat, S. Recha, and K.W. Benz*, Journal of Vac. Sci. Technol. B 16(3) (1998) 1627.
- [5] *D.T.J. Hurle*, Handbook of Crystal Growth (North-Holland, Amsterdam, 1994), vol.2b.
- [6] *M. Schulz and H. Weiss*, Landolt-Bornstein, New Series (Springer, Berlin) 1984.
- [7] *G.Kh. Azhdarov, T. Kucukomerogly, A. Varilci, M. Altunbas, A. Kobya, P. G. Azhdarov*, Journal of Crystal Growth, 226 (2001) 437.
- [8] *G.Kh. Ajdarov*, Izvestiya VUZov Rossii, Materiali elektronnoy tekhniki, 2 (2004) 47.
- [9] *G.Kh. Ajdarov, R.Z. Kyazimzade*, Tezisi dok. Natsionalnoy konferensii po rostu kristallov, Moskva (2004) c. 109.

V.K. KAZIMOVA, Z.M. ZEYNALOV, H.X. ƏJDƏROV

**Si-LA KƏSİRSİZ QİDALANAN ƏRİNTİDƏN MODERNLƏŞMİŞ BRİDJMAN ÜSULU İLƏ ALINAN
BİRCİNSLİ Ge-Si KRİSTALLARINDA İNDİUM AŞQARININ PAYLANMASI**

Pfann yaxınlaşması çərçivəsində modernizə edilmiş Bridjman üsulu ilə ərintini kəsirsiz Si ilə qidalandırma rejimində alınan bircinsli Ge-Si kristallarında indium aşqarının paylanma məsələsi nəzəri həll edilib. Aşqarın seqreqasiya əmsalının Ge-Si kristalının tərkibindən asılılığı və ərintinin qidalandırma nəticəsində dəyişilən həcmi aşqarın kristal boyunca konsentrasiyasına əhəmiyyətli təsiri göstərilib.

В.К. КАЗИМОВА, З.М. ЗЕЙНАЛОВ, Г.Х. АЖДАРОВ

**РАСПРЕДЕЛЕНИЕ ПРИМЕСИ ИНДИЯ В ОДНОРОДНЫХ КРИСТАЛЛАХ ТВЁРДЫХ РАСТВОРОВ
Ge-Si, ВЫРАЩЕННЫХ МЕТОДОМ БРИДЖМЕНА В РЕЖИМЕ НЕПРЕРЫВНОЙ ПОДПИТКИ
РАСПЛАВА КРЕМНИЕМ**

В пфанновском приближении решена задача распределения примеси индия в однородных монокристаллах Ge-Si, выращенных методом Бриджмена с использованием затравки и подпитывающего слитка кремния. Построены концентрационные профили примеси индия вдоль оси кристаллизации слитков различного состава, демонстрирующие существенное влияние на эти характеристики изменения объёма расплава, связанного с его подпиткой и зависимости коэффициента сегрегации примеси от композиции кристалла.

Received: 22.06.05

Fizika

**Azərbaycan Milli Elmlər Akademiyası
Fizika-Riyaziyyat və Texnika Elmləri Bölməsi
Fizika İnstitutu**

Ü Ə İ

Aşağı sıxlıqlı polietilen və TlInSe_2 kompozisiyalarının derivatoqrafik tədqiqi.	3
. E.M. Qocayev, R.M. Sərdarlı, S.S. Osmanova, N.A. Eyubova, E.Ə. Allahyarov	
Üzvi yarımqeçirici vanadium ftalosianin əsasında nazik təbəqəli strukturlarda elektrikke- çiriciliyinin mexanizmiM.M. Pənahov, S.A. Sədrəddinov, C.H. Cabbarov, B.Ş. Barxalov	7
MnIn_2S_4 və MnGaInS_4 monokristallarında termostimullaşmış depolyarizasiya cərəyanları.	
. N.N.Niftiyev, O.B. Tağıyev	10
Sıxılmış qazların və mayələrin istilikkeçirməsinin termiki təzyiqdən asılılığının nəzəri tədqiqi. . . .	
. C.Y. Naziyev	12
WZNW modelinin laksa cütü halında təqdim olunması. M.A. Muxtarov	15
Allatostatin iv neyropeptidinin su mühitində yan zəncirlərinin dinamik xüsusiyyətləri	
. M.A. Musayev, L.İ. Vəliyeva, İ.N. Əliyeva, N.M. Qojayev	17
Faza keçidi oblastında gümüş xalkoqenidlərdə nizamlılıq parametrlərinin yayınlılığı. . . S.A. Əliyev	24
Nambu-Yona-Lazinio modelində çoxkvarklı Qrin funksiyaları üçün tənliklər. R.Q. Cəfərov	27
Optik kanallardakı multiplikativ maneələrin təsirinin ayrıncı parametrlə qiymətləndirilməsi.	32
. R.A. Abdullayev, M. Yüksək	
Elektron - optik çevirici ekranının küy şüalanmasının səbəbləri haqda.	
. H.N. Vəzirov, N.İ. İbrahimov	36
Keyn tipli yarımqeçirici kvant tellərində kənar hallar . . .A.M. Babayev, Ş. Çakmaktepe, A. Kökçe	39
Əsas yaxınlaşmadan sonrakı tərtibdə qlüonun Qrin funksiyası. L.A. Əliyeva, S.A. Hacıyev	45
Protonların təsirlə nuklonların nüvədən qoparılması. M.M.Mirabutalıbov	50
$I^{\pm}N \Rightarrow I^{\pm}BX$ yarımqeçirici dərin qeyri elastiki reaksiyalarda elektrozəif proseslər	
. S.K. Abdullayev, A.İ. Muxtarov, S.M. Rəhimova	53
Elektrosintez prosesində Cu_{2-x}S təbəqələrinin maqnitohəssas komponent ilə (Sm) ləqirlənməsi	
. E.N. Zamanova, L.A. Əliyeva, S.M. Bağirova, M.N. Elçiyev, Q.Q. Hüseynov	59
Laylı sistemlərdə elektromaqnit şüalanmanın əksolunmasının tezlikli xüsusiyyətləri.	
. M.A. Sadıxov, S.T. Əzizov, A.S. Zeynalova	62
Dehidrogenləşmə katalizatorlarının tərkibindəki $\gamma\text{-Al}_2\text{O}_3$ üzərinə hopdurulmuş Cr, Co, Ni, Bi və K ionlarının halının DƏES və rentgenoqrafiya metodları ilə tədqiqi.	
. N.A. Əliyev, S.Ə. Camalova, R.B. Haqverdiyev, S.G. Fərəcova, T.F. Allahyarova, A.Ə. Qasimov	65
Metanol – su qarışığı R- ρ -T asılılığının -30°S –dən 30°S –dən temperatur və 1-200 bar təzyiq intervalında təcrübi tədqiqi.F.Q. Abdullayev, O.A. Ağayeva, Yu.A. Cəbiyev, D.A. Cəfərova	70
Si-la kəsirsiz qidalanan ərintidən modernləşmiş bridcman üsulu ilə alınan birjinsli Ge-Si kristallarında indium aşqarının paylanması. V.K. Kazımova, Z.M. Zeynalov, H.X. Əjdərov	73

СОДЕРЖАНИЕ

Дериватографические исследования композиций полиэтилен низкой плотности и TlInSe_2	3
.....Э.М. Годжаев, Р.М. Сардарлы, С.С. Османова, Н.А. Эюбова, Э.А. Аллахъяров	
Механизм электропроводности в тонкопленочной структуре на основе органического полупроводника фталоцианина ванадия.	7
.....М.М. Панахов, С.А. Садрадинов, Дж. Г. Джаббаров, Б.Ш. Бархалов	
Токи термостимулированной деполяризации в монокристаллах MnIn_2S_4 и MnGaInS_4	10
.....Н.Н. Нифтиев, О.Б. Тагиев	
Теоретическое исследование зависимости теплопроводности сжатых газов и жидкостей от термического давления.	12
.....Дж.Я. Назиев	
Представление модели WZNW в виде пары Лакса.	15
.....М.А. Мухтаров	
Динамические свойства боковых цепей нейропептида аллатостатина IV в водной среде.	17
.....М.А. Мусаев, Л.И. Велиева, И.Н. Алиева, Н.М. Годжаев	
Размытие параметра упорядочения в халькогенидах серебра в области фазового перехода.	24
.....С.А.Алиев	
Уравнения для многокварковых функций Грина в модели Намбу-Иона-Лазинию.	27
.....Р.Г. Джафаров	
Оценка оптического канала с мультипликативными помехами с помощью параметра разделения.	32
.....Р.А. Абдуллаев, М. Юксек	
О возможных причинах фонового излучения экрана электронного-оптического преобразователя	36
.....Х.Н. Везиров, Н.И. Ибрагимов	
Краевые состояния в квантовой проволоке кейновского полупроводника.	39
.....А.М. Бабаев, Ш. Чакмактепе, А. Кокче	
Функция Грина глюона в следующем порядке за главным приближением.	45
.....Л.А. Алиева, С.А. Гаджиев	
Реакция выбивания нуклонов из ядер протонами.	50
.....М.М. Мирабуталыбов	
Электрослабые асимметрии в полуинклюзивных глубоко неупругих реакциях $l^+N \Rightarrow l^+BX$	53
.....С.К. Абдуллаев, А.И. Мухтаров, С.М. Рагимова	
Легирование пленок Cu_{2-x}S магниточувствительной компонентой (Sm) в процессе электросинтеза	59
.....Э.Н. Заманова, Л.А. Алиева, С.М. Багирова, М.Н. Елчиев, Г.Г. Гусейнов	
Частотные характеристики отражения электромагнитного излучения в слоистых системах.	62
.....М.А. Садыхов, С.Т. Азизов, А.С. Зейналова	
Исследование состояния ионов Cr, Co, Ni, Bi и K, нанесенных на $\gamma\text{-Al}_2\text{O}_3$ в составе катализатора дегидрирования, методами ЭСДО и рентгенографии.	65
.....Н.А. Алиев, С.А. Джамалова, Р.Б. Ахвердиев, С.Г. Фараджева, Т.Ф. Аллахъярова, А.А. Касимов	
Экспериментальное исследование P- ρ -T зависимости растворов метанол-вода в пределах температур от -30°C до 30°C и давлений 1-200 бар.	70
.....Ф.Г. Абдуллаев, О.А. Агаева, Ю.А. Джабиев, Д.А. Джафарова	
Распределение примеси индия в однородных кристаллах твердых растворов Ge-Si, выращенных методом Бриджмена в режиме непрерывной подпитки расплава кремнием.	73
.....В.К. Кязимова, З.М. Зейналов, Г.Х. Аждаров	

CONTENTS

The derivative-graphical investigations of the polyethylene system of the low density (PELD) + x weigh % TlInSe ₂ (x=0; 1; 3; 5; 10; 40) . . .E.M.Gojayev, R.M.Sardarli, S.S.Osmanova, N.A.Eyubova, E.A.Allahyarov	3
The mechanism of electrical conductivity in thin-film structure on the basis of the organic semiconductor vanadium phthalocyanine. M.M. Panahov, S.A. Sadraddinov, J.N. Jabbarov, B.SH. Barkhalov	7
Currents of thermostimulated depolarization in MnIn ₂ S ₄ and MnGaInS ₄ single crystals.	10
. N.N. Niftiyev, O.B. Tagiyev	
Theoretical research of the dependence of thermal conductivity of compressed gases and liquids on thermal pressure. J.Y. Naziyev	12
Lax pair presentation of WZNW model. M.A. Mukhtarov	15
Dynamical properties of the allatostatin iv neuropeptide side chains in water solution.	17
. M.A. Musayev, L.I. Velieva, I.N. Alieva, N.M. Gojayev	
The blur of the order parameter in argentum chalcogenide in the region of the phase transition.	24
. S.A. Aliyev	
The equations for the multi-quark green function in nambu-jona-lazinio model. R.G. Jafarov	27
The estimation of optical channel with multiplicative noise by using of separating parameter.	32
. R.A. Abdullayev, M. Yuksek	
Possible causes of screen background radiation of electro-optical transformer (EOT).	36
. X.N. Vezirov, N.I. Ibragimov	
Edge states in a Kane type semiconductor quantum wire. M. Babayev, Ş. Çakmaktepe, A. Kökçe	39
The gluons Green function in NLO. L.A. Alieva, S.A. Gadjiev	45
The reaction of dislodging of nucleones by the protons from the nucleuses. M.M. Mirabutalibov	50
The electroweak asymmetries in the semi-inclusive deep-inelastic reactions $l^+N \Rightarrow l^+BX$	53
. S.K. Abdullayev, A.I. Mukhtarov, S.M. Ragimova	
The doping of Cu _{2-x} S magnitosensitive and component (Sm) films in electrosynthesis process.	59
. E.N. Zamanova, L.A. Aliyeva, S.M. Bagirova, M.N.Yolchiyev, G.G. Guseynov	
The frequency characteristics of the reflection of the electromagnetic radiation in the layered systems.	62
. M.A. Sadichov, S.T. Azizov, A.S. Zeynalova	
The investigation of the states of Cr, Co, Ni, Bi and K ions, deposited on γ -Al ₂ O ₃ in the composition of the dehydrogenation catalyst by ESDO and rentgenography methods.	65
. N.A. Aliyev, S.A. Jamalova, R.B. Akhverdiyev, S.G. Faradjeva, T.F. Allahyarova, A.A. Kasimov	
The experimental investigation of P - ρ - T dependence of methanol-water solutions in the temperature intervals from -30°C till 30°C and pressure 1-200 bar.	70
. F.G. Abdullayev, O.A. Agayeva, U.A. Jabiyev, D.A. Jafarova	
The distribution of indium impurity in the Ge-Si homogeneous crystals of the solid solutions, grown up by Bridgman method in the mode of the continuous replenishment of the melt by the silicon.	73
. V.K.Kazimova, Z.M.Zeynalov, G.H. Ajdarov	